TECHNISCHE UNIVERSITÄT MÜNCHEN

Fakultät für Chemie

Lehrstuhl für Pharmazeutische Radiochemie

Development of PSMA inhibitors for molecular imaging and radio-guided surgery of prostate cancer

Stephanie Robu

Vollständiger Abdruck der von der Fakultät für Chemie der Technischen Universität München zur Erlangung des akademischen Grades eines

Doktors der Naturwissenschaften (Dr. rer. nat.)

genehmigten Dissertation.

Vorsitzender: Prof. Dr. Dr. h.c. Horst Kessler

Prüfer der Dissertation:

1. Prof. Dr. Hans-Jürgen Wester
2. Priv.-Doz. Dr. Matthias Eiber

Die Dissertation wurde am 24.10.2018 bei der Technischen Universität München eingereicht und durch die Fakultät für Chemie am 06.12.2018 angenommen.

Danksagung

Die vorliegende Arbeit wurde im Zeitraum von April 2012 bis September 2016 an der Fakultät für Chemie am Lehrstuhl für Pharmazeutische Radiochemie der Technischen Universität München unter der Leitung von **Prof. Dr. Hans-Jürgen Wester** angefertigt.

Mein besonderer Dank gilt Herrn **Prof. Dr. Hans-Jürgen Wester** für die äußerst interessante Themenstellung und vor allem für die kompetente Unterstützung und sein Vertrauen, das er mir entgegengebracht hat. Des Weiteren bedanke ich mich für die großzügige Förderung und seine Gesprächsbereitschaft bei kleinen und großen wissenschaftlichen Problemen.

Ferner danke ich Frau **Prof. Dr. Margret Schottelius** für Ihre stets uneingeschränkte Unterstützung und die hilfreichen Diskussionen bei wissenschaftlichen Fragestellungen und Problemen.

Zudem möchte ich Herrn **Prof. Dr. Markus Schwaiger** für die Bereitstellung der technischen Ausrüstung und den guten Arbeitsbedingungen am Klinikum rechts der Isar danken und allen Mitarbeitern der Nuklearmedizin des Klinikum rechts der Isar, besonders Herrn **PD Dr. Matthias Eiber** und **PD Dr. Tobias Maurer** für die stets gute Zusammenarbeit. Zudem danke ich Herrn **Michael Herz** für die Routineherstellung von [^{18}F]Fluorid und **Sybille Reder**, sowie **Markus Mittelhäuser** für ihre Unterstützung bei den *in vivo* Versuchen.

Ein ganz spezieller Dank gilt meinen Laborkollegen **Dr. Martina Wirtz**, **Dr. Theresa Osl**, **Dr. Andreas Poschenrieder**, **Dr. Alexander Schmidt**, **PD Dr. Johannes Notni**, **PD Dr. Behrooz Yousefi**, **Alexander Wurzer**, **Dr. Jakub Šimeček**, **Thomas Günther**, **Dr. Frauke Richter**, **Dr. Roswitha Beck**, **Matthias Konrad**, **Daniel Di Carlo** sowie **Monika Beschorner** und **Sven Hintze** für eine sehr schöne und unvergessliche Zeit im Labor und für das gute Arbeitsklima.

Mein größter Dank gilt meiner Familie und insbesondere meinen Eltern, die mich während meines Studiums bis zum Abschluss der Promotion uneingeschränkt und in jeglicher Form unterstützt und motiviert haben.

Work on the presented PhD thesis resulted in the following publications:

Weineisen M, **Robu S**, Schottelius M, Wester H-J. Novel and Established Radiopharmaceuticals for Diagnosis and Therapy of Prostate Carcinoma. *Nuklearmediziner* 2015; 38(02): 89-98.

Robu S*, Schottelius M*, Eiber M, Maurer T, Gschwend J, Schwaiger M, Wester H-J. Preclinical Evaluation and First Patient Application of ^{99m}Tc-PSMA-I&S for SPECT Imaging and Radioguided Surgery in Prostate Cancer. *J. Nucl. Med*. 2017; 58(2): 235-242.

Maurer T*, **Robu S***, Schottelius M, Schwamborn K, Rauscher I, van den Berg N, van Leeuwen F W B, Haller B, Horn T, Heck M M, Gschwend J E, Schwaiger M, Wester H-J, Eiber M. ^{99m}Technetium-based Prostate-specific Membrane Antigen-radioguided Surgery in Recurrent Prostate Cancer. *Eur Urol*. 2019; 75(4):659-666.

Robu S*, Schmidt A, Eiber M, Schottelius M, Günther T, Yousefi B, Schwaiger M, Wester H-J. Synthesis and Preclinical Evaluation of novel ^{18}F-labeled Glu-urea-Glu-based PSMA inhibitors for Prostate Cancer Imaging: a comparison with ^{18}F-DCFPyl and ^{18}F-PSMA-1007. *EJNMMI Res*. 2018; 8(1):30-40.

Studies described in the PhD thesis resulted in the following conference presentations:

S. Robu, M. Schottelius, H.-J. Wester. Der Frizzled 2 Rezeptor als Target für die molekulare Bildgebung; 12-14th September **2013**, 21th Meeting of Radiochemistry and Radiopharmacy Work Groups (AGRR), Pamhagen, Austria.

S. Robu, M. Schottelius, A. Kohlmeier, M. Weineisen, F. Hoffmann, M. Schwaiger, H.-J. Wester. Novel [Tc-99m]MaS3-analogs of PSMA-I&T for SPECT-imaging of metastatic prostate cancer; 22-25th April **2015**, 53th Symposium of German Society of Nuclear Medicine (DGN), Hannover, Germany.

S. Robu, M. Schottelius, M. Eiber, T. Maurer, J.E. Gschwend, M. Schwaiger, H.-J. Wester. Entwicklung und erste Evaluierung von ^{99m}Tc-PSMA-I&S für die SPECT und RGS. 20-23th April **2016**, 54th Symposium of German Society of Nuclear Medicine (DGN), Dresden, Germany.

Studies described in this PhD thesis resulted in the following award lecture:

S. Robu, M. Schottelius, M. Eiber, T. Maurer, J. E. Gschwend, M. Schwaiger, H.-J. Wester. Entwicklung und klinische Evaluierung von [^{99m}Tc]PSMA-I&S für die SPECT und RGS. 22-23th September 2016, Jörg-Mahlstedt Gedächtnispreis, 46th Symposium of the Professional Organization of German Nuclear Medicine, Berlin, Germany.

Abstract

Prostate cancer (PCa) is estimated to be the most common malignancy in man worldwide. Despite the reduction of death rates, PCa still remains a serious health care issue with high clinical need for better characterization and treatment of the disease. To address these issues, imaging techniques have the potential to make significant contributions to the initial diagnosis, staging, determination of the extent of disease recurrence, and measurement of the response to treatment. Due to the high and consistent expression in PCa, the prostate specific membrane antigen (PSMA) has emerged as one of the most extensively explored targets for molecular imaging and targeted therapy, using highly specific PSMA radioligands. In recent years, several urea-based PSMA inhibitors have been clinically introduced, which have already had a remarkable impact on the clinical management of PCa. The primary goal of this work was the development of novel PSMA inhibitors for PET imaging (^{18}F), SPECT imaging, and for radioguided-surgery (^{99m}Tc) of PCa.

In general, a combination of solution and solid phase peptide synthesis afforded the rapid synthesis of the PSMA inhibitors, based on either a KuE- or a EuE-binding motif conjugated over a linker unit to a radiometal chelator or a radiolabeled prosthetic group. Binding affinities towards PSMA (IC_{50}) and internalization kinetics of the respective radiolabeled inhibitors were determined using LNCaP cells and ((^{125}I)I-BA)KuE as internal reference. *In vivo* metabolite analyses, biodistribution studies and µPET imaging was carried out using CD-1 nu/nu mice and LNCaP-tumor-bearing CB-17-SCID mice.

The adaptation of the **(^{68}Ga/^{177}Lu/^{111}In)PSMA-I&T**-based theranostic concept towards ^{99m}Tc-labeling chemistry, led to the corresponding more cost-effective and promising substitute **^{99m}Tc-PSMA-I&S** (**I & S for I**maging and **S**urgery). The established ^{99m}Tc-labeling strategy ensured fast and reliable radiosynthesis for clinical application. The investigated structural modifications of **^{99m}Tc-PSMA-I&S** resulted in comparable *in vitro* and *in vivo* PSMA-targeting characteristics compared to the lead compound **^{111}In-PSMA-I&T**. The combined effects of enhanced internalization kinetics and prolonged half-life of intact tracer in the blood combined with continuing clearance of background activity promoted excellent tumor-to-background ratios in SPECT imaging of an exemplary patient using **^{99m}Tc-PSMA-I&S** (up to 21h p.i.). These favorable tracer characteristics allowed the successful intraoperative detection and complete resection of all ^{68}Ga-PSMA-11 PET positive metastatic lesions during first-in-human **^{99m}Tc-PSMA-I&S**-based radioguided-surgery (RGS). The follow up data of 31 consecutive patients with evidence of recurrent PCa, undergoing **^{99m}Tc-PSMA-I&S**-based RGS, demonstrated the high potential of this surgical technique for the detection of even small tumor deposits in PCa patients with high specificity, sensitivity, as well as accuracy.

The short-term outcomes indicated that **^{99m}Tc-PSMA-I&S**-based RGS might positively influence disease progression and delay the need for further systemic treatment. Although, **^{99m}Tc-PSMA-I&S** was developed as a gamma probe for intraoperative guidance the acquired data also hint towards the unexpected potential of **^{99m}Tc-PSMA-I&S** as an SPECT imaging agent for first-line diagnosis of metastasized PCa.

To address the continuously growing clinical demand for ^{18}F-labeled PSMA ligands, two novel EuE-based PSMA inhibitors, **EuE-k-^{18}F-FBAO** and **EuE-k-β-a^{18}F-FPyl** were developed for the diagnosis of PCa. The KuE binding motif was replaced by a EuE-based binding unit conjugated to an optimized linker structure and different ^{18}F-labeled aromatic groups for chemo-selective labeling strategies. The highly hydrophilic chemical structure of both **EuE-based PSMA inhibitors** resulted in enhanced PSMA affinities and markedly higher internalization efficiencies in LNCaP cells compared to the recently introduced tracers **^{18}F-DCFPyl** and **^{18}F-PSMA-1007**. Therefore, **EuE-k-^{18}F-FBAO** and **EuE-k-β-a^{18}F-FPyl** revealed markedly higher tumor accumulation in µPET and biodistribution studies in LNCaP-tumor xenografts in comparison to the reference ligands (1h p.i.). In addition, both **EuE-based radioligands** showed favorable pharmacokinetics *in vivo* with straightforward clearance kinetics and almost no uptake in non-target tissue, allowing for high-contrast imaging at early time points. Although both **^{18}F-labeled EuE-based inhibitors** exhibited excellent and (partly) superior *in vitro* and *in vivo* PSMA-targeting characteristics in comparison to **^{18}F-DCFPyl** and **^{18}F-PSMA-1007**, **EuE-k-^{18}F-FBAO** appeared to be more promising for further investigation than **EuE-k-β-a^{18}F-FPyl**, due to the more reliable radiosynthesis and the faster clearance kinetics with comparable high tumor uptake. **EuE-k-^{18}F-FBAO** was investigated in a proof-of-concept study for the diagnostic application in a patient with metastatic castration resistant prostate carcinoma (mCPRC). Due to the intense uptake of **EuE-k-^{18}F-FBAO** in lymph- and bone metastases, the fast renal wash-out, and minimal blood pool retention of the tracer high-contrast PCa PET imaging was achieved at 1h p.i..

Zusammenfassung

Den Schätzungen zur Folge gehört das Prostatakarzinom (PCa) zu der weltweit häufigsten bösartigen Tumorerkrankung des Mannes. Trotz sinkender Mortalitätsrate ist eine bessere Charakterisierung und Behandlung der Erkrankung von höchster klinischer Notwendigkeit. Bildgebende Verfahren leisten einen bedeutenden Beitrag zur Initialdiagnose, dem Staging, zur Bestimmung des Ausbreitungsgrades eines PCa-Rezidivs, als auch zur Beurteilung des Therapieansprechens. Das Prostata-spezifische Membranantigen (PSMA) gehört, aufgrund der hohen und konsistenten Expression beim PCa, zu der am meist erforschten Zielstruktur für die molekulare Bildgebung und zielgerichtete Therapie mittels hoch spezifischer Harnstoff-basierter PSMA Radioliganden. Das primäre Ziel dieser Arbeit war die Entwicklung neuer PSMA Inhibitoren für die PET (^{18}F) und SPECT Bildgebung, sowie für die Radioguided Surgery (^{99m}Tc) des PCa.

Eine Kombination aus Flüssig- und Festphasenpeptidsynthese ermöglichte eine schnelle Synthese der PSMA Inhibitoren. Die Struktur der PSMA-Liganden basierte entweder auf einem KuE- oder EuE-Bindungsmotiv, das über einen Peptidlinker an einen Radiometall-chelator oder eine radiomarkierte prosthetische Gruppe konjugiert wurde. Zur Bestimmung der PSMA Bindungsaffinitäten (IC_{50}) und Internalisierungskinetiken, der jeweiligen radiomarkierten Inhibitoren, wurden PSMA exprimierende LNCaP Zellen und ((^{125}I)I-BA)KuE als interne Referenz verwendet. *In vivo* Metabolitenanalysen, Biodistributionsstudien und Kleintier-PET Untersuchungen wurden in CD-1 nu/nu Mäusen und LNCaP-Tumor tragenden CB-17 SCID Mäusen durchgeführt.

Die Anpassung des theranostischen Konzepts von **(^{68}Ga/^{177}Lu/^{111}In)PSMA-I&T** an die Anforderungen der ^{99m}Tc-Markierungschemie, führte zur Entwicklung des kostengünstigeren und vielversprechenden Analogons **^{99m}Tc-PSMA-I&S** (**I & S** for **I**maging and **S**urgery). Eine etablierte ^{99m}Tc-Markierungsstrategie gewährleistete die schnelle und zuverlässige Radiosynthese für die klinische Anwendung. Das strukturell modifizierte **^{99m}Tc-PSMA-I&S** zeigte vergleichbar gute *in vitro* und *in vivo* PSMA-gerichtete Eigenschaften im Vergleich zur Leitstruktur **^{111}In-PSMA-I&T**. In einer ersten Patientenstudie mit **^{99m}Tc-PSMA-I&S** wurde gezeigt, dass die Kombination aus erhöhter Internalisierung, verlängerter Verfügbarkeit des intakten Tracers im Blut und die kontinuierliche Clearance von Hintergrundaktivität zu exzellenten Tumor-zu-Hintergrund Verhältnissen in der SPECT Bildgebung führte (bis zu 21h nach Injektion). Diese vorteilhaften Tracereigenschaften ermöglichten die erfolgreiche intraoperative Detektion und vollständige Resektion aller ^{68}Ga-PSMA-11 PET positiven Metastasen während der Erstanwendung der **^{99m}Tc-PSMA-I&S**-basierten Radioguided Surgery (RGS) am Patienten. Die Folgedaten von 31 konsekutiven Patienten mit

nachgewiesenen PCa Rezidiv, die mittels **^{99m}Tc-PSMA-I&S** RGS operiert wurden, demonstrierten das vielversprechende Potential dieser Operationstechnik für die Detektion selbst sehr kleiner Läsionen mit hoher Sensitivität, Spezifität und Genauigkeit. Die vorläufigen Ergebnisse deuten darauf hin, dass die **^{99m}Tc-PSMA-I&S**-basierte RGS zum einen die Progression der Erkrankung als auch die Notwendigkeit einer weiteren Behandlung positiv beeinflussen könnte. Obwohl **^{99m}Tc-PSMA-I&S** vorwiegend als Radioligand für die intraoperative Detektion von Lymphknotenmetastasen entwickelt wurde, weisen die vorläufigen Daten zudem auf ein unerwartetes Potential von **^{99m}Tc-PSMA-I&S** als Tracer für die SPECT Bildgebung zur Primärdiagnose von metastasierten PCa hin.

Aufgrund der steigenden klinischen Nachfrage nach ^{18}F-markierten PSMA Liganden, wurden die zwei neuen EuE-basierten PSMA Inhibitoren, **EuE-k-^{18}F-FBAO** und **EuE-k-β-a^{18}F-FPyl**, für die Bildgebung des PCa entwickelt. Das KuE-Bindemotiv wurde gegen eine EuE-Bindungseinheit ausgetauscht, die über optimierte Linkerstrukturen an verschiedene ^{18}F-markierte aromatische Gruppen, zur chemo-selektiven Markierung, konjugiert wurde. Die hydrophile Struktur der **EuE-basierten PSMA Inhibitoren** führte, im Vergleich zu den kürzlich veröffentlichten Tracern **^{18}F-DCFPyl** und **^{18}F-PSMA-1007,** zu verbesserten PSMA Affinitäten und einer deutlich höheren Internalisierungseffizienz in LNCaP Zellen. Zudem zeigten **EuE-k-^{18}F-FBAO** und **EuE-k-β-a^{18}F-FPyl,** verglichen mit den Referenzliganden, eine signifikant höhere Tumoranreicherung im Kleintier-PET und in Biodistributionsstudien in LNCaP-Tumor Xenografts (1h p.i.). Beide **EuE-basierten Radioliganden** zeigten neben einer vorteilhaften Pharmakokinetik *in vivo*, kaum Anreicherung in PSMA-negativen Organen, wodurch eine kontrastreiche PET-Bildgebung zu frühen Zeitpunkten ermöglicht wurde. Aufgrund der zuverlässigeren Radiosynthese, der schnelleren Ausscheidungskinetik mit vergleichbar hoher Tumoranreicherung, schien **EuE-k-^{18}F-FBAO** im Vergleich zu **EuE-k-β-a^{18}F-FPyl** vielversprechender für die weitere klinische Anwendung. Folglich wurde **EuE-k-^{18}F-FBAO** in einer Machbarkeitsstudie (Prof-of-Concept) für die diagnostische Anwendung an einem Patienten mit metastasierten kastrationsresistenten PCa (mCRPC) untersucht. Aufgrund der hohen Anreicherung von **EuE-k-^{18}F-FBAO** in Lymph- und Knochenmetastasen und der schnellen renalen Ausscheidung des Tracers, konnte bereits eine Stunde nach Injektion eine PET Bildgebung des PCa mit hohem Bildkontrast erzielt werden.

List of Abbreviations

aa	Amino acids
BPH	Benign prostate hyperplasia
Bq/mL	Bequerel per mL
CT	Computed tomography
DCE-MRI	Dynamic-contrast-enhanced MRI
DMF	Dimethyl formamide
DMSO	Dimethyl sulfoxide
DWI-MRI	Diffusion-weighted MRI
DRE	Digital rectal exams
EC	Electron capture
EDDA	Ethylenediamine diacetic acid
EuE	(2R,2'R)-2,2'-(carbonylbis(azanediyl))diglutaric acid
EuK	((S)-5-amino-1-carboxypentyl)carbamoyl)-L-glutamic acid
FDA	Food and Drug Administration
^{18}F-FBA	^{18}F-Fluorobenzaldehyde
^{18}F-FDG	^{18}F-Fluorodeoxyglucose
^{18}F-FPyl-TFP	6-^{18}F-fluoronicotinic acid 2,3,5,6-tetrafluorophenyl ester
FOLH I	Folate Hydrolase I
GCPII	Glutamate carboxypeptidase II
GRPR	Gastrin-releasing peptide receptor
GS	Gleason score
HF	Hydrogen fluoride
HOAt	1-hydroxy-7-azabenzotriazole
HYNIK	2-hydrazinonicotinamide
INC	Investigational new drug application
IC_{50}	Half maximal inhibitory concentration
IT	Isomeric transition
$K_{2.2.2}$	Kryptofix 2.2.2®
MAG_3	Mercaptoacetyltriglycine
MAS_3	Mercaptoacetylserine
mCRPC	Metastatic castration resistant prostate carcinoma
MeCN	Acetonitrile
MIP	Maximum intensity projection
MRI	Magnetic resonance imaging

n.c.a.	No carrier added
NAAG	N-acetyl aspartylgutamate
NAALADase	N-acetylated-γ-linked acidic dipeptidase
$Na_2BH_3CO_2$	Sodium boranocarbonate
N_3S-adipate	Mercaptoacetamidoadipoylglycylglycine
PADA	Picoylamine diacetic acid
PCa	Prostate cancer
PET	Positron emission tomography
PHI	Prostate health index
PMT	Photomultiplier tubes
PSA	Prostate-specific antigen
PSMA	Prostate-specific membrane antigen
p2PSA	Serum isoform [-2]proPSA
RCP	Radiochemical purity
RCY	Radiochemical yield
RGS	Radio-guided surgery
SA	Specific activity
SAAC	Single-amino-acid chelator
$SnCl_2$	Stannous choride
SPE	Solid phase extraction
SPECT	Single-photon emission computed tomography
SUV	Standardized uptake value
Tricine	N-(Tri(hydroxymethyl)methyl)glycine)
%ID/mL	Percent injected dose per mL

Table of Contents

I. Introduction

1. Prostate Cancer

Prostate cancer (PCa) is estimated to be the most common type of cancer in man and the fifth leading cause of cancer death worldwide [1]. Early diagnosis and staging of PCa are of upmost importance for an effective treatment of the disease.

At present, elevated prostate-specific antigen (PSA) levels and digital rectal exams (DRE) are established methods for the initial diagnosis of PCa with further confirmation by needle biopsy and histological analysis [2]. In spite of ongoing debate surrounding PSA screening, as a reliable indicator for PCa, early detection of the disease by measuring the amount of PSA in the blood has shown to substantially reduce PCa mortality [3-6]. However, the value of elevated PSA is controversial, since higher PSA levels also occur in non-cancerous prostate conditions, such as prostatitis and benign prostate hyperplasia (BPH) [7-9]. Therefore, PSA screening can lead to overdiagnosis and unnecessary treatments associated with side effects, such as urinary incontinence, bowl problems, and erectile dysfunction from radical prostectomy [10-12]. To complement PSA screening and to reduce the risk of overdiagnosis, new blood and urine biomarkers, like the prostate health index (PHI) and the noncoding mRNA sequence PCA3 have been investigated to improve primary diagnosis of PCa and to separate low-risk cancers from more aggressive forms [13-15].

After PCa diagnosis and histological confirmation by transrectal sonography-guided needle biopsy, PCa patients are classified in risk groups according their DRE results, their Gleason score (GS), which is determined by stained sections of biopsy specimens, and their PSA level, in low-, intermediate-, or high risk patients [16]. The curative treatment options for low to intermediate risk patients with localized disease include radical prostatectomy, radiation therapy, and brachytherapy.

The staging of metastasis (primarily located in lymph node and bones) in intermediate or high risk PCa patients is carried out by computed tomography (CT) or whole-body magnetic resonance imaging (MRI) of the lower abdomen, accompanied by ^{99m}Tc bone scintigraphy [16, 17]. Compared to local disease, the initial therapy for advanced PCa is the hormone treatment, consisting of androgen-deprivation, usually combined with radiotherapy to reduce or eliminate the tumor [16, 17]. However, tumor recurrence is very common following hormonal therapy and most patients develop metastatic castration resistant prostate carcinoma (mCRPC) with low survival rates [18-20].

2. Imaging Modalities for the Diagnosis of Prostate Cancer

Modern functional imaging techniques have the potential to make significant contributions to the initial diagnosis and staging of PCa, measurement of response to treatment and early detection of recurrent disease [21, 22]. Most state-of-the-art imaging techniques are non-invasive and provide dynamic real-time data.

For the local detection of PCa, MRI has emerged as the imaging technique of choice after inconclusive or negative biopsy findings [23]. Dynamic-contrast-enhanced MRI (DCE-MRI) and diffusion-weighted MRI (DWI-MRI) often enable a more precise examination of the prostate than MRI alone [24-29]. For evaluation of spread to lymph nodes and visceral organs both CT and MRI are used. These techniques provide only anatomorphological information. Thus, metastatic lymph nodes are detected on the basis of increased size. However, in prostate cancer almost 80% of metastatic lymph nodes are too small for the detection using anatomorphological imaging [30, 31].

To overcome the limitations of CT and MRI and to reliably identify lymphatic spread, the combination of anatomorphological with radionuclide-based imaging techniques, such as positron emission tomography (PET) or single-photon emission computed tomography (SPECT) has been extensively investigated in the context of functional imaging of PCa [32, 33].

2.1 Molecular Imaging - the Principle of PET and SPECT Imaging

PET and SPECT imaging techniques are associated with radiolabeled tracers, which allow the *in vivo* visualization of tumor-specific metabolic processes or target-structures on a molecular level to provide functional information of biochemical processes [34]. For this purpose, a radiolabeled probe that exhibits high (low nM) affinity towards a biological target structure (receptors, enzymes, and transporters) overexpressed by the cells in a tissue of interest, can be exploited to visualize the density of the expressed targets after injection of such a probe by means of PET or SPECT (Figure 1) [35-43]. To provide both functional and anatomorphological information by scanning in one single device, hybrid scanners, such as PET/CT, SPECT/CT, and PET/MRI are used [44-51].

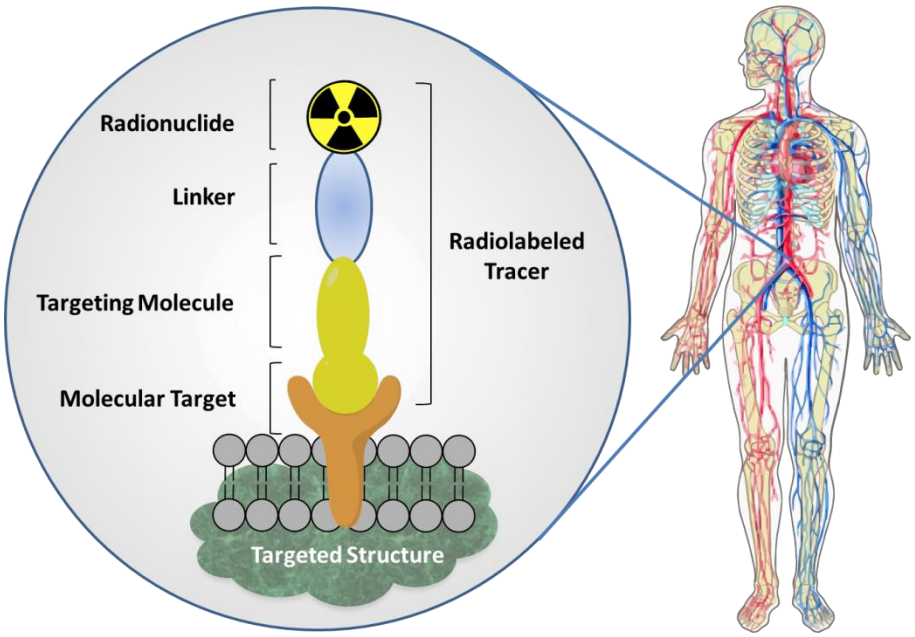

Figure 1: Schematic representation of the molecular imaging concept using radiolabeled molecules, which bind to specific molecular targets overexpressed on target structures.

SPECT and PET imaging is based on the detection of photons, which are emitted during the radioactive decay of radionuclides that have been used to radiolabel suitable radiopharmaceuticals (tracers).

In PET imaging, photon pairs, which are emitted in opposite direction after positron-electron annihilation are visualized (Figure 2). The decay of a neutron-deficient isotope is characterized by positron release from the atomic nucleus by β^+-decay, which loses its kinetic energy by interaction with atoms in the surrounding tissue (ionization, electronic excitation, *bremsstrahlung*). At this stage, it encounters its antiparticle (an electron) from the surrounding matters to form a positronium, which mutually annihilates whereby their masses are converted into two almost 511 keV γ-rays. The photons are emitted in approximate opposite direction (~180°) [52, 53]. When leaving the investigated body, these two γ-rays can be detected by two detectors or a circular array of multiple detector pairs (of scintillation crystals) placed around the patient. The output is only generated when the incident photon pairs from positron annihilation are detected in coincidence by opposite detector pairs and when detection occurs simultaneously, typically within a time window of 6-12 ns [54]. This coincidence event represents a line in space and allows the localization of the annihilation occurrence. Subsequently, due to the acquisition of a large number of coincidence events along all lines and many angles, a-three dimensional image is reconstructed from the two-dimensional projections via mathematical algorithms [55, 56].

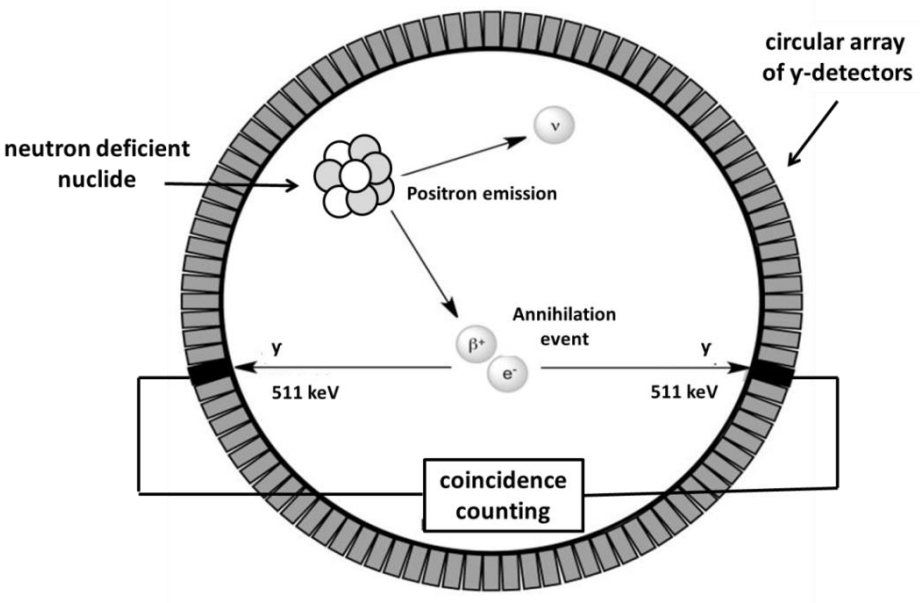

Figure 2: Schematic representation of a radioisotope decay by β^+-emission. The emitted positron combines with an electron to a positronium that annihilates into two 511 keV photons, which are detected by two opposite detector units, electronically connected via a coincident circuit – modified image from [57].

For quantification of the radiotracer uptake and tissue distribution, the projections are additionally corrected for random coincidences, scatter, attenuation, and dead time [53, 55, 58]. The reconstructed PET data in a region of interest are expressed as Bq per mL (Bq/mL) or in standardized uptake values (SUV) [59]:

$$\mathrm{SUV} = \frac{\text{activity concentration in image } \left[\frac{\mathrm{kBq}}{\mathrm{mL}}\right] \text{ x body weight [kg]}}{\text{injected activity [kBq]}}$$

The ultimate spatial PET resolution of approximately 4-6 mm for clinical and 1-2 mm for preclinical PET scanners is determined by the emission energy of the positron and thus the positron range, the density of the surrounding tissue and by non-colinearity of annihilation photon pairs when the positronium has a residual kinetic energy at the moment of annihilation [54, 60-67]. In order to measure changes of the targeted (patho)biological processes over time, dynamic PET scans are performed. Thereafter, PET acquisition data are summed up in different time frames (e.g. 30 s to 10 min), reconstructed separately and thus allow to visualize the distribution kinetics continuously over the entire acquisition period or in dedicated time intervals as 3D dataset [55, 68].

In contrast, SPECT measures single photons emitted by γ-emitting isotopes (Table 2), which are detected and recorded by a set of rotating γ-cameras (scintillation detectors, Anger cameras). To acquire a series of two-dimensional projection images, acquisition is performed at multiple angles by rotation of two or three camera heads around the longitudinal axis of the patient (Figure 3). The detectors contain NaI(Tl)-crystals, which convert γ-energy by means of photo effect, compton scattering and, when the energy of the photon is >1022 keV, pair production, to a certain amount of light. The resulting light (3-4 eV scintillation photons) is absorbed by photocathodes, resulting in the formation of photoelectrons that are amplified. For the latter processes photomultiplier tubes (PMTs) are coupled optically to the back face of the crystal, and are finally converted into an electrical signal (mA) [69-71]. NaI(Tl)-crystals show optimum performance for γ-rays in the range of 120-300 keV, therefore NaI(Tl)-crystal containing detectors are ideal for the detection of 141 keV γ-rays emitted by the most widely used imaging isotope ^{99m}Tc [70, 72]. To define the direction of the detected γ-rays, the γ-camera is equipped with a collimator that absorbs most of the non-orthogonal gamma radiation that would otherwise be also detected (Figure 3) [69].

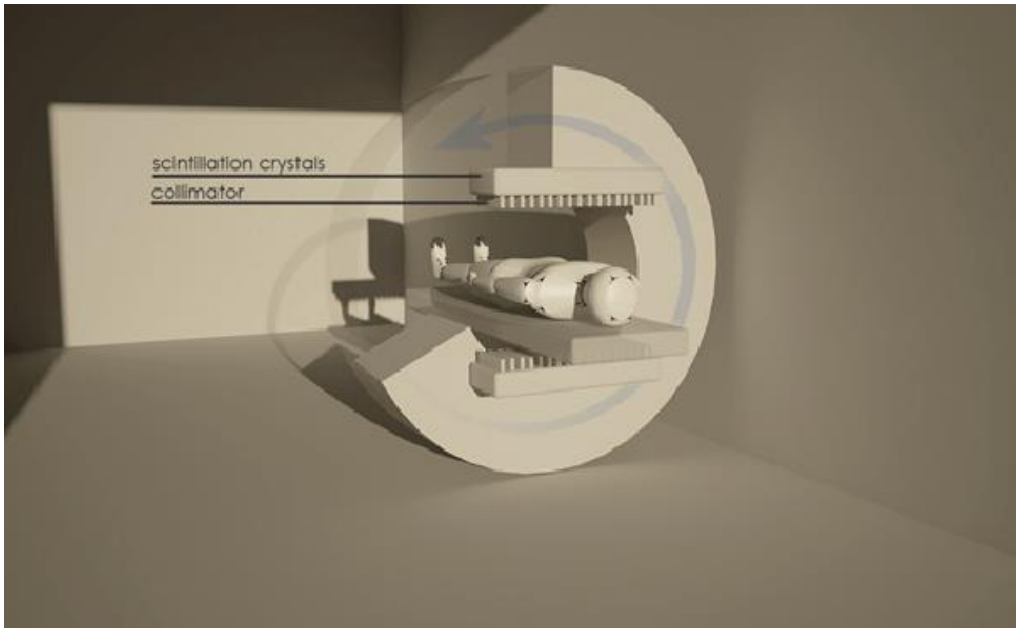

Figure 3: SPECT measures γ-rays emitted by radioisotope decay, which were detected by a γ-camera consisting of a collimator, scintillation crystal, light guide, array of PMTs and related electronics for image acquisition – modified image from © 2014 Haralampieva DG, *et al*. Published in [73] under CC BY 3.0 license. Available from: http://dx.doi.org/10.5772/59356.

The resolution of SPECT (8-10 mm for clinical and down to 0.4 mm for preclinical scanners) is determined by the thickness of the collimator walls (septa), the number of collimator holes, and the distance of the detector from the γ-source [67, 70, 74, 75]. After conversion to a

digital signal and image reconstruction by several algorithms a three-dimensional image of the radiotracer distribution in the patient is created [76, 77].

In general, both modalities have become extremely important in the clinics. However, PET imaging possesses significant advantages, like higher spatial resolution and higher sensitivity. Moreover, PET allows for quantitative imaging and thus allows to quantify the absolute radioactivity uptake in a tissue of interest due to the development and validation of options to correct photon scatter, photon attenuation, and partial volume artefacts, owing to the technical advantages offered by positron decay and coincidence detection [78, 79]. Nevertheless, due to the lower prize and the broad availability of suitable ^{99m}Tc-radiopharmaceuticals, the overall number of worldwide installed devices is still approximately 10-times higher than the number of PET scanners, i.e. in countries with less developed nuclear medicine infrastructure [80]. A selection of important SPECT and PET radionuclides with their physical characteristics, production and common labeling modes is given in Table 1 and 2.

Table 1: Selected SPECT-isotopes used for radiolabeling of biomolecules: physical characteristics, production mode and common labeling methods. Data presented in the table were obtained from [53, 81-83] and http://www.nndc.bnl.gov/nudat2/chartNuc.jsp. IT – Isomeric transition; EC – Electron capture.

Nuclide	half-life	Decay mode (%)	γ-Energy [keV]	Production mode	Labeling methods
^{99m}Tc	6.0 h	IT (> 99)	141	Generator ^{99}Mo/^{99m}Tc	Direct labeling or bifunctional chelators
^{123}I	13.2 h	EC (100)	159 529	Cyclotron ^{124}Xe(p,2n)^{123}Cs→ ^{123}Xe→^{123}I ^{124}Xe(p,pn)^{123}I ^{123}Te(p,n)^{123}I	Direct labeling or prosthetic group
^{67}Ga	3.3 d	EC (100)	93 185 300	Cyclotron ^{nat}Zn(p,x)^{67}Ga ^{68}Zn(p,2n)^{67}Ga	Bifunctional chelators
^{111}In	2.8 d	EC (100)	171 245	Cyclotron ^{111}Cd(p,n)^{111m,g}In ^{112}Cd(p,2n) ^{111m,g}In	Bifunctional chelators

Table 2: Selected PET-isotopes used for radiolabeling of biomolecules: physical characteristics, production mode and common labeling methods. Data presented in the table were obtained from [53, 81-84] and http://www.nndc.bnl.gov/nudat2/chartNuc.jsp. E – Energy; EC – Electron capture.

Nuclide	half-life	Decay mode (%)	Maximum β+- Energy (abundance) [MeV]	Production mode	Labeling methods
^{18}F	109.7 min	EC + β^+(100) β^+(97)	0.6	Cyclotron ^{18}O(p,n)^{18}F ^{20}Ne(d,α)^{18}F	Direct labeling, prosthetic groups
^{68}Ga	67.8 min	EC + β^+(100) β^+(89)	1.9	Generator ^{68}Ge/^{68}Ga	Bifunctional chelator
^{64}Cu	12.7 h	EC + β^+(62) β^+(18) β^-(39)	0.7	Cyclotron ^{64}Ni(p,n)^{64}Cu ^{66}Zn(d,α)^{64}Cu	Bifunctional chelator
^{89}Zr	78.4 h	EC + β^+(100) β^+(23)	0.9	Cyclotron ^{89}Y(p,n)^{89}Zr	Bifunctional chelator
^{124}I	4.2 d	EC + β^+(100) β^+(23)	2.1	Cyclotron ^{124}Te(p,n)^{124}I ^{125}Te(p,2n)^{124}I	Direct labeling, prosthetic groups
^{11}C	20.4 min	EC + β^+(100) β^+(99.8)	1.0	Cyclotron ^{10}B(d,n)^{11}C ^{11}B(p,n)^{11}C ^{14}N(p,α)^{11}C	Prosthetic groups
^{15}O	2.0 min	EC + β^+(100) β^+(99,9)	1.7	Cyclotron ^{14}N(d,n)^{15}O ^{15}N(p,n)^{15}O ^{16}O(p,pn)^{15}O	Direct labeling, prosthetic groups
^{44}Sc	4.0 h	EC + β^+(100) β^+(94)	1.5	Generator ^{44}Ti/^{44}Sc	Bifunctional chelator

3. PSMA as a Target for Molecular Imaging of Prostate Cancer

For the imaging of PCa several metabolic tracers, like ^{18}F-FDG and radiolabeled cholines have been evaluated. These tracers showed limited sensitivity for initial staging, lymph node detection, as well as for restaging of biochemical recurrence in patients, especially at low PSA level and PSA-doubling rate [85-92]. Therefore, extensive research has been undertaken to develop PCa targeted agents, that bind with high affinity and selectivity to PCa cells, to fulfill the urgent need for the non-invasive detection of molecular and cellular processes, that are overexpressed in PCa and that reflect the overall kinetics of the disease [93-96]. Among these approaches, the prostate-specific membrane antigen (PSMA) is the most promising target for PCa diagnosis and therapy [95, 97-99].

3.1 Enzymatic Activity and Expression Pattern of PSMA

The human prostate-specific membrane antigen (PSMA), also termed glutamate carboxypeptidase II (GCPII), Folate Hydrolase 1 (FOLH 1) or N-Acetylated-Alpha-Linked Acidic Dipeptidase I (NAALADase I) is an enzyme from the family of zinc-metallopeptidases [100-106].

PSMA is expressed in the normal prostate epithelium, the kidneys, the proximal tubuli of the kidneys, the salivary glands, the nervous system glia, and the small bowel [107-110].

The molecular functions of PSMA within the nervous system glia and the small bowel are still not fully elucidated. In the nervous system PSMA acts as “NAALADase” and hydrolyses the abundant neurotransmitter N-acetyl-L-aspartyl-L-glutamate (NAAG) in N-acetyl-L-aspartate and L-glutamate (Figure 4) [111-114].

In contrast, PSMA in the small intestine acts as “folate hydrolase”. PSMA is responsible to hydrolyze the C-terminal glutamates of dietary folates, existing in the form of folyl-poly-γ-L-glutamates (Figure 4) [104, 115-117]. The resulting folate is actively transported across the intestinal wall into the blood stream [118]. The enzymatic role of PSMA and the in the prostate and the renal proximal tubules is still unclear, but it may be related to folate metabolism in these tissues [103, 119].

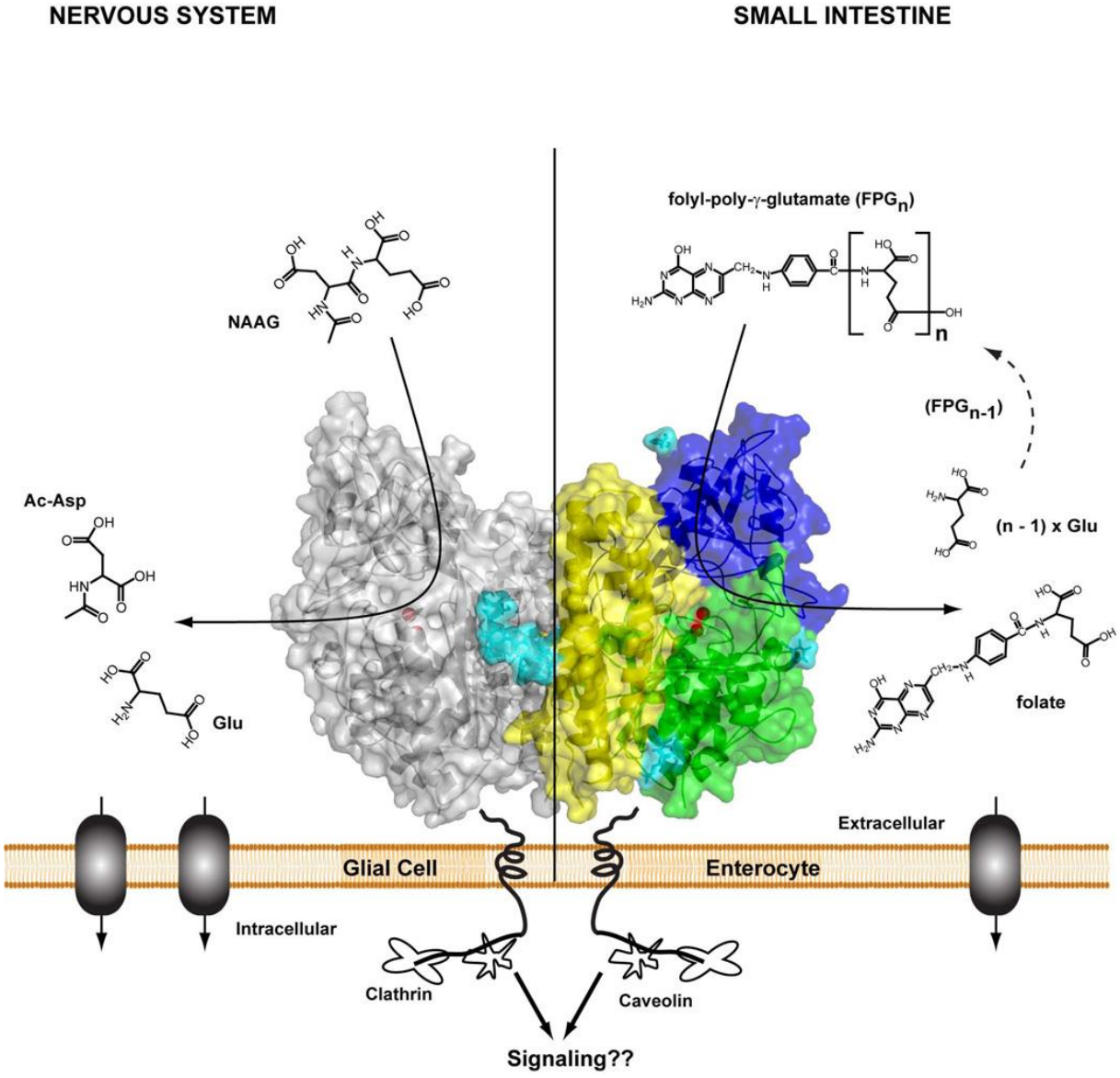

Figure 4: Crystal structure of the homodimer of human GCPII (PSMA). One monomer is shown in semitransparent surface representation. The individual domains of the extracellular part include the protease domain (green), the apical domain (blue) and the C-terminal domain (yellow). The second monomer is colored gray. N-linked sugar moieties are colored cyan, and the active-site Zn^{2+} ions are shown as red spheres. **Left panel**: GCPII catabolizes NAAG (peptidic neurotransmitter) in the mammalian nervous system. **Right panel**: GCPII hydrolyzes the C-terminal γ-glutamate tail of dietary folates at the plasma membrane of enterocytes – Figure was originally published in [120].

In contrast to the comparatively low expression levels of PSMA in nervous system glia and the small bowel, PSMA is up to 100 to 1000-fold overexpressed in PCa [121]. Expression levels of PSMA seem to be depended on malignancy, as PSMA upregulation increases from benign prostatic hyperplasmia to high-grade prostatic intraepithelial neoplasia to prostatic adenocarcinoma [122, 123]. It was found that PSMA expression correlates with increased aggressiveness of PCa and may have a functional role in the progression of higher-grade,

metastatic and castration-resistant PCa [98, 121, 124-126]. While the enzymatic function of PSMA in normal and diseased prostate is still unclear [127-129], the folate level seems to play an important role in tumor growth [130].

Due to its high and consistent expression in PCa and the high accessibility as a surface membrane protein, PSMA represents an ideal target for molecular imaging and targeted therapy using highly specific radiolabeled PSMA ligands, i.e. inhibitors.

3.2 PSMA Structure and Urea-based PSMA Inhibitor Design

The homodimeric transmembrane protein PSMA consists of 750 amino acids (aa) [131, 132] and is divided in three structural domains, including the intracellular N-terminal domain (19 aa), a hydrophobic transmembrane domain (24 aa) and the extracellular domain (707 aa) [101, 133]. The extracellular catalytic site of PSMA contains three structurally distinct domains: the protease domain, the apical domain, and the C-terminal domain (Figure 4). Each domain contributes residues implicated in substrate binding [101, 134, 135].

The PSMA internal ligand-binding cavity can be divided into three continuous parts: the dinuclear zinc active center, the S1´pharmacophore pocket, and an irregular shaped entrance funnel, connecting the active site to the external surface of PSMA (Figure 6) [136-138].

The main strategy for the development of PSMA inhibitors was the linkage of a glutamate moiety to a zinc-binding functionality, containing a linker/effector part. Furthermore, these three semi-independent parts can be tailored to suit experimental or clinical needs [137, 139]. By this time, small molecule PSMA inhibitors can be divided into three groups, distinguishable by their functionalities with affinity for zinc: 1) phosphonates, phosphoramidates [134, 140], 2) thiols [141, 142] and 3) urea-based glutamate heterodimers, which especially exhibit high substrate specificity to PSMA (Figure 5) [143-145].

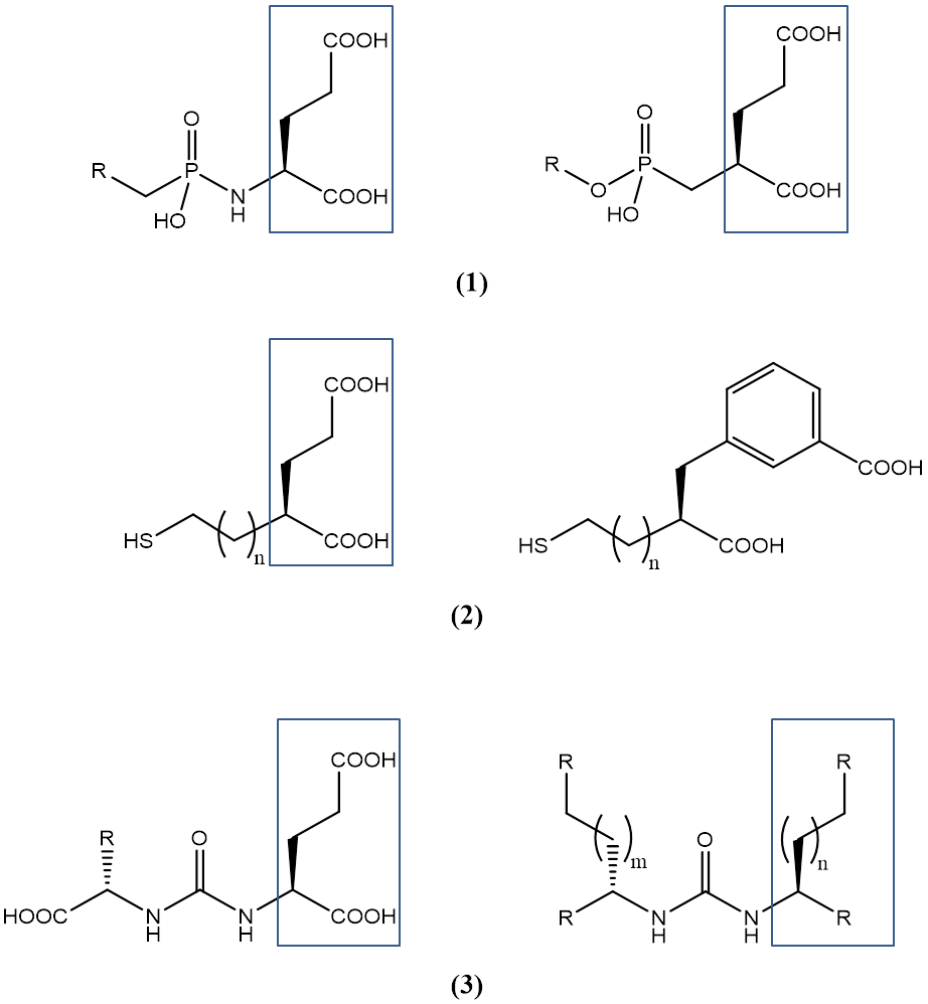

Figure 5: Classification of small molecule PSMA inhibitors: (**1**) phosphoramidates, phoshonates, (**2**) thiols and (**3**) urea-based glutamate heterodimers.

The active center of PSMA contains two zinc ions with an activated water molecule, which interact with the carbonyl oxygen of the ureido motif of the inhibitors. The active site is essential for hydrolytic function of PSMA, while urea-based inhibitors show resistance to hydrolysis of the enzyme and act as an amide-bioisostere (Figure 6) [143, 146, 147].

The S1' pharmacophore pocket (glutamate pocket) specifically binds L-glutamate or glutamate-like moieties at the C-terminal part of the inhibitor. SAR studies revealed low tolerance for substitutions at this position of the PSMA ligand (Figure 6) [145, 148-152].

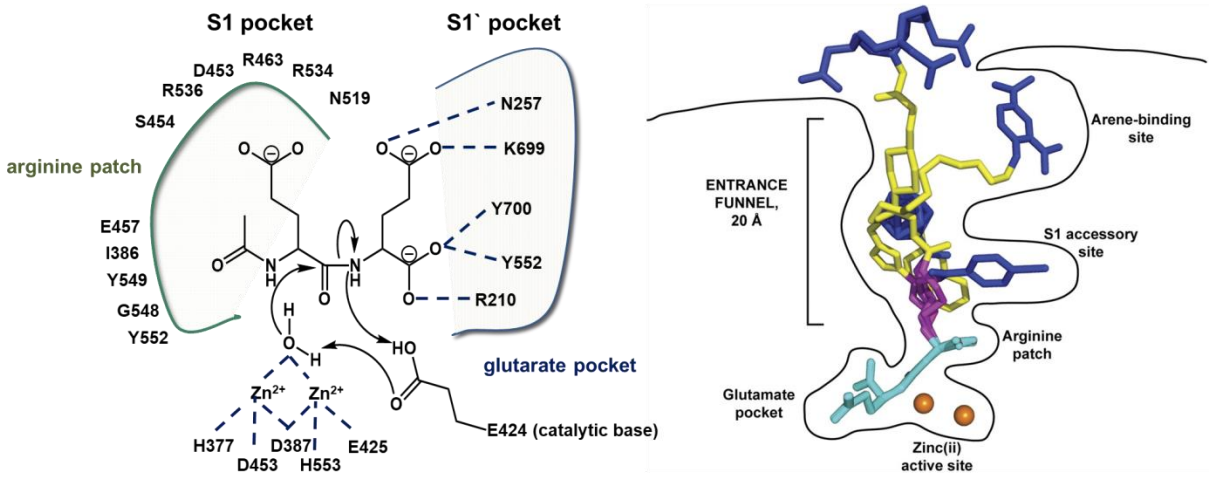

Figure 6: **Left:** Scheme of the catalytic site of PSMA, indicating the NAAG hydrolysis in the active center. **Right:** Presentation of an overlap of four Glu-urea–based ligands within the binding cavity of PSMA. All ligands show a structural overlap of pharmacophore modules (cyan), connected to a flexible proximal linker (magenta), and a functional spacer (yellow) of different lengths to address the respective pockets in the entrance funnel of PSMA with an effector moiety (blue). Zinc ions are shown as orange spheres. Figure was originally published in JNM [153]. © SNMMI Kopka K *et al*. Available from: http://jnm.snmjournals.org/content/58/Supplement_2/17S.

Compared to the S1´ site, the entrance funnel contains structural defined pockets e.g. the arginine patch, the S1 accessory pocket and the arene-binding site (Figure 6, 7). It has been shown, that modifications within the spacer/effector portion of Glu-urea-based inhibitors are well tolerated by PSMA because of the quite spacious entrance funnel, which can accommodate many diverse chemical groups and is therefore more flexible in terms of structural modifications of PSMA inhibitors [137, 143, 145, 149, 154-156].

A central feature of the S1 pocket is the “arginine patch”, which can transit between two distinct confirmations, and define therefore the size of the S1 accessory pocket (Figure 7) [134, 143, 157, 158]. The P1 carboxylate of the urea-based ligands contributes prominently to PSMA-inhibitor binding in the S1 pocket [143, 150]. Therefore, this structural feature should be preserved in urea-based inhibitors to retain high-affinity to PSMA [151].

In contrast, the P1 side chain is placed into a “hydrophobic part” of the S1 pocket with no significant interactions [143, 156]. However, depended on the lengths of the side chain and the appendage of a hydrophobic functionality at the P1 position, the hydrophobic pockets within the entrance funnel can be addressed and therefore, affinity towards PSMA may be increased [143, 156].

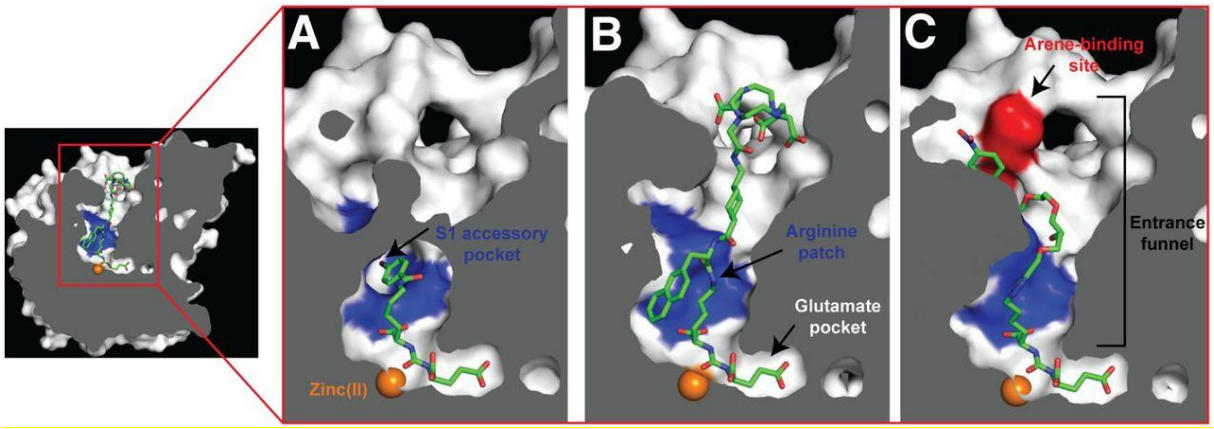

Figure 7: Presentation of the internal exemplary inhibitor-binding cavity of PSMA, consisting of a S1′ glutamate recognition pocket, zinc(II) active site, and irregularly shaped entrance funnel. The structural features of the entrance funnel are the arginine patch, S1 accessory hydrophobic pocket (blue), and arene-binding site (red), which can accommodate functional groups of different sizes and physicochemical characteristics. Figure was originally published in JNM 2017 [153]. © SNMMI Kopka K *et al.*; Available from: http://jnm.snmjournals.org/content/58/Supplement_2/17S.

3.3 PSMA – Internalization

PSMA is constitutively internalized like many surface membrane proteins. The internalization of PSMA is mediated by five N-terminal amino acids in the cytoplasmic tail, which are essential for internalization [159]. After interaction of the cytoplasmic tail with several scaffold proteins, like clathrin and filamin-A, endocytosis occurs predominantly in a clathrin-dependent manner [159-162].

It has been described that internalization of PSMA can be significantly enhanced by binding of PSMA-specific antibodies or small molecule inhibitors at an increased rate and extent [163, 164]. The ability of PSMA to undergo constitutive internalization and the rate and extent of radioligand internalization are important requirements for the *in vivo* tumor accumulation and retention of the tracer in targeted tissue, resulting in high-contrast *in vivo* imaging and therapeutic efficiency [165, 166]. However, it is still unclear which structural features of PSMA-inhibitors influence the internalization efficiency and whether there is a correlation between PSMA-affinity and internalization.

3.4 Radiolabeled Probes for the Diagnosis of Prostate Cancer

The dual nature of PSMA, acting as an receptor as well as an enzyme, has paved the way for the development of several approaches to target PSMA via radiolabeled molecules [139, 167-170]. Based on the macromolecular protein structure of PSMA, specific monoclonal antibodies have been developed, showing selective and specific binding to either the extracellular or intracellular domain of PSMA [169, 171-178]. However, the use of antibodies for PCa diagnosis showed major disadvantages, including the long circulatory half-life, poor tumor penetration and low tumor-to-background ratios. In contrast, small molecule inhibitors exhibit favorable pharmacokinetics, rapid diffusion in the extravascular space and faster blood clearance, resulting in higher tumor-to-background ratios [170]. Therefore, due to the enzymatic nature of PSMA the development of low molecular weight anti-PSMA inhibitors has been triggered in recent years [139, 167, 168]. Especially urea-based PSMA inhibitors for SPECT and PET imaging show promising results in clinical assessment for PCa diagnosis [170, 179, 180].

3.4.1 Clinical Assessment of Urea-based SPECT Tracers

Highly promising radioiodinated urea-based inhibitors are ^{123}I-MIP-1072 and ^{123}I-MIP-1095 (Figure 8). Due to the higher lipophilicity of ^{123}I-MIP-1095, ^{123}I-MIP-1072 exhibits significantly faster clearance from PSMA-negative tissues and is excreted over the kidneys/bladder [181]. However, ^{123}I-MIP-1095 showed 5-fold higher affinity towards PSMA and enhanced tumor-uptake in animal models, which might be explainable due to additional hydrophobic interactions of the tracer with sites outside of the PSMA binding pocket [182]. Initial clinical studies of both tracers revealed high-contrast imaging of both bone and lymph node metastasis and demonstrated the suitability of these agents for the diagnosis of PCa [181].

Due to the favorable nuclide characteristics, ^{99m}Tc remains the radionuclide of choice for SPECT imaging. Different ^{99m}Tc-labeled urea-based PSMA inhibitors have been developed and (pre)clinically evaluated [183-185]. Previous studies, investigating the influence of different chelators and linker lengths with respect to the overall performance of the derived ^{99m}Tc-labeled Glu-urea-Lys-based PSMA ligands, revealed that the charge, polarity, and hydrophilicity contribute to efficient PSMA-targeting and pharmacokinetics of the respective inhibitors [139, 186, 187].

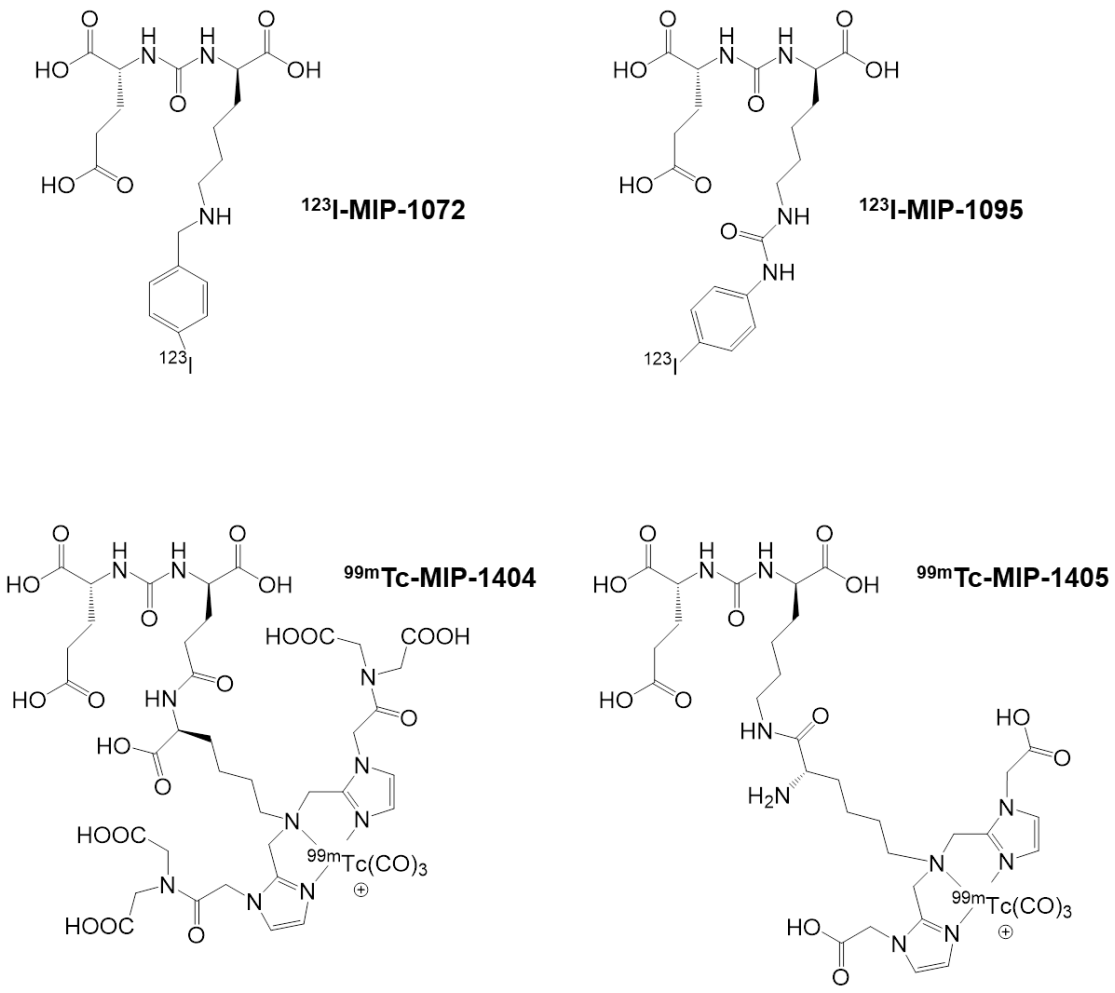

Figure 8: Chemical structures of radioiodinated and ^{99m}Tc-labeled PSMA inhibitors, which are currently under clinical investigation for SPECT imaging of PCa.

Molecular Insight Pharmaceuticals developed two promising inhibitors, termed ^{99m}Tc-MIP-1404 and ^{99m}Tc-MIP-1405, and implemented an exploratory investigational new drug application (IND) to transfer them to the clinic (Figure 8) [139]. The urea-based inhibitors MIP-1404 and MIP-1405 were conjugated to a single-amino-acid chelator (SAAC) and radiolabeled using ^{99m}Tc-based tricarbonyl chemistry [183, 188]. Both tracers revealed impressive results for diagnostic imaging of PCa in preclinical and clinical studies [183, 185]. These tracers cleared rapidly from the circulation and showed persistent uptake in PSMA-expressing tissues, the lacrimal, and parotid glands and in bone-/lymph node metastasis as early as 1 h p.i.. Furthermore, more bone metastases were visualized using these agents in comparison to conventional bone scans (Figure 9) [183, 185]. Due to the shift towards hepatobiliary excretion and therefore lower activity in the urinary bladder, ^{99m}Tc-MIP-1404 exhibited a clear advantage for the detection of PCa in the gland and pelvis at early stages of the disease compared to ^{99m}Tc-MIP-1405. ^{99m}Tc-MIP-1404 is currently under clinical investigation in a phase 2 trial (Figure 9) [185, 189].

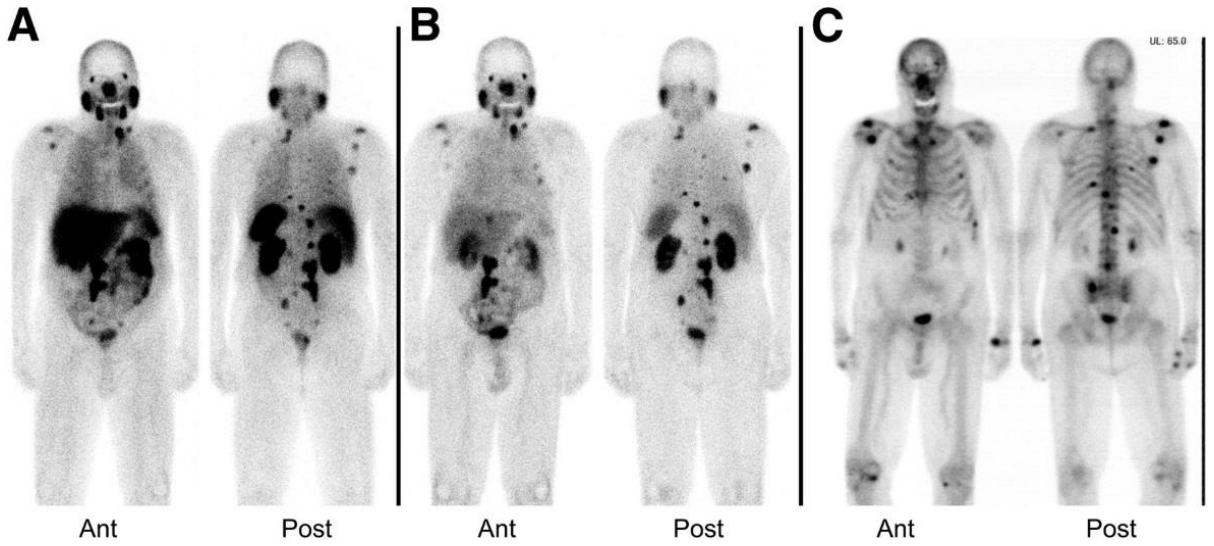

Figure 9: Comparative SPECT imaging of ^{99m}Tc-MIP-1404 (**A**) or ^{99m}Tc-MIP-1405 (**B**) in the same patient with metastatic PCa (4 h p.i.), in comparison to standard bone scan (**C**). Figure was originally published in JNM 2014 [185] © SNMMI, Vallabhajosula S, *et al*. Available from: http://jnm.snmjournals.org/content/55/11/1791.

3.4.2 Clinical Assessment of Urea-based PET Tracers

So far, the most extensively studied PET Tracer for PCa imaging is ^{68}Ga-HBED-CC-Ahx-KuE (^{68}Ga-PSMA-11) (Figure 10). Several clinical studies demonstrated the potential of ^{68}Ga-PSMA-11 for the detection of primary tumors, as well as for metastatic PCa lesions with high sensitivity and specificity (Figure 12) [190-202]. A retrospective study demonstrated the positively association of PSA level and androgen deprivation therapy with tumor uptake of ^{68}Ga-PSMA-11 and has been proven that ^{68}Ga-PSMA-11 PET/CT imaging is crucial for the restaging, planning and monitoring of therapy, as well as for the evaluation of recurrence [193, 203]. However, ^{68}Ga-PSMA-11 shows high background uptake in the liver, kidneys, and the salivary and lacrimal glands. Hence, several pitfalls have been reported, like pathological uptake of ^{68}Ga-PSMA-11 in coeliac ganglia [204], resulting in difficulties interpreting PET images.

In preclinical studies, a novel inhibitor ^{68}Ga-PSMA-617 showed superiority to ^{68}Ga-PSMA-11 concerning the *in vitro* and *in vivo* PSMA-targeting characteristics (Figure 10) [205]. An initial clinical assessment of the theranostic tracer, which could be either labeled with ^{177}Lu or ^{68}Ga, revealed high contrast imaging of PCa lesions. However, due to high plasma protein binding, only at late imaging time points (3-4 h p.i.) [206].

Another promising tracer for PET imaging of PCa is ^{68}Ga-PSMA-I&T (Figure 10, 11) [207]. The DOTAGA-conjugated ligand allows labeling with both ^{68}Ga and ^{177}Lu, and thus can be

used for diagnostic and therapeutic purposes. An initial study of ^{68}Ga-PSMA-I&T PET/CT PCa imaging revealed high uptake in primary lesions, as well as lymph node, bone, and liver metastases (Figure 12). Subsequently, biodistribution and radiation data were evaluated in five patients, showing promising dosimetry and high imaging contrast at 1 h p.i [208].

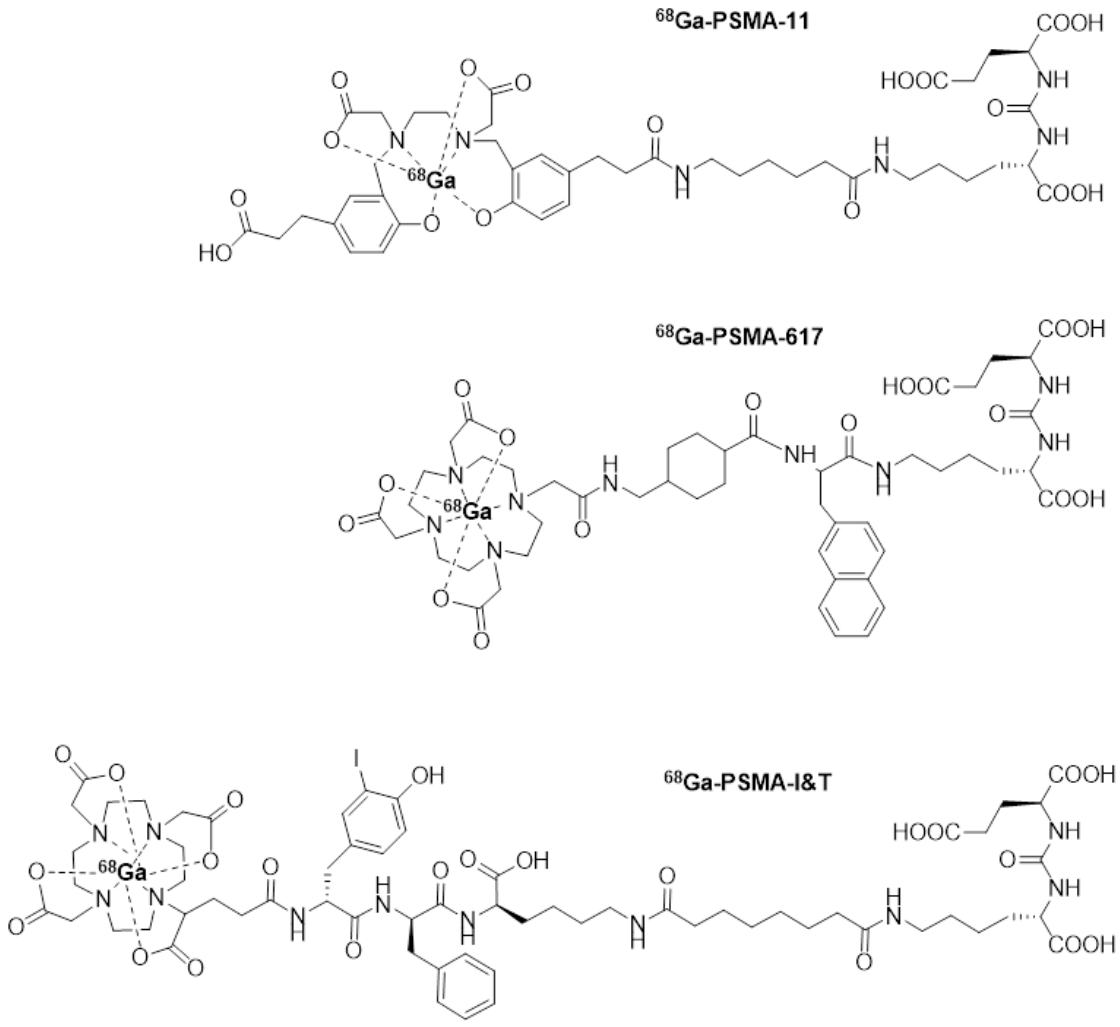

Figure 10: Chemical structures of ^{68}Ga-labeled PSMA inhibitors, which are currently under clinical investigation.

One of the first clinically investigated ^{18}F-labeled PSMA ligand was ^{18}F-DCFBC (Figure 11). ^{18}F-DCFBC PET/CT imaging demonstrated feasibility for the detection of high grade primary PCa and metastatic lesions [209] and may allow a more specific localization of high grade and clinically significant tumor lesions compared to MRI [210]. A major disadvantage of ^{18}F-DCFBC is the high plasma protein binding of the tracer, which results in slow clearance kinetics and high blood pool activity, which potentially interferes with the detection of lower avidity or smaller tumor lesions (Figure 12) [209, 211].

To overcome these limitations a second generation radiofluorinated PSMA inhibitor, termed ^{18}F-DCFPyl, was developed by the same group (Figure 11) [212]. Initial studies revealed five times higher PSMA affinities, enhanced tumor uptake with rapid plasma clearance, resulting in higher tumor-to-background ratios and lower accumulation in the liver compared to ^{18}F-DCFBC. However, a considerable kidney and salivary gland uptake of ^{18}F-DCFPyl was observed (Figure 12) [213]. An initial comparison of PSMA-based PCa imaging between ^{18}F-DCFPyl and ^{68}Ga-PSMA-11 PET/CT demonstrated promising results in detection of primary and metastatic PCa [211, 213], regarding higher sensitivity, higher tumor-to-background ratios and faster clearance of the ^{18}F-labeled compound [214]. Overall, this study suggests that ^{18}F-DCFPyl PET/CT imaging is superior to ^{68}Ga-PSMA-11 PET/CT for the diagnosis of PCa.

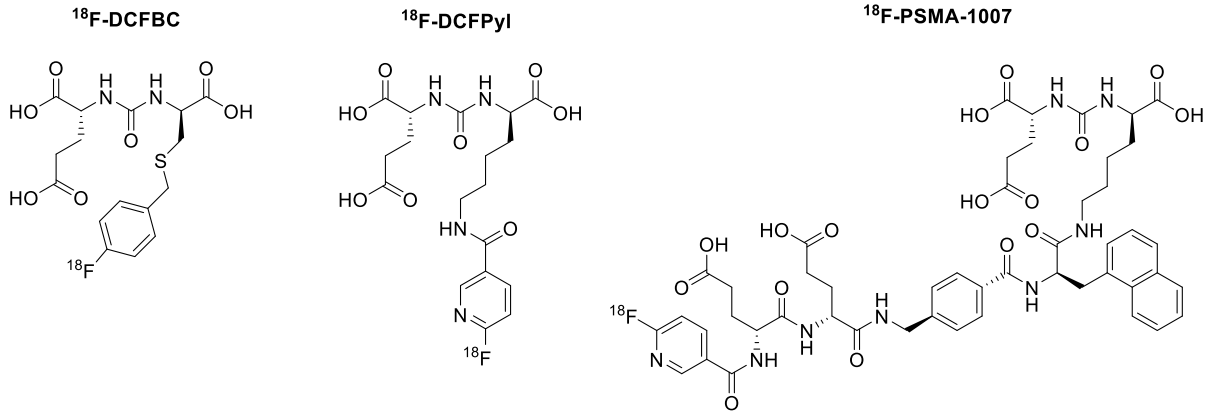

Figure 11: Chemical structures of ^{18}F-labeled PSMA inhibitors, which are currently under clinical investigation.

PSMA-1007, a novel ^{18}F-labeled tracer based on the scaffold of PSMA-617, was developed [206, 215]. A first-in-man study of a patient with mCRPC revealed similar tumor and organ uptake for ^{18}F-PSMA-1007 and ^{177}Lu-PSMA-617 [216]. Further studies in patients demonstrated a comparable radiation dosimetry of ^{18}F-PSMA-1007 to ^{18}F-DCFPyl and high-contrast imaging for both tracers with excellent sensitivity for the detection of small lymph node metastasis (Figure 12) [217, 218]. The predominant hepatobiliary excretion with reduced urinary uptake of ^{18}F-PSMA-1007 might facilitate some advantages for local recurrence or pelvic lymph-node detection, whereas the fast renal excretion of ^{18}F-DCFPyl with lower hepatic background might favor the detection of liver metastases in late stages of PCa [217, 218]. Overall, a major disadvantage is the slow delivery of ^{18}F-PSMA-1007 combined with slow clearance kinetics, resulting in favorable tumor-to-background ratios and an increased tumor uptake up to 50% at late imaging time points (3h p.i.) [217].

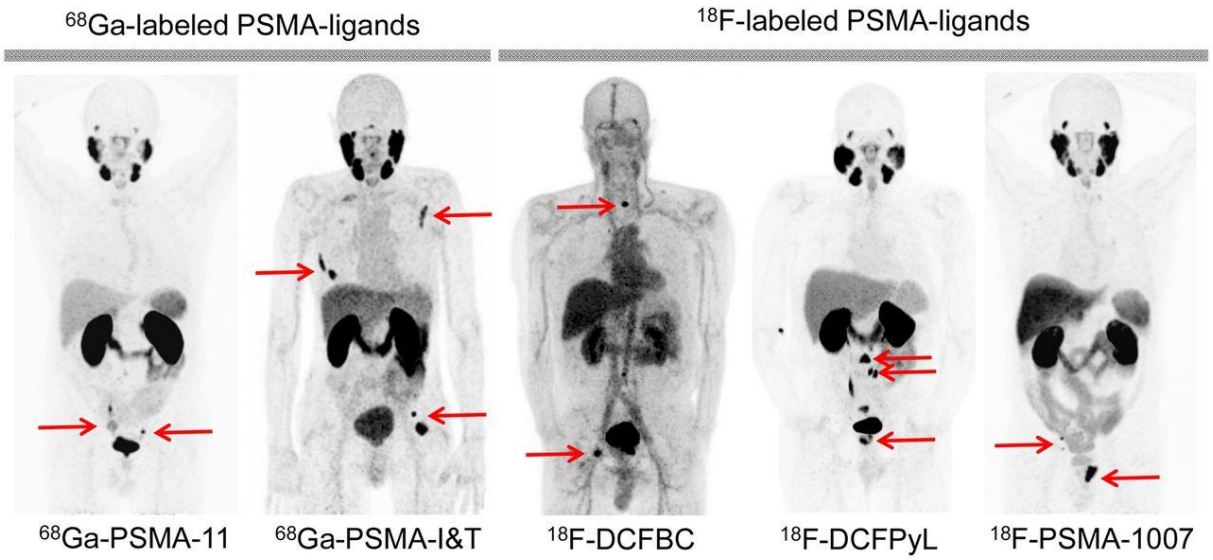

Figure 12: MIP images of ^{68}Ga- and ^{18}F-labeled PSMA inhibitors most commonly used for PET imaging. Images were acquired at different centres. The specific tumor uptake in different numbers of lesions uptake is indicated by red arrows and depended on extent of disease in respective patients. Figure was originally published in JNM 2014 [219] © SNMMI, Eiber M, *et al*. Available from: http://jnm.snmjournals.org/content/58/Supplement_2/67S.

3.5 The Concept of Radio-guided Surgery

Besides endoradiotherapy, other therapeutic strategies such as PSMA-targeted radio-guided surgery (RGS) have been developed [220]. To supplement the theranostic approach, PSMA-I&T (Figure 10) was labeled with ^{111}In and successfully used as a gamma probe for the specific intraoperative detection of small metastatic lymph nodes and atypically located lesions [220, 221]. This therapeutic strategy offers the localization of small metastatic lymph nodes and micro metastases during surgery, which can potentially cause recurrence of the disease. After preoperative ^{68}Ga-PSMA-11 PET/CT, ^{111}In-PSMA-I&T was injected 24 h before surgery. All visible lesions on PET/CT were detected with intraoperative guidance, using a gamma probe with live acoustic feedback of the count rate. All resected specimen were further confirmed by *ex vivo* histopathology to bear PSMA-expressing metastatic disease (Figure 13). It has been shown that ^{111}In-PSMA-I&T RGS enables the detection of even subcentimeter lesions, as well as tumor deposits, that could not be visualized on preoperative ^{68}Ga-PSMA-11 PET scans, which clearly demonstrates the sensitivity of this method [219, 220]. A follow-up study, summarizing the data of 30 patients (after salvage PSMA RGS), was highly promising and indicated the beneficial influence of ^{111}In-PSMA I&T RGS on further disease progression [219, 222].

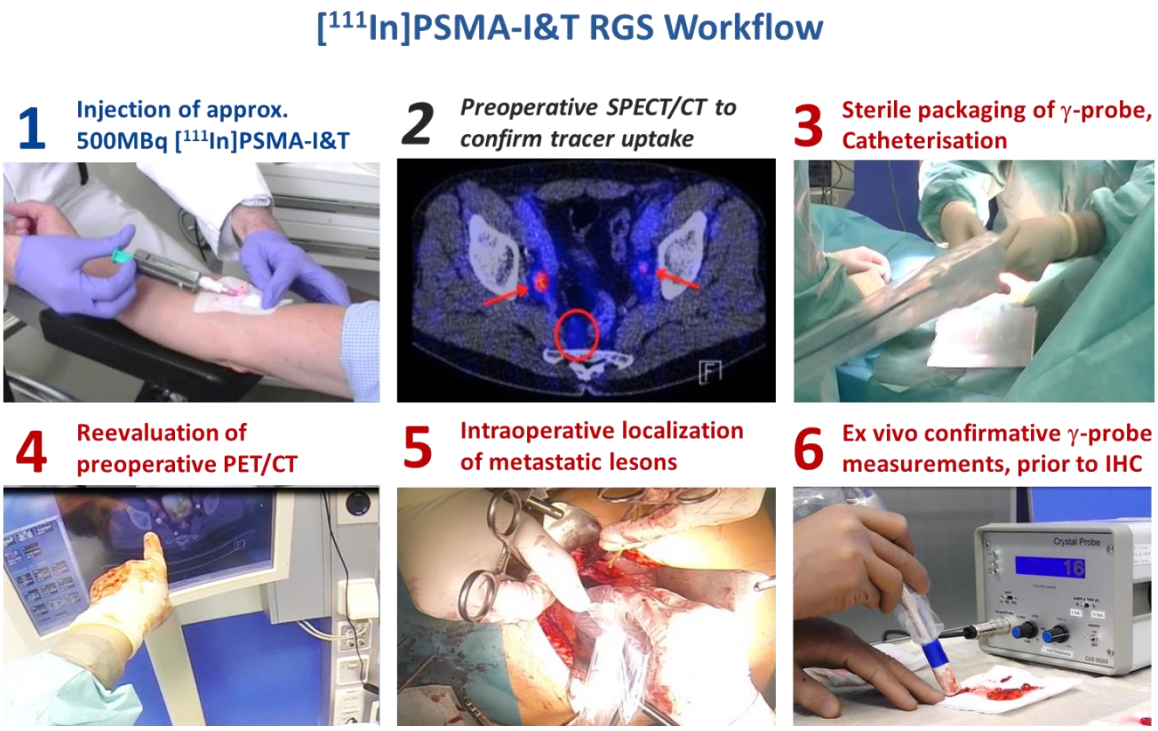

Figure 13: Representation of the clinical workflow of ^{111}In-PSMA-I&T RGS.

II. Introduction to Selected Methods

In this chapter, selected methods described in the publications, such as nuclide production and labeling methods are pinpointed.

1. ^{18}F-Radiochemistry

1.1 ^{18}F-Production and Properties

Due to the unique physical and nuclear properties, ^{18}F is the most important radioisotope in PET imaging. The half-life of 109.7 min enables multi-step syntheses of radiopharmaceuticals and permits longer imaging protocols to investigate processes of slower tracer kinetics [223]. The low maximum positron energy of 0.63 MeV (E_{mean} = 0.25 MeV) results in a short maximum positron range in tissue (2.2 mm), which gives the highest spatial resolution in comparison to other positron emitters [84, 224]. ^{18}F predominantly decays by positron emission (97%) and did not accompany gamma rays, resulting in lower radiation dose of the patient and making the reconstruction of PET images easier [84].

The most commonly used production of nucleophilic n.c.a. ^{18}F-F_{aq}^- is the bombardment of ^{18}O-enriched water (> 98%) with high energy protons (typically ~15 MeV) [225, 226]. The production can be performed either in a cyclotron or a linear particle accelerator. The target for the ^{18}O(p,n)^{18}F reaction consists of resistant silver or niobium material, which is chemically stable under extreme conditions during the irradiation process [227, 228]. The yield of ^{18}F production is dependent on the target volume, the proton energy, the bombardment time, and the beam current. 120 min of bombardment with a beam current of about 60 µA usually yield about 120 GBq of ^{18}F with high specific activity (SA) (6.3 x 10^{19} Bq/mol) [53]. The produced ^{18}F-HF in the target water can easily be trapped on a anion exchange cartridge and can be separated from the target water and traces of ^{13}N [223]. Due to high production yields, multiple doses of ^{18}F-labeled tracers can be produced in one synthesis, enabling centralized production and commercial distribution in greater areas.

1.2 ^{18}F-Radiolabeling

The most common method to prepare radiofluorinated compounds is the aliphatic and aromatic nucleophilic substitution of halides and sulfonates (e.g. tosylates, triflates, nosylates and mesylates) by n.c.a $^{18}F^-$ [57]. The nucleophilicity and solubility of $^{18}F^-$ in aqueous solution is increased by the use of phase-transfer catalysts (e.g Kryptofix 2.2.2® ($K_{2.2.2}$) or quaternary ammonium derivatives), forming bulky counter cation $^{18}F^-$ anion complexes. To remove water, the chemically inert hydrated $^{18}F^-$ anions have to be dried azeotropically under reduced pressure with acetonitrile (MeCN). For radiolabeling reaction polar aprotic solvents like DMF, MeCN and DMSO were used to improve the ionic dissociation of $^{18}F^-$ with the bulky counter cation [229-232]. Direct ^{18}F-labeling of organic molecules work only well without acidic protons (or NH_2, OH, SH - groups) within the precursor. In this case the introduction of $^{18}F^-$ by nucleophilic substitution is only possible by using protecting group strategy, resulting in time-consuming more-step reactions [233]. Finally, purification and formulation steps are necessary.

More complex molecules, like peptides, contain several reactive nucleophilic moieties or acidic protons, which makes direct ^{18}F-labeling by nucleophilic substitution nearly impossible. The labeling of peptides via small ^{18}F-labeled prosthetic groups overcome these limitations [234-239]. For this purpose several ^{18}F-fluoroalkylation/-acylation agents have been developed [234, 235, 238, 240-244]. These ^{18}F-labeled prosthetic groups have to be synthesized in advance and afterwards, reaction with $–NH_2$, -OH or other nucleophilic group of the targeted biomolecule is carried out. To separate the labeled prosthetic groups from the precursor, purification is indispensable before conjugation to the biomolecule. To avoid multiple reaction sites in the biomolecule, other reactive groups (where radiolabeling is undesired) have to be chemically protected.

To circumvent the complicated syntheses of fully protected labeling precursors and to avoid additional time-consuming deprotection steps after ^{18}F-labeling with prosthetic groups, more site-specific labeling strategies have been developed [245-247]. A promising approach is the chemo-selective ligation of ^{18}F-labeled aldehydes, such as 4-^{18}F-fluorobenzaldehyde (^{18}F-FBA), which selectively forms an oxime bond with aminooxy-derivated peptides under mild and aqueous reaction conditions [245, 248, 249]. This ^{18}F-labeling synthon reacts site-specifically and in high RCYs in the presence of a whole spectrum of functional groups within the peptide precursor [246, 247]. The use of aniline as a nucleophilic catalyst, significantly accelerate oxime ligation [249, 250].

Another promising approach for selective peptide radiolabeling is the use of preactivated ,6-^{18}F-fluoronicotinic acid 2,3,5,6-tetrafluorophenyl ester (^{18}F-FPyl-TFP) as prosthetic group [212, 245, 251, 252]. After one-step radiosynthesis of ^{18}F-FPyl-TFP and subsequent SPE cartridge purification, peptide conjugation can be carried out under mild basic conditions in good conjugation yields without addition of coupling reagents [213, 251].

Recently, a new approach for efficient, time-saving and reliable ^{18}F-labeling of aliphatic and aromatic prosthetic groups via nucleophilic substitution, such as ^{18}F-FPyl-TFP and ^{18}F-FBA, was described [253, 254]. Thereby, $^{18}F^-$ is directly eluted with a quaternary trimethylammonium precursor salt, dissolved in an alcoholic solution. After evaporation and addition of a dipolar aprotic solvent, the ^{18}F-labeling is carried out under heating. Via SPE cartridge purification the ^{18}F-labeled compound can be easily separated from the precursor salt. High chemical yields up to 80-90% can be achieved in short synthesis time (app. 5-10 min). This highly promising “minimalist” approach needs neither azeotropic drying steps, nor base or any other additives, like cryptands or crown ethers, which may facilitate automatization of ^{18}F-radiolabeling for clinical routine.

2. ^{99m}Tc-Radiochemistry

2.1 ^{99m}Tc-Production and Properties

More than 80% of all nuclear medicine investigations apply radiopharmaceuticals labeled with ^{99m}Tc. Among other radionuclides for SPECT imaging, ^{99m}Tc holds a prominent position due to its optimal gamma energy, its availability from ^{99}Mo/^{99m}Tc generators, the relatively low costs, and the reliable labeling procedures based on kit preparations. Other advantages are: ^{99m}Tc emits only photons, rather than positrons or negative ß-particles, and the primarily short half-life results in low radiation burden of the patients [255-257].

The elution of ^{99m}Tc-pertechnetate ($^{99m}TcO_4^-$) from the ^{99}Mo/^{99m}Tc generator (molybdate (MoO_4^{2-}) is absorbed on an Al_2O_3 matrix) is carried out using isotonic saline. The parent radionuclide ^{99}Mo spontaneously decays through several ß-particle transitions to metastable ^{99m}Tc (87 %) and to long-lived ^{99}Tc ($t_{1/2}$ = 212000 years). Subsequently, the metastable ^{99m}Tc decays to ^{99}Tc ($t_{1/2}$ = 6.02 h), under emission of gamma radiation (140.5 keV) [255-259].

$^{99m}TcO_4^-$ shows neglible chemical reactivity and cannot bind directly to any ligand. Therefore, reduction to lower oxidation states in the presence of suitable ligands is necessary for molecule labeling; otherwise colloidal $^{99m}TcO_2$ is formed in aqueous media. For the reduction

of $^{99m}TcO_4^-$ the stannous ion ($SnCl_2$), is usually used as reductant. After reduction of $^{99m}TcO_4^-$ to a lower oxidation state in the presence of ligands, coordination complexes of ^{99m}Tc (acting as Lewis acid) and functional groups (act as Lewis bases) are formed [255]. Depending on the ligand, ^{99m}Tc is stabilized in different oxidation states, predominantly, penta- or hexacoordinated complexes containing a $^{99m}TcO_2^+$ or a $^{99m}TcO^+$ core. In the presence of other suitable ligands the formation of other cores and complexes of lower oxidation states (IV, III, I) are possible. Ligands for ^{99m}Tc-complexation containing one donor group, such as an amine, thiol, phosphine, oxime or isonitrile, form monodentate complexes with the ^{99m}Tc-core. Moreover, ligands with two or even more donor groups from a single molecule (chelate) can bind to one ^{99m}Tc-core [255, 257, 260]

2.2 ^{99m}Tc-Labeling of Peptides

For the design of target-specific ^{99m}Tc-labeled peptides, ^{99m}Tc is usually attached to the peptide via different chelating units. The quest for the optimal chelator should be in accordance with the target-specific biomolecule. Important therefore is, that the chelating unit should not affect the potency nor alter the *in vivo* properties of the peptide and the chelate ^{99m}Tc-complex should preferably be an integral part of the biomolecule [184, 186, 257, 261-263].

Different amino- and/or amido $N_xS_{(4-x)}$-based tetradentate chelators (e.g. DADT, MAMA) for complexation of a $^{99m}Tc(V)$-oxo core ($[^{99m}TcO]^{3+}$) have been extensively investigated for the ^{99m}Tc-labeling of biomolecules (Figure 14). However, many of these systems show upon complex formation multiple isomers, differing in their pharmacokinetic properties [255, 257, 260, 264-268]. Expansion of this functionalized peptide approach resulted in the development of peptide-bound chelators, such as N_3S-adipate (mercaptoacetamido-adipoylglycylglycine), MAG_3 (mercaptoacetyltriglycine) and its more hydrophilic counterpart MAS_3 (mercaptoacetylserine), which belong to the mostly used chelators for peptide labeling (Figure 14) [260, 269-272]. The use of these chelators for peptide labeling requires heating to 80-100°C for 10–20 min, due to their relatively slow complexation kinetics.

Another widely applied ^{99m}Tc-labeling strategy is the use of HYNIK (2-hydrazinonicotinamid)-peptide complexes (Figure 14) [255, 273-275]. HYNIK may coordinate the ^{99m}Tc-core via a monodentate diazenido- or bidentate-mode, involving the hydrazine and heterocyclic nitrogens [276, 277]. To saturate the hexacoordination sphere of the $^{99m}Tc(V)$-core with donor groups, co-ligands like EDDA (ethylenediamine diacetic acid) and tricine (N-(Tri(hydroxymethyl)methyl)glycine) are used to increase ^{99m}Tc-complex formation [260, 278,

279]. The choice of the appropriate co-ligand, as well as combinations thereof have an influence on the *in vivo* stability of the ^{99m}Tc-complex, as well as on the tracer kinetics [260, 262, 264, 278, 280].

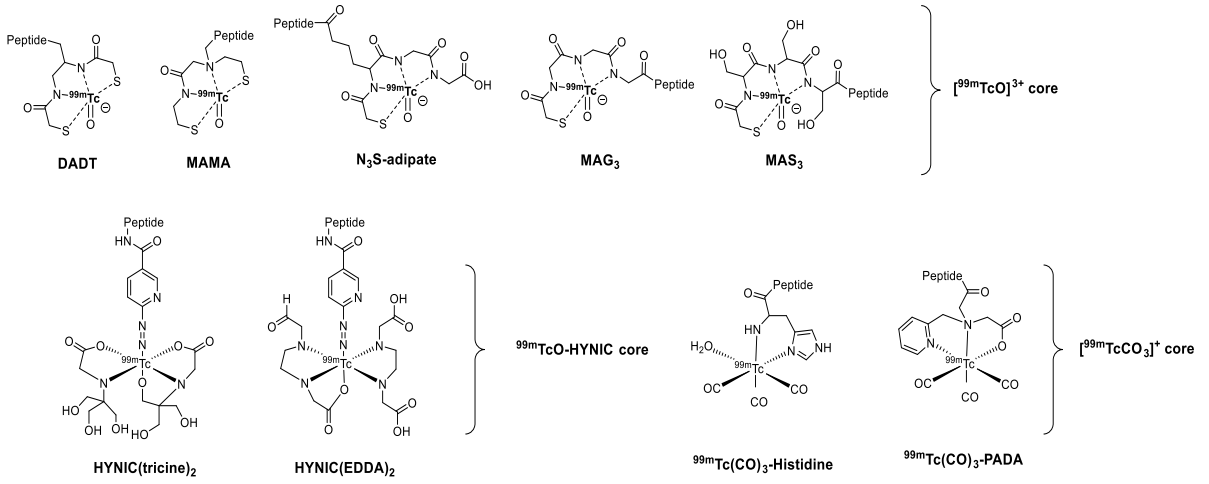

Figure 14: Peptide labeling via the $[^{99m}TcO]^{3+}$, the ^{99m}Tc-HYNIC, and $[^{99m}Tc(CO)_3]^+$ core, using different chelating systems (the site of peptide attachment is indicated).

In addition, several suitable tridentate and bidentate chelators, such as picolylamine diacetic acid (PADA) and histidine have been developed for the complexation of an $^{99m}Tc(CO)_3$ core (Figure 14) [281, 282]. The preparation is carried out in two steps: firstly, the formation of an $[^{99m}Tc(CO)_3(H_2O)_3]^+$ aquaion, using sodium boranocarbonate ($Na_2BH_3CO_2$) and secondly, by replacement of the labile water molecules by tri-/bidentate ligands [283]. These complexes exhibit high *in vivo* stability, however bidentate chelates can be further stabilized by addition of a monodentate ligand (phosphines, isocyanides, or aromatic amines), forming the fully coordinated “2+1” mixed ligand system [255, 260, 284-287].

2.3 ^{99m}Tc-Kit Labeling

Kit preparations have been greatly simplified the ^{99m}Tc-labeling procedures. Generally, the ^{99m}Tc-eluate ($^{99m}TcO_4^-$ in saline) is added to a sterile kit, initiating the direct labeling of the precursor [258]. The commercially available kits given the need to provide easy labeling procedures for clinical routine production and contain all chemical compounds that are necessary for the labeling in lyophilized form.

The standard reducing agent used for kit preparations is $SnCl_2$. The reducing agent is usually in high excess compared to other kit components, due to the oxidation sensitivity by air or radiolysis [288].

The formation of colloidal $^{99m}TcO_2$ is avoided by coordination of the reduced ^{99m}Tc species in the presence of the functionalized precursor. To provide a suitable pH for the labeling procedure, buffers are important components [257].

Further additives in kit formulations are antioxidants, catalysts, accelerators, and fillers [289, 290]. Antioxidants, such as ascorbic acid, prevent reoxidation to increase the stability of ^{99m}Tc-radiopharmaceuticals [291]. Intermediary coordination ligands such as citrate or tartrate can act as catalysts and stabilize reduced ^{99m}Tc, if complex formation with the precursor is slow [292]. Accelerators increase the rate of complex formation [292] and inert fillers (e.g. lactose) achieve rapid solubilization of the vial content [290]. For kit-based synthesis of new ^{99m}Tc-labeled tracers many variables, such as optimized composition of all kit ingredients, the reaction time, temperature, and pH have to be explored during the developmental phase to obtain high RCYs and only the desired product [257].

III. Objectives

Due to the high and consistent expression of PSMA and the high accessibility as a cell-surface membrane protein, it represents an excellent target for molecular imaging of PCa. Therefore, targeting of PSMA using highly specific radiolabeled inhibitors is of upmost clinical relevance for the diagnosis and (re)staging of PCa, as well as for the selection of PCa treatment.

Driven by the clinical interest for the intraoperative detection of small and atypically localized PCa lymph node metastases and based on the introduction of ^{111}In-PSMA-I&T for PSMA-targeted radioguided surgery (RGS) and SPECT imaging, this theranostic tracer concept should be adapted to the requirement of ^{99m}Tc-chemistry [220, 221]. Decisive factors for the development of a corresponding ^{99m}Tc-labeled analog are the suboptimal nuclear properties of ^{111}In, its high costs, and its limited availability, which restricts the application of ^{111}In-PSMA-I&T for clinical routine. Besides the selection of an optimal ^{99m}Tc-labeling strategy, to ensure fast and robust radiolabeling, the major focus should be directed towards the enhancement of the lead structure of PSMA-I&T to design a novel gamma probe with improved PSMA-targeting characteristics.
To investigate the clinical impact of ^{99m}Tc-PSMA-based RGS for removal of recurrent PCa lesions and on further disease progression, the feasibility and short-term outcomes of ^{99m}Tc-PSMA-based RGS should be analyzed in a small cohort of patients, with recurrent PCa after radical prostectomy, in collaboration with the Department of Nuclear Medicine and the Department of Urology of the TUM.

In addition, the severe limitations of ^{68}Ga for PET imaging result in a continuously growing clinical demand for ^{18}F-labeled PSMA ligands. Thus, the second aim of this thesis was the development of novel ^{18}F-labeled PSMA tracers, exploiting optimized ^{18}F-labeling strategies, as well as the enhanced experience concerning the structural requirements for ligand design for optimal PSMA binding. To ensure a valid comparative assessment of the new tracers, ^{18}F-DCFPyl and ^{18}F-PSMA-1007 should be used as reference and should be preclinically co-evaluated, using the same assays and preclinical test systems [212, 215].

All radiolabeled ligands investigated in this thesis should be preclinically evaluated, using comparative and robust systems to determine the *in vitro,* as well as the *in vivo* PSMA-targeting characteristics (affinity (IC_{50}), internalization efficiency, lipophilicity, metabolic stability, *in vivo* biodistribution, and µPET imaging). Initial first proof-of-concept studies in humans should be conducted to assess the potential of the novel PSMA inhibitors in a clinical setting.

IV. Results

In this chapter the reported projects of the development of PSMA-targeting radiopharmaceuticals for PET-, SPECT imaging, and RGS are outlined. The scientific details are available in the attached original peer-reviewed publications (Appendix VIII).

1. Novel and Established Radiopharmaceuticals for Diagnosis and Therapy of Prostate Carcinoma

Weineisen M, **Robu S**, Schottelius M, Wester H-J. *Nuk.* **2015**; 38(02): 89-98.
DOI: 10.1055/s-0035-1549863

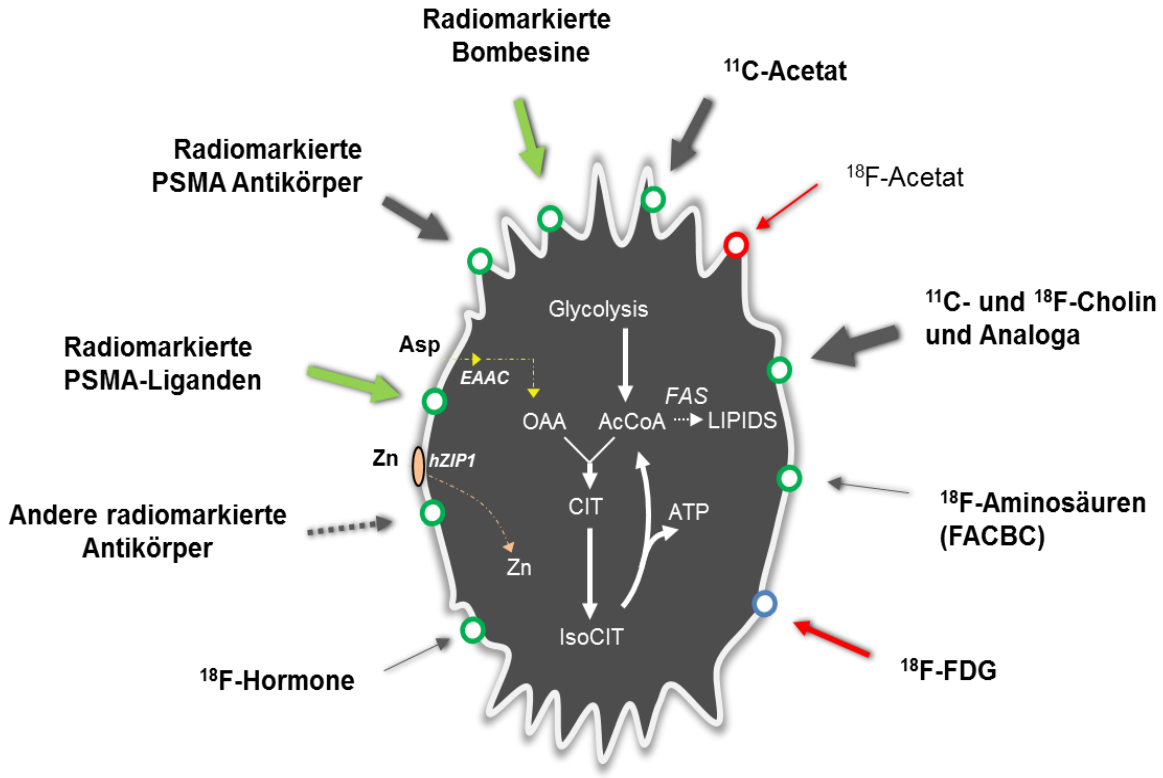

Figure 15: Various classes of radiopharmaceuticals for molecular imaging and therapy of PCa. Figure was originally published in [293] © Georg Thieme Verlag KG.

In this review recent developments of radiopharmaceuticals for the diagnosis and therapy of PCa were summarized, evaluated and assessed with respect to clinical applications. Due to the limited sensitivity of conventional imaging techniques, combination of PET/CT, SPECT/CT, and PET/MRI is developing a remarkable change on the clinical management of PCa [294]. For the enhanced detection of locally recurrent or metastatic PCa, metabolic processes and various targets have been addressed by molecular imaging.

The potential of metabolic ^{18}F-FDG PET imaging is limited by the low glycolytic rate of most PCas [295, 296]. Further advances for the detection of recurrent PCa have been achieved by investigation of PET tracers targeting the lipid metabolism, like ^{18}F/^{11}C-choline derivatives and ^{11}C-acetate [85, 297-299]. However, especially in patients with low PSA levels a poor sensitivity and specificity for initial staging and lymph node detection of biochemical PCa recurrence have been reported [86-88]. ^{18}F-FACBC, an amino acid transport imaging agent, was approved by the FDA, showing comparable detection rates in recurrent PCa to those of the choline derivatives [219, 300, 301].

Receptor specific ligands labeled with a broad range of radionuclides for PET and SPECT imaging have been developed for the diagnosis of PCa. The detection of primary tumors using Gastrin-releasing peptide receptor (GRPR)-targeted tracers exhibited promising results, demonstrating the clinical potential of these tracer class for initial staging of PCa [302].

Due to the overexpression of the prostate-specific membrane antigen (PSMA) it represents a promising target for both imaging and therapeutic interventions of PCa, using radiolabeled antibodies, as well as highly specific small molecule inhibitors [28, 303-306]. Small molecules have a clear advantage over much larger constructs, such as antibodies, due to their faster clearance from the blood and increased tumor permeability, resulting in rapid and persistent uptake in tumor lesions with minimal retention in non-targeted tissue [137]. Several studies demonstrated the remarkable potential of radiolabeled small molecule PSMA inhibitors in early diagnosis, staging of high-risk patients, anatomic localization of metastases and therapy planning [137, 219]. Treatment options for PCa patients with metastatic disease were for some time restricted to androgen-deprivation therapy and chemotherapy, which causes potentially serious adverse effects [219, 307, 308]. For the additional treatment of bone metastasis ^{223}Ra-dichloride (Xofigo) was approved by the FDA and EMA [309]. Due to the urgent need for additional therapy options for patients with soft-tissue metastasizing disease, methods have been developed to label PSMA inhibitors, either with ^{68}Ga or ^{177}Lu, enabling their use as theranostics, which offers promising perspectives for PSMA-targeted therapy [139]. Initial data of endoradiotherapeutic applications of these novel ligands in patients with metastatic PCa demonstrated highly promising molecular and morphological treatment responses [137, 139, 219].

2. Preclinical Evaluation and First Patient Application of ^{99m}Tc-PSMA-I&S for SPECT Imaging and Radioguided Surgery in Prostate Cancer

Robu S*, Schottelius M*, Eiber M, Maurer M, Gschwend J, Schwaiger M, Wester H-J. *J Nucl Med.* **2017**; 58:235-242. DOI: 10.2967/jnumed.116.178939

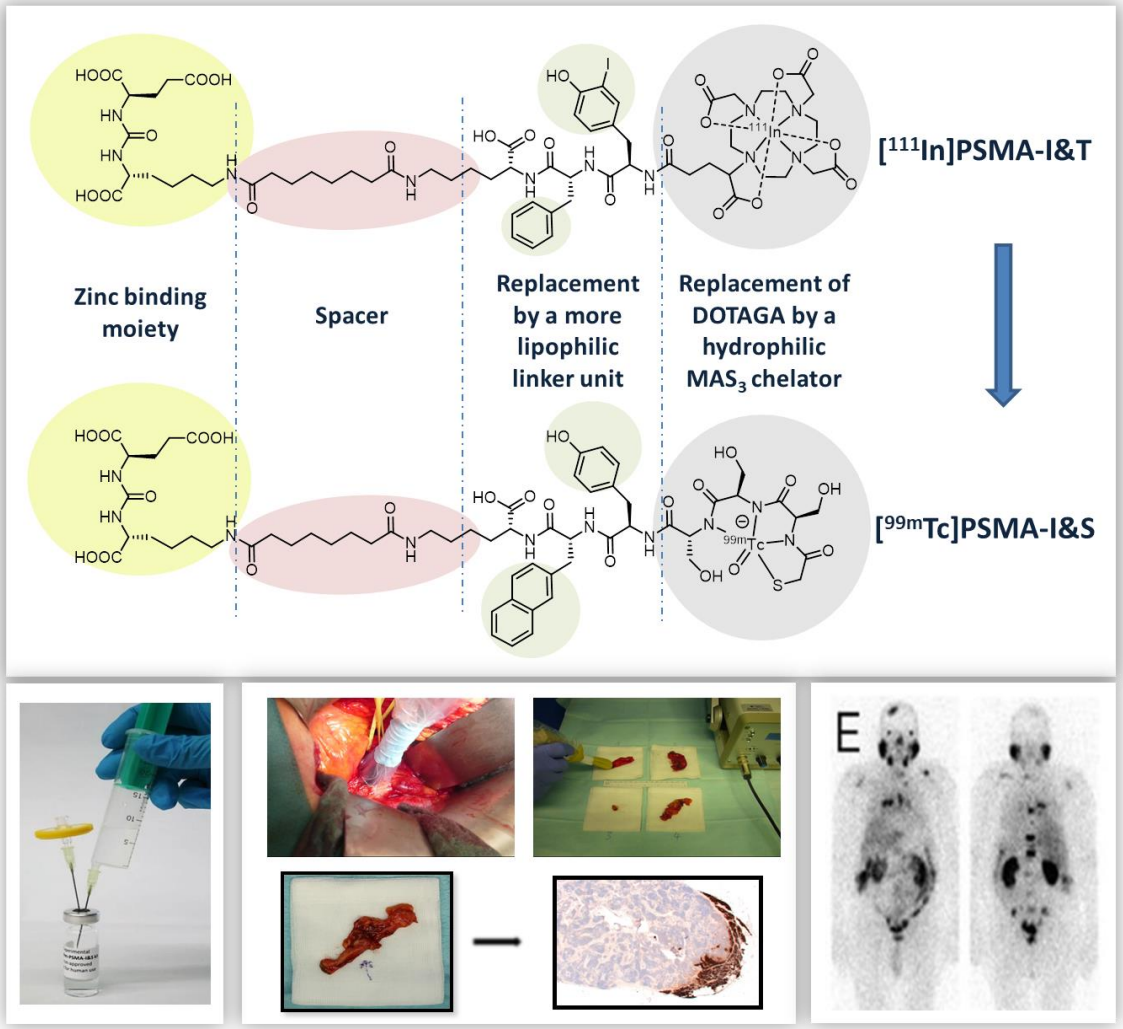

Figure 16: Adaption of the theranostic tracer concept of ^{111}In-PSMA-I&T towards the requirements of ^{99m}Tc-chemistry: Ligand design of the gamma probe ^{99m}Tc-PSMA-I&S for PSMA-targeted RGS and SPECT imaging.

Initial studies demonstrated the suitability of ^{111}In-PSMA-I&T for preoperative PCa SPECT imaging and radio-guided surgery (RGS), however, the inherent limitations associated with the use of ^{111}In as radionuclide restricted the broader clinical use [220, 221]. To meet the clinical need for a more cost-effective alternative with favorable nuclide characteristics, the aim of this study was to adapt the PSMA-I&T-based theranostic concept towards ^{99m}Tc-labeling chemistry. This publication describes the synthesis and (pre)clinical evaluation of a novel PSMA inhibitor for SPECT imaging and RGS, termed ^{99m}Tc-PSMA-I&S (for **I**maging and **S**urgery).

Due to the ease and efficiency of MAG_3-based ^{99m}Tc-labeling, the DOTAGA-chelator in PSMA-I&T was replaced by a MAG_3-derived more hydrophilic all-D-serine chelating moiety (MAS_3), leading to high *in vivo* stability of ^{99m}Tc-PSMA-I&S. The peptidic linker of ^{111}In-PSMA-I&T was replaced by an optimized more lipophilic linker unit, resulting in nearly identical PSMA affinities and internalization kinetics for both tracers. In comparison to ^{111}In-PSMA-I&T, the chelator and linker-unit exchange leads to higher lipophilicity and therefore considerable higher plasma protein binding of ^{99m}Tc-PSMA-I&S (94%). This was mirrored in the biodistribution data, where ^{99m}Tc-PSMA-I&S showed delayed clearance kinetics but identical high uptake in PSMA-positive tissues and tumors in LNCaP-xenografts (1 h p.i.).

The pronounced plasma protein binding also led to a relatively slow whole body clearance in an exemplary PCa patient, which resulted in steadily increased tracer accumulation in PCa lesions over time, as a result of the prolonged availability of intact ^{99m}Tc-PSMA-I&S in the blood and its enhanced internalization efficiency in PSMA-expressing tumor lesions. This synergistic effect of persistent tracer uptake in tumor tissue and continuing clearance of background activity resulted in excellent lesion-to-background ratios at late imaging times points (≥ 5 h p.i.). These combined effects represent a major prerequisite for RGS in a clinical setting, because the success of RGS relies on high lesion-to-background contrast at time of surgery, which is performed on the day after injection for practical reasons [220].

A preoperative SPECT/CT scan showed high ^{99m}Tc-PSMA-I&S uptake in all suspect lesions, previously identified with ^{68}Ga-HBED-CC-PSMA PET/CT, allowing for exact intraoperative identification and resection during RGS. The first-in-human studies suggested improved performance of ^{99m}Tc-PSMA-I&S in comparison to ^{111}In-PSMA-I&T, based on the enhanced tracer uptake in tumor tissue and consequently higher imaging contrast in preoperative SPECT. Although, ^{99m}Tc-PSMA-I&S was mainly developed for the adaptation on the requirements for RGS, the quality of SPECT images obtained with ^{99m}Tc-PSMA-I&S are well comparable to those of promising PSMA inhibitors, such as ^{99m}Tc-MIP-1404 [183, 185].

Moreover, to facilitate the distribution and one-site production for clinical applications, a robust and reliable synthesis procedure was developed, which is highly compatible with the daily clinical workflow, allowing the synthesis of ^{99m}Tc-PSMA-I&S in consistently high radiochemical yield and purity (≥ 98%, > n=200).

3. ^{99m}Technetium-based Prostate-specific Membrane Antigen-radioguided Surgery in Recurrent Prostate Cancer

Maurer T*, **Robu S***, Schottelius M, Schwamborn K, Rauscher I, van den Berg N, van Leeuwen F W B, Haller B, Horn T, Heck M M, Gschwend J E, Schwaiger M, Wester H-J, Eiber M. *Eur Urol*. 2019;75(4):659-666. DOI: 10.1016/j.eururo.2018.03.013

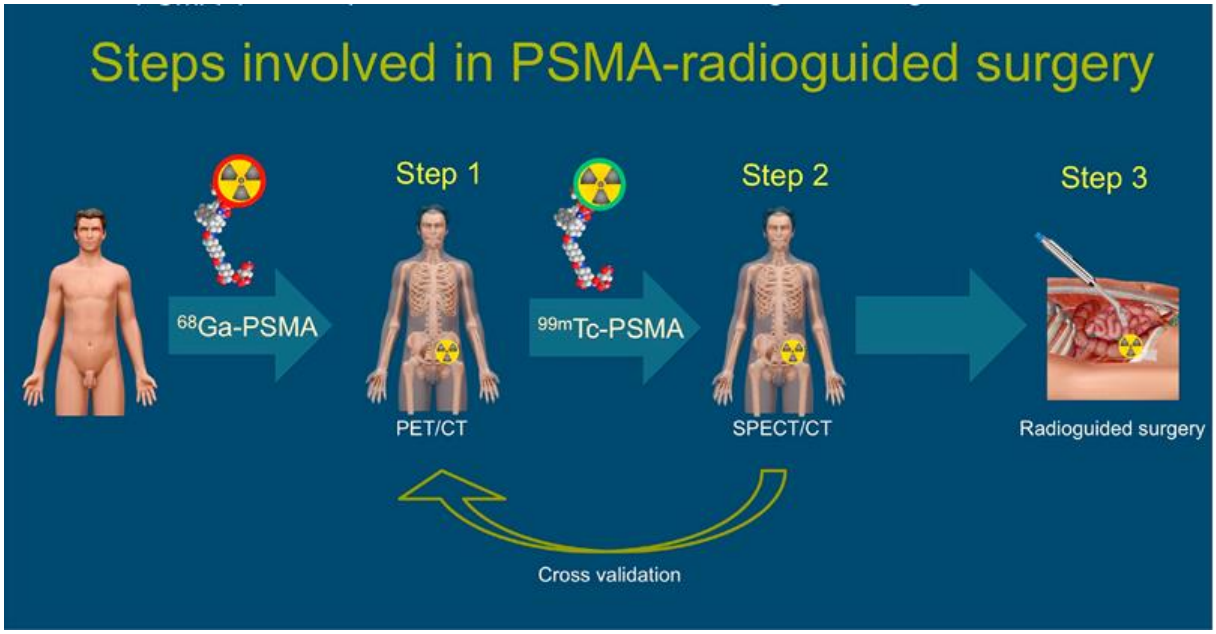

Figure 17: Overview of the procedure for ^{99m}Tc-PSMA-I&S based RGS: After selection of patients based on ^{68}Ga-PSMA-11-PET/CT scan, subsequent ^{99m}Tc-PSMA-I&S SPECT/CT is performed to confirm tracer uptake in the same lesions. ^{99m}Tc-PSMA-I&S based RGS is carried out on the next day, performing *in vivo*/*ex vivo* gamma probe measurements to reliable identify metastatic PCa lesions during surgery. Image is originally published in [310].

The use of radiolabeled inhibitors for PSMA-targeted PET allows the improved visualization of metastatic lesions in patients with early biochemical recurrence. In addition, the salvage surgery has gained increasing interest to delay further disease progression, especially in patients with locoregional oligometastatic disease [311-313]. The reliable identification of small or atypical located lesions during salvage surgery is still challenging. The theranostic concept of radiolabeled PSMA ligands was expanded beyond endoradiotherapy towards radio-guided surgery (RGS), using ^{99m}Tc-PSMA-I&S for preoperative SPECT imaging and primary as a gamma probe for the intraoperative detection of lymph node metastasis.

This publication describes the feasibility and short-term outcomes of ^{99m}Tc-PSMA-I&S based RGS for intraoperative detection and surgical removal of recurrent PCa lesions. The retrospective study summarizes the data of 31 consecutive patients with evidence of

recurrent PCa on ^{68}Ga-PSMA-11-PET after radical prostatectomy, undergoing salvage surgery using ^{99m}Tc-PSMA-I&S as a gamma probe for intraoperative guidance.

In every patient, all lesions detected on preoperative ^{68}Ga-PSMA-11 PET could be identified and removed by ^{99m}Tc-PSMA-I&S based RGS. To investigate the radioactive rating (positive vs. negative) of all resected tissue specimens, the findings were compared with *ex vivo* histopathological analysis. In total, 58 of 132 (46 positive and 86 negative by *ex vivo* gamma probe measurement) removed surgical specimens were confirmed to bear PSMA-expressing metastatic disease by *ex vivo* histopathology, resulting therefore in 12 false negative findings for gamma probe measurement. These 12 low-volume small sized lymph node metastases, confirmed by histopathology, could neither be detected on preoperative ^{68}Ga-PSMA-11-PET nor during surgery. Thus, it seems to be advisable to dissect surrounding tissue to remove possible adjacent micrometastases. The radioactive rating of ^{99m}Tc-PSMA-I&S based RGS showed in correlation to *ex vivo* histopathology therefore, a specificity of 100%, and a sensitivity of 83.6% and an accuracy of 93.0%.

No adverse effects, related to the administration of ^{99m}Tc-PSMA-I&S, were observed. The short-term outcome for 30 patients after salvage PSMA-RGS revealed a PSA decline of greater than 50% and greater than 90% in 24 (80%) and 17 (57%) of 30 patients, respectively. A reduction in the PSA-level below 0.2 ng/ml was observed in 20 patients. After a median follow-up of 13.8 month, 10 patients (33.3%) remained biochemical recurrence-free and 20 patients (65%) continued to be treatment-free at a median follow-up of 12.2 month. In the remaining 11 of 31 patients (35%) further PCa-specific treatment was given after a median of 3.7 months.

In summary, it has been proven that ^{99m}Tc-PSMA-targeted RGS is a feasible surgical technique to reliable identify metastatic lymph nodes in PCa patients with biochemical recurrence and facilitates the surgical removel of metastatic lesions. RGS might positively influence the disease progression and delay the need for further systemic treatment. However, its long-term impact on outcome has to be further evaluated and the identification of suitable patients on the basis of ^{68}Ga-PSMA-PET, as well as the consideration of clinical variables are essential for satisfactory results [219, 220].

4. Synthesis and Preclinical Evaluation of novel ^{18}F-labeled Glu-urea-Glu-based PSMA inhibitors for Prostate Cancer Imaging: a comparison with ^{18}F-DCFPyl and ^{18}F-PSMA-1007

Robu S*, Schmidt A, Eiber M, Schottelius M, Günther T, Yousefi B H, Schwaiger M, Wester H-J. *EJNMMI Res.* 2018; 8(1):30-40. DOI: 10.1186/s13550-018-0382-8

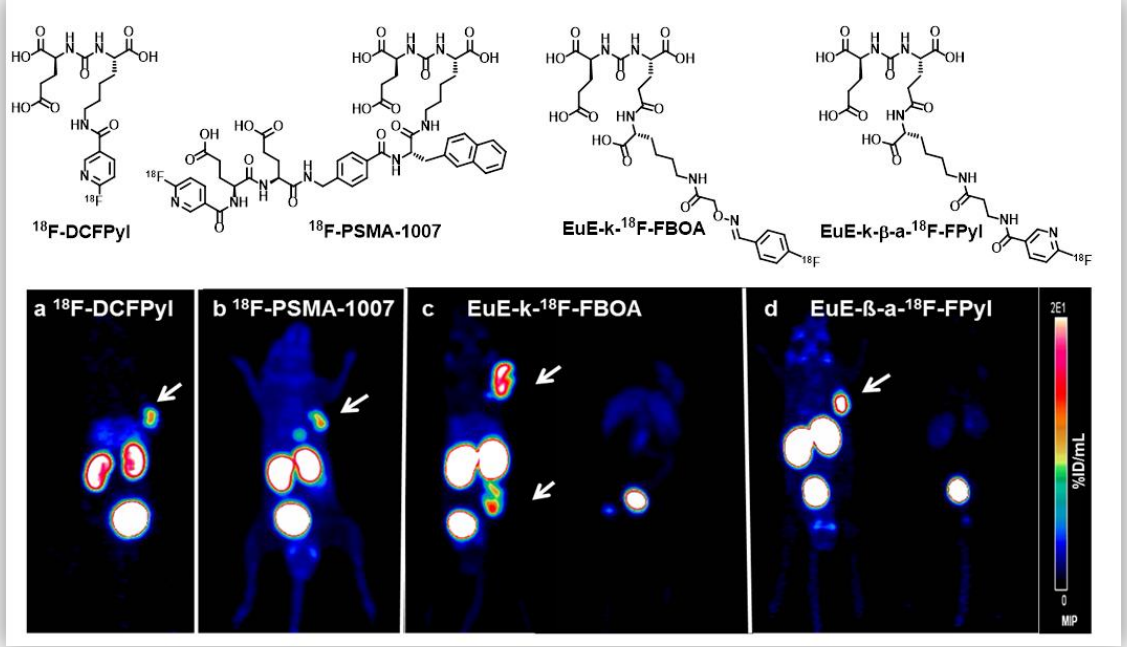

Figure 18: Comparative µPET scans of **(a)** ^{18}F-DCFPyl; **(b)** ^{18}F-PSMA-1007 **(c) left:** EuE-k-^{18}F-FBOA, **right**: + blocking with 8 mg/kg PMPA; **(d) left:** EuE-k-β-a-^{18}F-FPyl, **right**: + blocking with 8 mg/kg (PMPA) (60-90 min p.i.; 0-20 % ID/mL; 0.9-1 MBq). Image modified from [314].

In this study two novel ^{18}F-labeled PSMA inhibitors based on a Glu-urea-Glu (EuE) binding motif were synthesized and preclinically evaluated, to address the continuously growing clinical demand for ^{18}F-labeled PSMA ligands. Both tracers, termed EuE-k-^{18}F-FBOA and EuE-k-ß-a-^{18}F-FPyl, were suitable for the chemo-selective labeling with either oxime ligation using ^{18}F-FBA or established acylation chemistry with ^{18}F-FPyl-TFP. To allow for a direct comparison, the recently introduced tracers ^{18}F-DCFPyl and ^{18}F-PSMA-1007 were included in the preclinical evaluation [212, 215].

Radiolabeling of the prosthetic groups was performed according to a previously published "minimalist approach", without the need of time-consuming azeotropic drying steps or any other additives or base [253, 254]. Radiolabeling of ^{18}F-FPyl-TFP revealed lower RCYs and RCP compared to ^{18}F-FBA, due to the hydrolysis of the labeled synthon and precursor salt, resulting therefore in decreased overall RCYs after conjugation to the peptidic precursor.

Both metabolic stable EuE-based ligands showed commensurable or even higher PSMA affinities combined with enhanced internalization rates in PSMA-expressing cells in comparison to ^{18}F-DCFPyl and ^{18}F-PSMA-1007.

Due to the high hydrophilicity and low plasma protein binding (app. 13%) of both ^{18}F-labeled EuE-based tracers, almost no unspecific uptake in non-target tissue was observed in µPET imaging. The markedly higher uptake in tumor lesions (up to 50%), compared to the reference ligands, resulted in higher contrast µPET imaging using EuE-k-^{18}F-FBOA and EuE-k-ß-a-^{18}F-FPyl. These data were confirmed in a comparative *in vivo* biodistribution study of all four radioligands (1h and 2h p.i.). The comparable high hydrophilicity and low blood pool retention of the ^{18}F-labeled EuE-based tracers and ^{18}F-DCFPyl leads to similar tracer pharmacokinetics with fast renal clearance and low activity levels in the blood and non-target tissue. In comparison to EuE-k-ß-a-^{18}F-FPyl, EuE-k-^{18}F-FBOA showed significantly decreased kidney accumulation and additionally faster clearance kinetics, resulting in better tumor-to-organ, especially tumor-to-kidney ratios as early as 1 h p.i.. In contrast, due to the less hydrophilic character (logP= -1.6) and its high plasma protein binding (98%), ^{18}F-PSMA-1007 showed predominantly hepatobiliary excretion and higher uptake in non-target tissue, caused by higher activity levels in the blood.

Although, both ^{18}F-labeled EuE-based inhibitors exhibited excellent *in vivo* and *in vitro* PSMA-targeting characteristics, EuE-k-^{18}F-FBOA seems to be more promising for further investigation, due to the faster clearance kinetics with comparable high tumor uptake, resulting therefore in better high-contrast µPET imaging as early as 1 h p.i..

A proof-of-concept study of a 79 year old patient with mCPRC (PSA 392 ng/ml) using EuE-k-^{18}F-FBOA showed minimal blood pool retention and high contrast PET imaging at 1 h p.i.. Even tiny subcentimeter lymph node metastases were detectable, due to the intense uptake of EuE-k-^{18}F-FBOA.

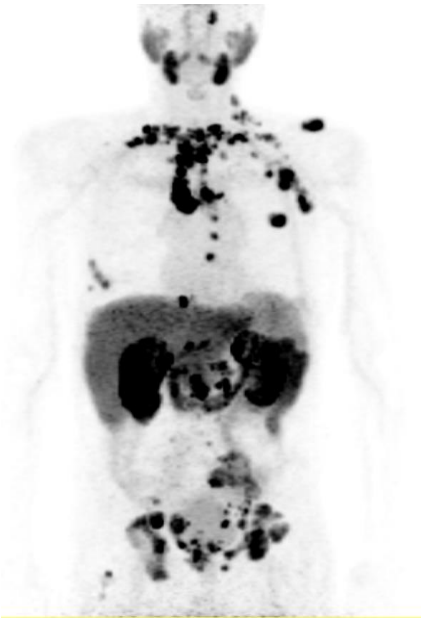

Figure 19: First in-man study of a 79 year old patient with mCPRC using EuE-k-^{18}F-FBOA.

V. Summary and Outlook

Initial proof-of-concept studies using ^{111}In-PSMA-I&T for preoperative SPECT imaging and primary as a gamma probe for the intraoperative detection of lymph node metastasis demonstrated the feasibility of this theranostic approach [220, 221]. However, the suboptimal nuclear properties and high costs of ^{111}In restricted the use of ^{111}In-PSMA-I&T in clinical routine. One main objective of the presented theses was therefore, the development of a corresponding ^{99m}Tc-labeled analog for SPECT and radio-guided surgery (RGS), termed ^{99m}Tc-PSMA-I&S (I&S for **I**maging and **S**urgery).

The modified peptidic structure of ^{99m}Tc-PSMA-I&S resulted in comparable *in vitro* and *in vivo* PSMA-targeting characteristics to ^{111}In-PSMA-I&T. Initial patient studies revealed, that the combination of prolonged availability of intact tracer in the blood and high internalization efficiency of ^{99m}Tc-PSMA-I&S promoted efficient tracer accumulation in tumor lesions over time and led to steadily increasing lesion-to-background ratios up to 21 h after injection. These tracer characteristics fulfill perfectly the requirements for RGS, which is performed on the day after injection. In addition, preoperative SPECT/CT imaging with ^{99m}Tc-PSMA-I&S showed high specific uptake in all metastatic lesions, identified in a previous ^{68}Ga-PSMA-11 PET scan, allowing for the successful intraoperative detection and complete dissection of all PET-positive lesions during first-in-human RGS. Initial patient data also hint towards the unexpected potential of ^{99m}Tc-PSMA-I&S as a SPECT imaging agent.

Based on the promising data obtained in this study, ^{99m}Tc-PSMA-I&S is a cost-effective and superior substitute for ^{111}In-PSMA-I&T for SPECT imaging, as well as PSMA-targeted RGS. In addition, a clear advantage of ^{99m}Tc-PSMA-I&S includes its fast and efficient radiolabeling for convenient implementation in the clinical workflow.

The retrospective study, summarizing the data of 31 consecutive patients with evidence of recurrent PCa after radical prostatectomy, has demonstrated that the use of ^{99m}Tc-PSMA-I&S as a gamma probe facilitates targeted molecular surgery, as it allows the specific intraoperative detection and dissection of all lesions detected on preoperative ^{68}Ga-PSMA-11 PET. In addition, the correlation with histopathology demonstrated a high specificity, sensitivity, as well as accuracy for the intraoperative identification of even small tumor deposits in PCa patients using ^{99m}Tc-PSMA-I&S. The short-term follow-up data indicate a high potential of ^{99m}Tc-PSMA-I&S RGS, to positively influence disease progression, which might delay the need of further systemic treatment. However, this has to be further proven in prospective clinical trials.

The high potential clinical value of ^{99m}Tc-PSMA-I&S RGS is supported by currently ongoing proof-of-concept studies in up to now more than 200 patients, which help to support the

integration of PSMA-targeted RGS into the clinics. In addition, further evaluations with emphasis on the suitability of ^{99m}Tc-PSMA-I&S as SPECT probe are currently under assessment, to support the notion of first-line diagnosis of metastasized PCa by SPECT imaging in centers where PET is not available.

The second aim of this thesis was the development of novel ^{18}F-labeled PSMA inhibitors for the diagnostic imaging of PCa. We designed two ^{18}F-labeled PSMA inhibitors based on a novel EuE (Glu-urea-Glu) binding core, named EuE-k-^{18}F-FBOA and EuE-k-ß-a-^{18}F-FPyl. Both tracers contain an optimized hydrophilic linker structure and an ^{18}F-labeled aromatic moiety, suitable for the labeling with either chemo-selective oxime ligation using ^{18}F-FBA or established acylation chemistry with ^{18}F-FPyl-TFP as prosthetic group. To ensure a valid assessment of the novel EuE-based inhibitors, they were evaluated in a comparative preclinical study with the recently introduced tracers ^{18}F-DCFPyl and ^{18}F-PSMA-1007 [212, 215].

The two step radiolabeling of the ^{18}F-labeled EuE-based ligands allowed preparation with moderate RCYs and high RCP. In contrast to the acylation approach using ^{18}F-FPyl-TFP, the oxime ligation for the synthesis of EuE-k-^{18}F-FBOA resulted in enhanced RCYs with less precursor peptide needed.

Regarding the ligand design, we focused on the improvement of the structural requirements for favorable *in vivo* and *in vitro* PSMA-targeting characteristics. In comparison to the reference ligands ^{18}F-DCFPyl and ^{18}F-PSMA-1007, both ^{18}F-labeled EuE-based PSMA inhibitors revealed enhanced PSMA affinities combined with higher internalization efficiency, which leads to approximately 50% higher tumor accumulation in µPET and biodistribution studies in LNCaP-tumor xenografts. Since hydrophilicity and extend of plasma protein binding significantly contributes to the *in vivo* performance of a given radiopharmaceutical, ^{18}F-PSMA-1007 showed high tracer uptake in non-target tissue and predominantly hepatobiliary excretion, due to the less hydrophilic character and its high plasma protein binding (98%). In contrast, ^{18}F-DCFPyl exhibited pharmacokinetics quite similar to those obtained for the highly hydrophilic ^{18}F-labeled EuE-based PSMA inhibitors, which revealed straightforward clearance kinetics and almost no uptake in non-target tissue. Though, in contrast to EuE-k-ß-a-^{18}F-FPyl, EuE-k-^{18}F-FBOA showed significantly lower uptake in the kidneys with additionally faster clearance kinetics combined with similar high tumor uptake, resulting therefore in improved high-contrast µPET imaging as early as 1 h p.i..

Based on the more promising preclinical results, a first-in-human study using EuE-k-^{18}F-FBOA has been conducted. This proof-of-concept study revealed potential for high contrast imaging of metastatic PCa and clearly underlines successful translation to a clinical setting.

However, the time-consuming multistep radiosynthesis of EuE-k-^{18}F-FBOA, with only moderate overall RCYs, restricted the use of this tracer in the daily clinical practice. The optimization of the radiolabeling procedure, to facilitate the automatization for synthesis in clinical routine, was not further pursued after this thesis. Instead, the findings of this study, concerning the structure of the EuE-based ligands for enhanced PSMA-targeting, provided the basis for the synthesis of novel ^{18}F-labeled EuE-based compounds, combining more innovative ^{18}F-labeling strategies, to ensure fast and efficient radiolabeling and convenient implementation into the clinics.

VI. Reprint Permissions

All manuscripts were reproduced by permission of the corresponding journals. The detailed bibliographic data of the respective articles can be found in chapter IV. Original publications can be found in the appendix VIII.

1. Nuklearmediziner Publication

Weineisen M, **Robu S**, Schottelius M, Wester H-J. Novel and Established Radiopharmaceuticals for Diagnosis and Therapy of Prostate Carcinoma. *Nuklearmediziner* 2015; 38(02): 89-98.

GEORG THIEME VERLAG KG LICENSE TERMS AND CONDITIONS

Oct 10, 2018

This Agreement between Ms. Stephanie Robu Klinikum rechts der Isar -- Stephanie Robu ("You") and Georg Thieme Verlag KG ("Georg Thieme Verlag KG") consists of your license details and the terms and conditions provided by Georg Thieme Verlag KG and Copyright Clearance Center.

The publisher has provided special terms related to this request that can be found at the end of the Publisher's Terms and Conditions.

License Number	4423541225343
License date	Sep 07, 2018
Licensed Content Publisher	Georg Thieme Verlag KG
Licensed Content Publication	Nuklearmediziner Der
Licensed Content Title	Neue und bewährte Radiopharmaka für die Diagnostik und Therapie des Prostatakarzinoms
Licensed Content Author	M. Weineisen, S. Robu, M. Schottelius, H.-J. Wester
Licensed Content Date	Jan 1, 2015
Licensed Content Volume	38
Licensed Content Issue	02
Type of Use	Dissertation/Thesis
Requestor type	author of the original Thieme publication
Format	print and electronic
Portion	full article/document
Will you be translating?	no

Distribution quantity	6
Specified additional information	Dear Sir and Madam, in order to satisfy the criteria of my degree-granting institution (Technische Universität München), i need a written confirmation that i may reuse the following publication for my dissertation. By signing this form, you grant me confirmation, that the above stated work may be reused with appropriate citation to meet the criteria of my institution for submission of my dissertation. Sincerely, Stephanie Robu
Order reference number	
Title of your dissertation / thesis	Development of PSMA inhibitors for molecular imaging and radio-guided surgery of prostate cancer
Expected completion date	Jan 2019
Estimated size (number of pages)	110
Requestor Location	Ms. Stephanie Robu Klinikum rechts der Isar Ismaningerstrasse 22 München, 81675 Germany Attn: Ms. Stephanie Robu Klinikum rechts der Isar
Publisher Tax ID	DE 147638607
Billing Type	Invoice
Billing Address	Ms. Stephanie Robu Klinikum rechts der Isar Ismaningerstrasse 22 München, Germany 81675 Attn: Ms. Stephanie Robu Klinikum rechts der Isar
Total	0.00 EUR

Terms and Conditions

[…] Licenses for reuse in a dissertation/thesis are limited to the depositary copies (non-profit and password-protected) that have to be delivered within the university system. Any further use and follow-up publications require separate permission. […]

[…] **Special Terms**: Diese Einwilligung gilt für die Nutzung in Print und in elektronischer Form in den Pflichtexemplaren der o.g. wissenschaftlichen Arbeit. Der Artikel darf nur in der akzeptierten WORD-Version ohne Thieme-Layout veröffentlicht werden. Nutzung/Bereitstellung der von uns veröffentlichten PDF-Version ist ausdrücklich ausgeschlossen. Weitere Verwertungsrechte und die Erlaubnis zur Bereitstellung auf anderen, kommerziellen Servern werden nicht erteilt.

2. Journal of Nuclear Medicine Publication

Robu S*, Schottelius M*, Eiber M, Maurer T, Gschwend J, Schwaiger M, Wester H-J. Preclinical Evaluation and First Patient Application of ^{99m}Tc-PSMA-I&S for SPECT Imaging and Radioguided Surgery in Prostate Cancer. *J. Nucl. Med*. 2017; 58(2): 235-242.

J Nucl Med.

MD. Johannes Czernin

University of California at Los Angeles

Los Angeles, California

Stephanie Robu

Department of Nuclear Medicine

Klinikum rechts der Isar

Technical University Munich

Ismaningerstrasse 22

81675 München, Germany

stephanie.robu@tum.de

München, 07.09.2018

Reuse/Republication of the Entire Work in Theses or Collections

Dear Sir or Madam,

in order to satisfy the criteria of my degree-granting institution (Technische Universität München), I need a written confirmation that I may reuse the following publication for my dissertation:

Preclinical Evaluation and First Patient Application of ^{99m}Tc-PSMA-I&S for SPECT Imaging and Radioguided Surgery in Prostate Cancer. Robu S*, Schottelius M*, Eiber M, Maurer M, Gschwend J, Schwaiger M, Wester H-J. J Nucl Med. 2017; 58:235-242.

By signing this form, you grant me confirmation, that the above stated work may be reused with appropriate citation to meet the criteria of my institution of my dissertation.

Sincerely,

St. Rob

PhD Candidate

Stephanie Robu

07.09.2018

APPROVED

By Mark Sumimoto at 9:42 am, Sep 07, 2018

3. European Urology Publication

Maurer T*, **Robu S***, Schottelius M, Schwamborn K, Rauscher I, van den Berg N, van Leeuwen F W B, Haller B, Horn T, Heck M M, Gschwend J E, Schwaiger M, Wester H-J, Eiber M. ^{99m}Technetium-based Prostate-specific Membrane Antigen-radioguided Surgery in Recurrent Prostate Cancer. Article in press: *Eur Urol*. 2018; https://doi.org/10.1016/j.eururo.2018.03.013.

4. European Journal of Nuclear Medicine and Molecular Imaging Research Publication

Robu S*, Schmidt A, Eiber M, Schottelius M, Günther T, Yousefi B, Schwaiger M, Wester H-J. Synthesis and Preclinical Evaluation of novel ^{18}F-labeled Glu-urea-Glu-based PSMA inhibitors for Prostate Cancer Imaging: a comparison with ^{18}F-DCFPyl and ^{18}F-PSMA-1007. *EJNMMI Res*. 2018; 8(1):30-40. © The Author(s). 2018

VII. References

1. Torre, L.A., et al., Global cancer statistics, 2012. CA Cancer J Clin, 2015. **65**(2): p. 87-108.
2. Heidenreich, A., et al., EAU Guidelines on Prostate Cancer. Eur Urol, 2008. **53**(1): p. 68-80.
3. Schroder, F.H., et al., Screening and prostate-cancer mortality in a randomized European study. N Engl J Med, 2009. **360**(13): p. 1320-1328.
4. Schroder, F.H., et al., Prostate-cancer mortality at 11 years of follow-up. N Engl J Med, 2012. **366**(11): p. 981-990.
5. Crawford, E.D., et al., Efficiency of prostate-specific antigen and digital rectal examination in screening, using 4.0 ng/ml and age-specific reference range as a cutoff for abnormal values. Prostate, 1999. **38**(4): p. 296-302.
6. Tsodikov, A., et al., REconciling the effects of screening on prostate cancer mortality in the erspc and plco trials. Ann Intern Med, 2017. **167**(7): p. 449-455.
7. Smith, D.S., P.A. Humphrey, and W.J. Catalona, The early detection of prostate carcinoma with prostate specific antigen: the Washington University experience. Cancer, 1997. **80**(9): p. 1852-1856.
8. Neal, D.E., Jr., et al., Prostate specific antigen and prostatitis. I. Effect of prostatitis on serum PSA in the human and nonhuman primate. Prostate, 1992. **20**(2): p. 105-111.
9. Roehrborn, C.G., et al., Serum prostate-specific antigen as a predictor of prostate volume in men with benign prostatic hyperplasia. Urology, 1999. **53**(3): p. 581-589.
10. Heijnsdijk , E.A.M., et al., Quality-of-Life Effects of Prostate-Specific Antigen Screening. N Engl J Med, 2012. **367**(7): p. 595-605.
11. Draisma, G., et al., Lead times and overdetection due to prostate-specific antigen screening: estimates from the European Randomized Study of Screening for Prostate Cancer. J Natl Cancer Inst, 2003. **95**(12): p. 868-878.
12. Cooperberg, M.R., et al., The changing face of low-risk prostate cancer: trends in clinical presentation and primary management. J Clin Oncol, 2004. **22**(11): p. 2141-2149.
13. Mohammed, A.A., Biomarkers in prostate cancer: new era and prospective. Med Oncol, 2014. **31**(8): p. 140-145.
14. Hessels, D. and J.A. Schalken, The use of PCA3 in the diagnosis of prostate cancer. Nat Rev Urol, 2009. **6**(5): p. 255-261.
15. Loeb, S. and W.J. Catalona, The Prostate Health Index: a new test for the detection of prostate cancer. Ther Adv Urol, 2014. **6**(2): p. 74-77.

16. Parker, C., et al., Cancer of the prostate: ESMO Clinical Practice Guidelines for diagnosis, treatment and follow-up. Ann Oncol, 2015. **26** (Suppl_5): p. 69-77.
17. Cornford, P., et al., EAU-ESTRO-SIOG Guidelines on Prostate Cancer. Part II: Treatment of Relapsing, Metastatic, and Castration-Resistant Prostate Cancer. Eur Urol, 2017. **71**(4): p. 630-642.
18. Griffiths, K., et al., Hormonal treatment of advanced disease: some newer aspects. Semin Oncol, 1994. **21**(5): p. 672-687.
19. Tan, J.-L., et al., Androgen receptor targeted therapies in metastatic castration-resistant prostate cancer – The urologists' perspective. Urol Sci, 2017. **28**(4): p. 190-196.
20. Scher, H.I., et al., Design and End Points of Clinical Trials for Patients With Progressive Prostate Cancer and Castrate Levels of Testosterone: Recommendations of the Prostate Cancer Clinical Trials Working Group. J Clin Oncol, 2008. **26**(7): p. 1148-1159.
21. Kelloff, G.J., P. Choyke, and D.S. Coffey, Challenges in clinical prostate cancer: role of imaging. AJR Am J Roentgenol. 2009 Jun;192(6): p.1455-1470.
22. Trabulsi, E.J., W.G. Merriam, and L.G. Gomella, New imaging techniques in prostate cancer. Curr Urol Rep, 2006. **7**(3): p. 175-180.
23. Heidenreich, A., et al., EAU guidelines on prostate cancer. Part 1: screening, diagnosis, and treatment of clinically localised disease. Eur Urol, 2011. **59**(1): p. 61-71.
24. Futterer, J.J., et al., Prostate cancer localization with dynamic contrast-enhanced MR imaging and proton MR spectroscopic imaging. Radiology, 2006. **241**(2): p. 449-458.
25. Lim, H.K., et al., Prostate cancer: apparent diffusion coefficient map with T2-weighted images for detection--a multireader study. Radiology, 2009. **250**(1): p. 145-151.
26. Tan, C.H., et al., Diffusion-weighted MRI in the detection of prostate cancer: meta-analysis. AJR Am J Roentgenol, 2012. **199**(4): p. 822-829.
27. Sciarra, A., et al., Value of magnetic resonance spectroscopy imaging and dynamic contrast-enhanced imaging for detecting prostate cancer foci in men with prior negative biopsy. Clin Cancer Res, 2010. **16**(6): p. 1875-1873.
28. Maurer, T., et al., Current use of PSMA-PET in prostate cancer management. Nat Rev Urol, 2016. **13**(4): p. 226-235.
29. Yagci, A.B., et al., The value of diffusion-weighted MRI for prostate cancer detection and localization. Diagn Interv Radiol, 2011. **17**(2): p. 130-134.
30. Heesakkers, R.A., et al., MRI with a lymph-node-specific contrast agent as an alternative to CT scan and lymph-node dissection in patients with prostate cancer: a prospective multicohort study. Lancet Oncol, 2008. **9**(9): p. 850-856.

31. Hovels, A.M., et al., The diagnostic accuracy of CT and MRI in the staging of pelvic lymph nodes in patients with prostate cancer: a meta-analysis. Clin Radiol, 2008. **63**(4): p. 387-395.
32. Beer, A.J., et al., Radionuclide and hybrid imaging of recurrent prostate cancer. Lancet Oncol, 2011. **12**(2): p. 181-191.
33. Even-Sapir, E., Z. Keidar, and R. Bar-Shalom, Hybrid imaging (SPECT/CT and PET/CT)--improving the diagnostic accuracy of functional/metabolic and anatomic imaging. Semin Nucl Med, 2009. **39**(4): p. 264-275.
34. Vallabhajosula, S., Molecular imaging: radiopharmaceuticals for PET and SPECT. 2009: Springer Science & Business Media.
35. Kuhl, D.E., J. Hale, and W.L. Eaton, Transmission Scanning: A Useful Adjunct to Conventional Emission Scanning for Accurately Keying Isotope Deposition to Radiographic Anatomy. Radiology, 1966. **87**(2): p. 278-284.
36. Bowley, A.R., et al., A radioisotope scanner for rectilinear, arc, transverse section and longitudinal section scanning: (ASS--the Aberdeen Section Scanner). Br J Radiol, 1973. **46**(544): p. 262-271.
37. Jaszczak, R.J., et al., Radionuclide emission computed tomography of the head with 99mTc and a scintillation camera. Journal of nuclear medicine: official publication, Society of Nuclear Medicine, 1977. **18**(4): p. 373-380.
38. Wrenn, F.R., Jr., M.L. Good, and P. Handler, The use of positron-emitting radioisotopes for the localization of brain tumors. Science, 1951. **113**(2940): p. 525-527.
39. Sweet, W.H., The uses of nuclear disintegration in the diagnosis and treatment of brain tumor. N Engl J Med, 1951. **245**(23): p. 875-878.
40. Kuhl, D.E. and R.Q. Edwards, The Mark III Scanner: A Compact Device for Multiple-View and Section Scanning of the Brain. Radiology, 1970. **96**(3): p. 563-570.
41. Larsson, S.A., Gamma camera emission tomography. Acta Radiologica, 1980. 363: p. 1-75.
42. Cherry, S.R., et al., Total-body imaging: Transforming the role of positron emission tomography. Sci Transl Med, 2017. **9**(381).
43. Kuhl, D.E. and R.Q. Edwards, Image Separation Radioisotope Scanning. Radiology, 1963. **80**(4): p. 653-662.
44. Townsend, D.W., Dual-modality imaging: combining anatomy and function. J Nucl Med, 2008. **49**(6): p. 938-955.
45. Bockisch, A., et al., Hybrid imaging by SPECT/CT and PET/CT: proven outcomes in cancer imaging. Semin Nucl Med, 2009. **39**(4): p. 276-289.

46. Maurer, A.H., Combined imaging modalities: PET/CT and SPECT/CT. Health Phys, 2008. **95**(5): p. 571-576.
47. Beyer, T., et al., A combined PET/CT scanner for clinical oncology. J Nucl Med, 2000. **41**(8): p. 1369-1379.
48. Even-Sapir, E., et al., The new technology of combined transmission and emission tomography in evaluation of endocrine neoplasms. J Nucl Med, 2001. **42**(7): p. 998-1004.
49. Delso, G., et al., Performance measurements of the Siemens mMR integrated whole-body PET/MR scanner. J Nucl Med, 2011. **52**(12): p. 1914-1922.
50. Sauter, A.W., et al., Combined PET/MRI: one step further in multimodality imaging. Trends Mol Med, 2010. **16**(11): p. 508-515.
51. Pichler, B.J., et al., PET/MRI: paving the way for the next generation of clinical multimodality imaging applications. J Nucl Med, 2010. **51**(3): p. 333-336.
52. Turkington, T.G., Introduction to PET instrumentation. J Nucl Med Technol, 2001. **29**(1): p. 4-11.
53. Dietlein, M., K. Kopka, and M. Schmidt, Nuklearmedizin: Basiswissen und klinische Anwendung. 2017: Schattauer GmbH.
54. Cherry, S.R., J.A. Sorenson, and M.E. Phelps, Physics in nuclear medicine e-Book. 2012: Elsevier Health Sciences.
55. Cherry, S.R., J.A. Sorenson, and M.E. Phelps, chapter 18 - Positron Emission Tomography, in Physics in Nuclear Medicine (Fourth Edition), S.R. Cherry, J.A. Sorenson, and M.E. Phelps, Editors. 2012, W.B. Saunders: Philadelphia. p. 307-343.
56. Turkington, T.G., PET imaging basics, in Clinical PET-CT in Radiology. 2011, Springer. p. 21-28.
57. Cole, E.L., et al., Radiosyntheses using Fluorine-18: the Art and Science of Late Stage Fluorination. Curr Top Med Chem, 2014. **14**(7): p. 875-900.
58. Ziegler, S.I., Positron Emission Tomography: Principles, Technology, and Recent Developments. Nucl Phys A, 2005. **752**: p. 679-687.
59. Thie, J.A., Understanding the standardized uptake value, its methods, and implications for usage. J Nucl Med, 2004. **45**(9): p. 1431-1434.
60. Levin, C.S. and E.J. Hoffman, Calculation of positron range and its effect on the fundamental limit of positron emission tomography system spatial resolution. Phys Med Biol, 1999. **44**(3): p. 781-799.
61. Sanchez-Crespo, A., P. Andreo, and S.A. Larsson, Positron flight in human tissues and its influence on PET image spatial resolution. Eur J Nucl Med Mol Imaging, 2004. **31**(1): p. 44-51.

62. Moses, W.W., Fundamental Limits of Spatial Resolution in PET. Nuclear instruments & methods in physics research. Section A, Accelerators, spectrometers, detectors and associated equipment, 2011. **648** (Suppl 1): p. S236-S240.
63. Phelps, M.E., et al., Effect of positron range on spatial resolution. J Nucl Med, 1975. **16**(7): p. 649-652.
64. Colombino, P., B. Fiscella, and L. Trossi, Study of positronium in water and ice from 22 to -144 °C by annihilation quanta measurements. Il Nuovo Cimento (1955-1965), 1965. **38**(2): p. 707-723.
65. Saha, G.B., Performance characteristics of PET scanners, in Basics of PET Imaging. 2016, Springer. p. 121-142.
66. DiFilippo, F.P., et al., Small Animal Imaging using a Clinical Positron Emission Tomography/Computed Tomography and Super-Resolution. Mol Im, 2012. **11**(3): p. 210-219.
67. James, M.L. and S.S. Gambhir, A Molecular Imaging Primer: Modalities, Imaging Agents, and Applications. Phys Rev, 2012. **92**(2): p. 897-965.
68. Karakatsanis, N.A., et al., Dynamic whole body PET parametric imaging: I. Concept, acquisition protocol optimization and clinical application. Phys Med Biol, 2013. **58**(20): p. 7391-7418.
69. Peterson, T.E. and L.R. Furenlid, SPECT detectors: the Anger Camera and beyond. Phys Med Biol, 2011. **56**(17): p. R145-182.
70. Vallabhajosula, S., Chapter 6 - PET and SPECT Scanners. Springer, 2009: p. 59-81.
71. Groch, M.W. and W.D. Erwin, SPECT in the Year 2000: Basic Principles. J Nuc Med Technol, 2000. **28**(4): p. 233-244.
72. Cherry, S.R., J.A. Sorenson, and M.E. Phelps, chapter 4 - Decay of Radioactivity, in Physics in Nuclear Medicine (Fourth Edition). 2012, W.B. Saunders: Philadelphia. p. 31-42.
73. Haralampieva, D.G., et al., Non-Invasive Imaging Modalities for Clinical Investigation in Regenerative Medicine, Cells and Biomaterials in Regenerative Medicine. InTech, 2014. p.176-191.
74. van der Have, F., et al., U-SPECT-II: An Ultra-High-Resolution Device for Molecular Small-Animal Imaging. J Nucl Med, 2009. **50**(4): p. 599-605.
75. Fahey, F.H., et al., Sensitivity, resolution and image quality with a multi-head SPECT camera. J Nucl Med, 1992. **33**(10): p. 1859-1863.
76. Gullberg, G.T., et al., Dynamic single photon emission computed tomography--basic principles and cardiac applications. Phys Med Biol, 2010. **55**(20): p. R111-191.
77. Hutton, B.F., Recent advances in iterative reconstruction for clinical SPECT/PET and CT. Acta Oncologica, 2011. **50**(6): p. 851-858.

78. Bateman, T.M., Advantages and disadvantages of PET and SPECT in a busy clinical practice. J Nucl Cardiol, 2012. **19**(Suppl 1): p. S3-11.
79. Rahmim, A. and H. Zaidi, PET versus SPECT: strengths, limitations and challenges. Nucl Med Commun, 2008. **29**(3): p. 193-207.
80. Zimmermann, R.G., Why are investors not interested in my radiotracer? The industrial and regulatory constraints in the development of radiopharmaceuticals. Nuc Med Biol, 2013. **40**(2): p. 155-166.
81. Bhattacharyya, S. and M. Dixit, Metallic radionuclides in the development of diagnostic and therapeutic radiopharmaceuticals. Dalton Trans, 2011. **40**(23): p. 6112-6128.
82. Nayak, T.K. and M.W. Brechbiel, Radioimmunoimaging with longer-lived positron-emitting radionuclides: potentials and challenges. Bioconjug Chem, 2009. **20**(5): p. 825-841.
83. Chatalic, K., Towards Personalized Treatment for Prostate Cancer: GRPR- and PSMA-targeted theranostic agents for imaging and therapy of prostate cancer. 2016, Erasmus University Rotterdam.
84. Conti, M. and L. Eriksson, Physics of pure and non-pure positron emitters for PET: a review and a discussion. EJNMMI Phys, 2016. **3**(8): p. 1-9.
85. Krause, B.J., et al., The detection rate of [11C]choline-PET/CT depends on the serum PSA-value in patients with biochemical recurrence of prostate cancer. Eur J Nucl Med Mol Imaging, 2008. **35**(1): p. 18-23.
86. Kitajima, K., R.C. Murphy, and M.A. Nathan, Choline PET/CT for imaging prostate cancer: an update. Ann Nucl Med, 2013. **27**(7): p. 581-591.
87. Umbehr, M.H., et al., The role of 11C-choline and 18F-fluorocholine positron emission tomography (PET) and PET/CT in prostate cancer: a systematic review and meta-analysis. Eur Urol, 2013. **64**(1): p. 106-117.
88. Castellucci, P., et al., Early biochemical relapse after radical prostatectomy: which prostate cancer patients may benefit from a restaging 11C-Choline PET/CT scan before salvage radiation therapy? J Nucl Med, 2014. **55**(9): p. 1424-1429.
89. Krause, B.J., M. Souvatzoglou, and U. Treiber, Imaging of prostate cancer with PET/CT and radioactively labeled choline derivates. Urol Oncol, 2013. **31**(4): p. 427-435.
90. Salminen, E., et al., Investigations with FDG-PET scanning in prostate cancer show limited value for clinical practice. Acta Oncol, 2002. **41**(5): p. 425-429.
91. Liu, I.J., et al., Fluorodeoxyglucose positron emission tomography studies in diagnosis and staging of clinically organ-confined prostate cancer. Urology, 2001. **57**(1): p. 108-111.

92. Jadvar, H., et al., Prospective evaluation of 18F-NaF and 18F-FDG PET/CT in detection of occult metastatic disease in biochemical recurrence of prostate cancer. Clin Nucl Med, 2012. **37**(7): p. 637-643.
93. Beer, A.J., et al., Radionuclide and hybrid imaging of recurrent prostate cancer. Lancet Oncol, 2011. **12**(2): p. 181-191.
94. Bouchelouche, K., et al., PET/CT Imaging and Radioimmunotherapy of Prostate Cancer. Semin Nucl Med, 2011. **41**(1): p. 29-44.
95. Lütje, S., et al., PSMA Ligands for Radionuclide Imaging and Therapy of Prostate Cancer: Clinical Status. Theranostics, 2015. **5**(12): p. 1388-1401.
96. Ceci, F., et al., New aspects of molecular imaging in prostate cancer. Methods, 2017. **130**: p. 36-41.
97. Chang, S.S., Overview of prostate-specific membrane antigen. Rev Urol, 2004. **6**(Suppl_10): p. S13-18.
98. Perner, S., et al., Prostate-specific membrane antigen expression as a predictor of prostate cancer progression. Hum Pathol, 2007. **38**(5): p. 696-701.
99. Haberkorn, U., PSMA ligands for diagnosis and therapy of prostate cancer. Cancer Imaging, 2014. **14**(Suppl 1): p. O10-O10.
100. Zhou, J., et al., NAAG peptidase inhibitors and their potential for diagnosis and therapy. Nat Rev Drug Discov, 2005. **4**(12): p. 1015-1026.
101. Mesters, J.R., et al., Structure of glutamate carboxypeptidase II, a drug target in neuronal damage and prostate cancer. EMBO J, 2006. **25**(6): p. 1375-1384.
102. Carter, R.E., A.R. Feldman, and J.T. Coyle, Prostate-specific membrane antigen is a hydrolase with substrate and pharmacologic characteristics of a neuropeptidase. Proc Natl Acad Sci U S A, 1996. **93**(2): p. 749-753.
103. Tiffany, C.W., et al., Characterization of the enzymatic activity of PSM: comparison with brain NAALADase. Prostate, 1999. **39**(1): p. 28-35.
104. Pinto, J.T., et al., Prostate-specific membrane antigen: a novel folate hydrolase in human prostatic carcinoma cells. Clin Cancer Res, 1996. **2**(9): p. 1445-1451.
105. Fair, W.R., R.S. Israeli, and W.D. Heston, Prostate-specific membrane antigen. Prostate, 1997. **32**(2): p. 140-148.
106. Horoszewicz, J.S., E. Kawinski, and G. Murphy, Monoclonal antibodies to a new antigenic marker in epithelial prostatic cells and serum of prostatic cancer patients. Anticancer Res, 1987. **7**(5B): p. 927-935.
107. Mhawech-Fauceglia, P., et al., Prostate-specific membrane antigen (PSMA) protein expression in normal and neoplastic tissues and its sensitivity and specificity in prostate adenocarcinoma: an immunohistochemical study using mutiple tumour tissue microarray technique. Histopathology, 2007. **50**(4): p. 472-483.

108. Sacha, P., et al., Expression of glutamate carboxypeptidase II in human brain. Neuroscience, 2007. **144**(4): p. 1361-1372.
109. Silver, D.A., et al., Prostate-specific membrane antigen expression in normal and malignant human tissues. Clin Cancer Res, 1997. **3**(1): p. 81-85.
110. Israeli, R.S., et al., Expression of the prostate-specific membrane antigen. Cancer Res, 1994. **54**(7): p. 1807-1811.
111. Robinson, M.B., et al., Hydrolysis of the brain dipeptide N-acetyl-L-aspartyl-L-glutamate. Identification and characterization of a novel N-acetylated alpha-linked acidic dipeptidase activity from rat brain. J Biol Chem, 1987. **262**(30): p. 14498-14506.
112. Slusher, B.S., et al., Rat brain N-acetylated alpha-linked acidic dipeptidase activity. Purification and immunologic characterization. J Biol Chem, 1990. **265**(34): p. 21297-21301.
113. Berger, U.V., R.E. Carter, and J.T. Coyle, The immunocytochemical localization of N-acetylaspartyl glutamate, its hydrolysing enzyme NAALADase, and the NMDAR-1 receptor at a vertebrate neuromuscular junction. Neuroscience, 1995. **64**(4): p. 847-850.
114. Carter, R.E., A.R. Feldman, and J.T. Coyle, Prostate-specific membrane antigen is a hydrolase with substrate and pharmacologic characteristics of a neuropeptidase. Proc Natl Acad Sci U S A, 1996. **93**(2): p. 749-753.
115. Tasch, J., et al., A unique folate hydrolase, prostate-specific membrane antigen (PSMA): a target for immunotherapy? Crit Rev Immunol, 2001. **21**(1-3): p. 249-261.
116. Ghosh, A. and W.D. Heston, Tumor target prostate specific membrane antigen (PSMA) and its regulation in prostate cancer. J Cell Biochem, 2004. **91**(3): p. 528-539.
117. Heston, W.D., Characterization and glutamyl preferring carboxypeptidase function of prostate specific membrane antigen: a novel folate hydrolase. Urology, 1997. **49**(3A Suppl): p. 104-112.
118. Zhao, R., L.H. Matherly, and I.D. Goldman, Membrane transporters and folate homeostasis: intestinal absorption and transport into systemic compartments and tissues. Expert Rev Mol Med, 2009. **28**(11): e4.
119. Ristau, B.T., D.S. O'Keefe, and D.J. Bacich, The prostate-specific membrane antigen: lessons and current clinical implications from 20 years of research. Urol Oncol, 2014. **32**(3): p. 272-279.
120. Bařinka, C., et al., Glutamate Carboxypeptidase II in Diagnosis and Treatment of Neurologic Disorders and Prostate Cancer. Curr Med Chem, 2012. **19**(6): p. 856-870.

121. Wright, G.L., Jr., et al., Expression of prostate-specific membrane antigen in normal, benign, and malignant prostate tissues. Urol Oncol, 1995. **1**(1): p. 18-28.
122. Sweat, S.D., et al., Prostate-specific membrane antigen expression is greatest in prostate adenocarcinoma and lymph node metastases. Urology, 1998. **52**(4): p. 637-640.
123. Bostwick, D.G., et al., Prostate specific membrane antigen expression in prostatic intraepithelial neoplasia and adenocarcinoma. Cancer, 1998. **82**(11): p. 2256-2261.
124. Israeli, R.S., et al., Expression of the prostate-specific membrane antigen. Cancer Res, 1994. **54**(7): p. 1807-1811.
125. Wright, G.L., Jr., et al., Upregulation of prostate-specific membrane antigen after androgen-deprivation therapy. Urology, 1996. **48**(2): p. 326-334.
126. Sweat, S.D., et al., Prostate-specific membrane antigen expression is greatest in prostate adenocarcinoma and lymph node metastases. Urology, 1998. **52**(4): p. 637-640.
127. Schulke, N., et al., The homodimer of prostate-specific membrane antigen is a functional target for cancer therapy. Proc Natl Acad Sci U S A, 2003. **100**(22): p. 12590-12595.
128. Lapidus, R.G., et al., Prostate-specific membrane antigen (PSMA) enzyme activity is elevated in prostate cancer cells. The Prostate, 2000. **45**(4): p. 350-354.
129. Arundhati, G. and H.W. D.W., Tumor target prostate specific membrane antigen (PSMA) and its regulation in prostate cancer. J Cell Biochem, 2004. **91**(3): p. 528-539.
130. Rycyna, K.J., D.J. Bacich, and D.S. O'Keefe, Opposing roles of folate in prostate cancer. Urology, 2013. **82**(6): p. 1197-1203.
131. Murphy, G.P., et al., Current evaluation of the tissue localization and diagnostic utility of prostate specific membrane antigen. Cancer, 1998. **83**(11): p. 2259-2269.
132. Rawlings, N.D., D.P. Tolle, and A.J. Barrett, MEROPS: the peptidase database. Nucleic Acids Res, 2004. **32**(Database issue): p. D160-164.
133. Leek, J., et al., Prostate-specific membrane antigen: evidence for the existence of a second related human gene. Br J Cancer, 1995. **72**(3): p. 583-588.
134. Barinka, C., et al., Structural basis of interactions between human glutamate carboxypeptidase II and its substrate analogs. J Mol Biol, 2008. **376**(5): p. 1438-1450.
135. Barinka, C., et al., A high-resolution structure of ligand-free human glutamate carboxypeptidase II. Acta Crystallogr Sect F Struct Biol Cryst Commun, 2007. **63**(Pt 3): p. 150-153.
136. Pavlicek, J., J. Ptacek, and C. Barinka, Glutamate carboxypeptidase II: an overview of structural studies and their importance for structure-based drug design and

deciphering the reaction mechanism of the enzyme. Curr Med Chem, 2012. **19**(9): p. 1300-1309.

137. Kopka, K., et al., Glu-Ureido-Based Inhibitors of Prostate-Specific Membrane Antigen: Lessons Learned During the Development of a Novel Class of Low-Molecular-Weight Theranostic Radiotracers. J Nucl Med, 2017. **58**(Suppl 2): p. 17s-26s.
138. Rong, S.-B., et al., Molecular Modeling of the Interactions of Glutamate Carboxypeptidase II with Its Potent NAAG-Based Inhibitors. J Med Chem, 2002. **45**(19): p. 4140-4152.
139. Gourni, E. and G. Henriksen, Metal-Based PSMA Radioligands. Molecules, 2017. **22**(4): p.524-558.
140. Maung, J., et al., Probing for a hydrophobic a binding register in prostate-specific membrane antigen with phenylalkylphosphonamidates. Bioorg Med Chem, 2004. **12**(18): p. 4969-4979.
141. Stoermer, D., et al., Design, Synthesis, and Pharmacological Evaluation of Glutamate Carboxypeptidase II (GCPII) Inhibitors Based on Thioalkylbenzoic Acid Scaffolds. J Med Chem, 2012. **55**(12): p. 5922-5932.
142. Majer, P., et al., Synthesis and biological evaluation of thiol-based inhibitors of glutamate carboxypeptidase II: discovery of an orally active GCP II inhibitor. J Med Chem, 2003. **46**(10): p. 1989-1996.
143. Barinka, C., et al., Interactions between human glutamate carboxypeptidase II and urea-based inhibitors: structural characterization. J Med Chem, 2008. **51**(24): p. 7737-7743.
144. Kozikowski, A.P., et al., Design of remarkably simple, yet potent urea-based inhibitors of glutamate carboxypeptidase II (NAALADase). J Med Chem, 2001. **44**(3): p. 298-301.
145. Kozikowski, A.P., et al., Synthesis of urea-based inhibitors as active site probes of glutamate carboxypeptidase II: efficacy as analgesic agents. J Med Chem, 2004. **47**(7): p. 1729-1738.
146. More, S.S. and R. Vince, A metabolically stable tight-binding transition-state inhibitor of glyoxalase-I. Bioorg Med Chem Lett, 2006. **16**(23): p. 6039-6042.
147. Barinka, C., et al., A high-resolution structure of ligand-free human glutamate carboxypeptidase II. Acta Crystallogr Sect F Struct Biol Cryst Commun, 2007. **63**(Pt 3): p. 150-153.
148. Jackson, P.F., et al., Design and pharmacological activity of phosphinic acid based NAALADase inhibitors. J Med Chem, 2001. **44**(24): p. 4170-4175.
149. Oliver, A.J., et al., Conformational and SAR analysis of NAALADase and PSMA inhibitors. Bioorg Med Chem, 2003. **11**(20): p. 4455-4461.

150. Pavlicek, J., et al., Structural characterization of P1'-diversified urea-based inhibitors of glutamate carboxypeptidase II. Bioorg Med Chem Lett, 2014. **24**(10): p. 2340-2345.
151. Wang, H., et al., Bioisosterism of urea-based GCPII inhibitors: Synthesis and structure-activity relationship studies. Bioorg Med Chem Lett, 2010. **20**(1): p. 392-397.
152. Ferraris, D.V., K. Shukla, and T. Tsukamoto, Structure-activity relationships of glutamate carboxypeptidase II (GCPII) inhibitors. Curr Med Chem, 2012. **19**(9): p. 1282-1294.
153. Kopka, K., et al., Glu-Ureido–Based Inhibitors of Prostate-Specific Membrane Antigen: Lessons Learned During the Development of a Novel Class of Low-Molecular-Weight Theranostic Radiotracers. J Nucl Med, 2017. **58**(Supplement 2): p. 17S-26S.
154. Jackson, P.F., et al., Design, synthesis, and biological activity of a potent inhibitor of the neuropeptidase N-acetylated alpha-linked acidic dipeptidase. J Med Chem, 1996. **39**(2): p. 619-622.
155. Barinka, C., et al., Structural insight into the pharmacophore pocket of human glutamate carboxypeptidase II. J Med Chem, 2007. **50**(14): p. 3267-3273.
156. Zhang, A.X., et al., A Remote Arene-Binding Site on Prostate Specific Membrane Antigen Revealed by Antibody-Recruiting Small Molecules. J Am Chem Soc, 2010. **132**(36): p. 12711-12716.
157. Barinka, C., et al., Substrate specificity, inhibition and enzymological analysis of recombinant human glutamate carboxypeptidase II. J Neurochem, 2002. **80**(3): p. 477-487.
158. Mhaka, A., et al., Use of methotrexate-based peptide substrates to characterize the substrate specificity of prostate-specific membrane antigen (PSMA). Cancer Biol Ther, 2004. **3**(6): p. 551-558.
159. Rajasekaran, S.A., et al., A novel cytoplasmic tail MXXXL motif mediates the internalization of prostate-specific membrane antigen. Mol Biol Cell, 2003. **14**(12): p. 4835-4845.
160. Anilkumar, G., et al., Prostate-specific membrane antigen association with filamin A modulates its internalization and NAALADase activity. Cancer Res, 2003. **63**(10): p. 2645-2648.
161. Anilkumar, G., et al., Association of prostate-specific membrane antigen with caveolin-1 and its caveolae-dependent internalization in microvascular endothelial cells: implications for targeting to tumor vasculature. Microvasc Res, 2006. **72**(1-2): p. 54-61.

162. Goodman, O.B., Jr., et al., Interaction of prostate specific membrane antigen with clathrin and the adaptor protein complex-2. Int J Oncol, 2007. **31**(5): p. 1199-1203.
163. Liu, H., et al., Constitutive and antibody-induced internalization of prostate-specific membrane antigen. Cancer Res, 1998. **58**(18): p. 4055-4060.
164. Liu, T., et al., Pseudoirreversible inhibition of prostate-specific membrane antigen by phosphoramidate peptidomimetics. Biochemistry, 2008. **47**(48): p. 12658-12660.
165. Schottelius, M., et al., N-Terminal Sugar Conjugation and C-Terminal Thr-for-Thr(ol) Exchange in Radioiodinated Tyr3-octreotide: Effect on Cellular Ligand Trafficking in Vitro and Tumor Accumulation in Vivo. J Med Chem, 2005. **48**(8): p. 2778-2789.
166. Storch, D., et al., Evaluation of [99mTc/EDDA/HYNIC0]octreotide derivatives compared with [111In-DOTA0,Tyr3, Thr8]octreotide and [111In-DTPA0]octreotide: does tumor or pancreas uptake correlate with the rate of internalization? J Nucl Med, 2005. **46**(9): p. 1561-1569.
167. Will, L., et al., Radiolabeled prostate-specific membrane antigen small-molecule inhibitors. Q J Nucl Med Mol Imaging, 2017. **61**(2): p. 168-180.
168. Eder, M., et al., PSMA as a target for radiolabelled small molecules. Eur J Nucl Med Mol Imaging, 2013. **40**(6): p. 819-823.
169. Yao, D., et al., The utility of monoclonal antibodies in the imaging of prostate cancer. Semin Urol Oncol, 2002. **20**(3): p. 211-218.
170. Lutje, S., et al., PSMA Ligands for Radionuclide Imaging and Therapy of Prostate Cancer: Clinical Status. Theranostics, 2015. **5**(12): p. 1388-1401.
171. Franc, B.L., et al., Detection and localization of carcinoma within the prostate using high resolution transrectal gamma imaging (TRGI) of monoclonal antibody directed at prostate specific membrane antigen (PSMA)--proof of concept and initial imaging results. Eur J Radiol, 2013. **82**(11): p. 1877-1884.
172. Ponsky, L.E., et al., Evaluation of preoperative ProstaScint scans in the prediction of nodal disease. Prostate Cancer Prostatic Dis, 2002. **5**(2): p. 132-135.
173. Sodee, D.B., et al., Multicenter ProstaScint imaging findings in 2154 patients with prostate cancer. The ProstaScint Imaging Centers. Urology, 2000. **56**(6): p. 988-993.
174. Troyer, J.K., et al., Biochemical characterization and mapping of the 7E11-C5.3 epitope of the prostate-specific membrane antigen. Urol Oncol, 1995. **1**(1): p. 29-37.
175. Taneja, S.S., ProstaScint(R) Scan: Contemporary Use in Clinical Practice. Rev Urol, 2004. **6**(Suppl_10): p. S19-28.
176. Bander, N.H., et al., Targeting metastatic prostate cancer with radiolabeled monoclonal antibody J591 to the extracellular domain of prostate specific membrane antigen. J Urol, 2003. **170**(5): p. 1717-1721.

177. Tagawa, S.T., et al., Phase II study of Lutetium-177-labeled anti-prostate-specific membrane antigen monoclonal antibody J591 for metastatic castration-resistant prostate cancer. Clin Cancer Res, 2013. **19**(18): p. 5182-5191.
178. Vallabhajosula, S., et al., Pharmacokinetics and biodistribution of 111In- and 177Lu-labeled J591 antibody specific for prostate-specific membrane antigen: prediction of 90Y-J591 radiation dosimetry based on 111In or 177Lu? J Nucl Med, 2005. **46**(4): p. 634-641.
179. Osborne, J.R., et al., Prostate-specific membrane antigen-based imaging. Urol Oncol, 2013. **31**(2): p. 144-154.
180. Foss, C.A., et al., GCPII imaging and cancer. Curr Med Chem, 2012. **19**(9): p. 1346-1359.
181. Barrett, J.A., et al., First-in-man evaluation of 2 high-affinity PSMA-avid small molecules for imaging prostate cancer. J Nucl Med, 2013. **54**(3): p. 380-387.
182. Hillier, S.M., et al., Preclinical evaluation of novel glutamate-urea-lysine analogues that target prostate-specific membrane antigen as molecular imaging pharmaceuticals for prostate cancer. Cancer Res, 2009. **69**(17): p. 6932-6940.
183. Hillier, S.M., et al., 99mTc-labeled small-molecule inhibitors of prostate-specific membrane antigen for molecular imaging of prostate cancer. J Nucl Med, 2013. **54**(8): p. 1369-1376.
184. Lu, G., et al., Synthesis and SAR of 99mTc/Re-labeled small molecule prostate specific membrane antigen inhibitors with novel polar chelates. Bioorg Med Chem Lett, 2013. **23**(5): p. 1557-1563.
185. Vallabhajosula, S., et al., 99mTc-labeled small-molecule inhibitors of prostate-specific membrane antigen: pharmacokinetics and biodistribution studies in healthy subjects and patients with metastatic prostate cancer. J Nucl Med, 2014. **55**(11): p. 1791-1798.
186. Banerjee, S.R., et al., Synthesis and evaluation of technetium-99m- and rhenium-labeled inhibitors of the prostate-specific membrane antigen (PSMA). J Med Chem, 2008. **51**(15): p. 4504-4517.
187. Ray Banerjee, S., et al., Effect of chelators on the pharmacokinetics of (99m)Tc-labeled imaging agents for the prostate-specific membrane antigen (PSMA). J Med Chem, 2013. **56**(15): p. 6108-6121.
188. Maresca, K.P., et al., Novel polar single amino acid chelates for technetium-99m tricarbonyl-based radiopharmaceuticals with enhanced renal clearance: application to octreotide. Bioconjug Chem, 2010. **21**(6): p. 1032-1042.
189. Maresca, K., et al., Development of a simple kit for Tc-99m-MIP-1404, a single amino acid chelate (SAAC II) derived small molecule inhibitor of prostate specific membrane

antigen (PSMA) for imaging prostate cancer. J Nucl Med, 2012. **53**(supplement 1): p. 523.

190. Eder, M., et al., 68Ga-complex lipophilicity and the targeting property of a urea-based PSMA inhibitor for PET imaging. Bioconjug Chem, 2012. **23**(4): p. 688-697.
191. Afshar-Oromieh, A., et al., PET imaging with a [68Ga]gallium-labelled PSMA ligand for the diagnosis of prostate cancer: biodistribution in humans and first evaluation of tumour lesions. Eur J Nucl Med Mol Imaging, 2013. **40**(4): p. 486-495.
192. Afshar-Oromieh, A., et al., Comparison of PET imaging with a (68)Ga-labelled PSMA ligand and (18)F-choline-based PET/CT for the diagnosis of recurrent prostate cancer. Eur J Nucl Med Mol Imaging, 2014. **41**(1): p. 11-20.
193. Afshar-Oromieh, A., et al., The diagnostic value of PET/CT imaging with the (68)Ga-labelled PSMA ligand HBED-CC in the diagnosis of recurrent prostate cancer. Eur J Nucl Med Mol Imaging, 2015. **42**(2): p. 197-209.
194. Eiber, M., et al., Evaluation of Hybrid (6)(8)Ga-PSMA Ligand PET/CT in 248 Patients with Biochemical Recurrence After Radical Prostatectomy. J Nucl Med, 2015. **56**(5): p. 668-674.
195. Ceci, F., et al., (68)Ga-PSMA PET/CT for restaging recurrent prostate cancer: which factors are associated with PET/CT detection rate? Eur J Nucl Med Mol Imaging, 2015. **42**(8): p. 1284-1294.
196. Witkowska-Patena, E., A. Mazurek, and M. Dziuk, 68Ga-PSMA PET/CT imaging in recurrent prostate cancer: Where are we now? Cent European J Urol, 2017. **70**(1): p. 37-43.
197. Sterzing, F., et al., (68)Ga-PSMA-11 PET/CT: a new technique with high potential for the radiotherapeutic management of prostate cancer patients. Eur J Nucl Med Mol Imaging, 2016. **43**(1): p. 34-41.
198. Freitag, M.T., et al., Comparison of hybrid (68)Ga-PSMA PET/MRI and (68)Ga-PSMA PET/CT in the evaluation of lymph node and bone metastases of prostate cancer. Eur J Nucl Med Mol Imaging, 2016. **43**(1): p. 70-83.
199. Herlemann, A., et al., 68Ga-PSMA Positron Emission Tomography/Computed Tomography Provides Accurate Staging of Lymph Node Regions Prior to Lymph Node Dissection in Patients with Prostate Cancer. Eur Urol, 2016. **70**(4): p. 553-557.
200. Schlenkhoff, C.D., et al., 68Ga-Labeled Anti-Prostate-Specific Membrane Antigen Peptide as Marker for Androgen Deprivation Therapy Response in Prostate Cancer. Clin Nucl Med, 2016. **41**(5): p. 423-425.
201. Verburg, F.A., et al., Extent of disease in recurrent prostate cancer determined by [(68)Ga]PSMA-HBED-CC PET/CT in relation to PSA levels, PSA doubling time and Gleason score. Eur J Nucl Med Mol Imaging, 2016. **43**(3): p. 397-403.

202. Maurer, T., et al., Diagnostic Efficacy of (68)Gallium-PSMA Positron Emission Tomography Compared to Conventional Imaging for Lymph Node Staging of 130 Consecutive Patients with Intermediate to High Risk Prostate Cancer. J Urol, 2016. **195**(5): p. 1436-1443.
203. Giesel, F.L., et al., PSMA PET/CT with Glu-urea-Lys-(Ahx)-[(6)(8)Ga(HBED-CC)] versus 3D CT volumetric lymph node assessment in recurrent prostate cancer. Eur J Nucl Med Mol Imaging, 2015. **42**(12): p. 1794-1800.
204. Krohn, T., et al., [(68)Ga]PSMA-HBED uptake mimicking lymph node metastasis in coeliac ganglia: an important pitfall in clinical practice. Eur J Nucl Med Mol Imaging, 2015. **42**(2): p. 210-214.
205. Benesova, M., et al., Preclinical Evaluation of a Tailor-Made DOTA-Conjugated PSMA Inhibitor with Optimized Linker Moiety for Imaging and Endoradiotherapy of Prostate Cancer. J Nucl Med, 2015. **56**(6): p. 914-920.
206. Afshar-Oromieh, A., et al., The Theranostic PSMA Ligand PSMA-617 in the Diagnosis of Prostate Cancer by PET/CT: Biodistribution in Humans, Radiation Dosimetry, and First Evaluation of Tumor Lesions. J Nucl Med, 2015. **56**(11): p. 1697-1705.
207. Weineisen, M., et al., 68Ga- and 177Lu-Labeled PSMA I&T: Optimization of a PSMA-Targeted Theranostic Concept and First Proof-of-Concept Human Studies. J Nucl Med, 2015. **56**(8): p. 1169-1176.
208. Herrmann, K., et al., Biodistribution and radiation dosimetry for a probe targeting prostate-specific membrane antigen for imaging and therapy. J Nucl Med, 2015. **56**(6): p. 855-861.
209. Cho, S.Y., et al., Biodistribution, tumor detection, and radiation dosimetry of 18F-DCFBC, a low-molecular-weight inhibitor of prostate-specific membrane antigen, in patients with metastatic prostate cancer. J Nucl Med, 2012. **53**(12): p. 1883-1891.
210. Rowe, S.P., et al., (18)F-DCFBC PET/CT for PSMA-Based Detection and Characterization of Primary Prostate Cancer. J Nucl Med, 2015. **56**(7): p. 1003-1010.
211. Rowe, S.P., et al., PSMA-Based [(18)F]DCFPyL PET/CT Is Superior to Conventional Imaging for Lesion Detection in Patients with Metastatic Prostate Cancer. Mol Imaging Biol, 2016. **18**(3): p. 411-419.
212. Chen, Y., et al., 2-(3-{1-Carboxy-5-[(6-[18F]fluoro-pyridine-3-carbonyl)-amino]-pentyl}-ureido)-pen tanedioic acid, [18F]DCFPyL, a PSMA-based PET imaging agent for prostate cancer. Clin Cancer Res, 2011. **17**(24): p. 7645-7653.
213. Szabo, Z., et al., Initial Evaluation of [(18)F]DCFPyL for Prostate-Specific Membrane Antigen (PSMA)-Targeted PET Imaging of Prostate Cancer. Mol Imaging Biol, 2015. **17**(4): p. 565-574.

214. Dietlein, M., et al., Comparison of [(18)F]DCFPyL and [(68)Ga]Ga-PSMA-HBED-CC for PSMA-PET Imaging in Patients with Relapsed Prostate Cancer. Mol Imaging Biol, 2015. **17**(4): p. 575-584.
215. Cardinale, J., et al., Preclinical Evaluation of [18F]PSMA-1007: A New PSMA-Ligand for Prostate Cancer Imaging. J Nucl Med, 2016. **27**(116): p. 425-431.
216. Giesel, F.L., et al., 18F-Labelled PSMA-1007 shows similarity in structure, biodistribution and tumour uptake to the theragnostic compound PSMA-617. Eur J Nucl Med Mol Imaging, 2016. **43**(10): p. 1929-1930.
217. Giesel, F.L., et al., F-18 labelled PSMA-1007: biodistribution, radiation dosimetry and histopathological validation of tumor lesions in prostate cancer patients. Eur J Nucl Med Mol Imaging, 2017. **44**(4): p. 678-688.
218. Giesel, F., et al., Intra-individual comparison of (18)F-PSMA-1007 and (18)F-DCFPyL PET/CT in the prospective evaluation of patients with newly diagnosed prostate carcinoma: A pilot study. J Nucl Med, 2017. **59**(7): p.1076-1080.
219. Eiber, M., et al., Prostate-Specific Membrane Antigen Ligands for Imaging and Therapy. J Nucl Med, 2017. **58**(Supplement 2): p. 67S-76S.
220. Maurer, T., et al., Prostate-specific membrane antigen-radioguided surgery for metastatic lymph nodes in prostate cancer. Eur Urol, 2015. **68**(3): p. 530-534.
221. Schottelius, M., et al., [(111)In]PSMA-I&T: expanding the spectrum of PSMA-I&T applications towards SPECT and radioguided surgery. EJNMMI Res, 2015. **5**(1): p. 68-72.
222. Rauscher, I., et al., Value of 111In-prostate-specific membrane antigen (PSMA)-radioguided surgery for salvage lymphadenectomy in recurrent prostate cancer: correlation with histopathology and clinical follow-up. BJU International, 2017. **120**(1): p. 40-47.
223. Miller, P.W., et al., Synthesis of 11C, 18F, 15O, and 13N radiolabels for positron emission tomography. Angew Chem Int Ed Engl, 2008. **47**(47): p. 8998-9033.
224. Chen, K. and X. Chen, Positron Emission Tomography Imaging of Cancer Biology: Current Status and Future Prospects. Seminars in Oncology, 2011. **38**(1): p. 70-86.
225. Qaim S, M. and G. StÖCklin, Production of Some Medically Important Short-Lived Neutron-Deficient Radioisotopes of Halogens, in Radiochimica Acta. 1983. p. 25.
226. Ruth, T.J., A.P. Wolf, and M.J. Welch, Absolute Cross Sections for the Production of 18F via the 18O(p,n) 18F Reaction. J Comput Assist Tomogr, 1980. **4**(1): p. 138-139.
227. Printz, G. and O. Solin, Construction of an 18O-enriched water target for the routine production of [18O]fluoride. Acta radiologica. Supplementum, 1991. **376**: p. 59.
228. Langevelde, F., et al., Production of multi Curie [18F] fluoride using a niobium target chamber at small PET cyclotrons. 2002. p-12-16.

229. Furuya, T., C.A. Kuttruff, and T. Ritter, Carbon-fluorine bond formation. Curr Opin Drug Discov Devel, 2008. **11**(6): p. 803-819.
230. Liotta, C.L. and H.P. Harris, Chemistry of naked anions. I. Reactions of the 18-crown-6 complex of potassium fluoride with organic substrates in aprotic organic solvents. J Am Chem Soc, 1974. **96**(7): p. 2250-2252.
231. Christe, K.O., et al., Syntheses, properties, and structures of anhydrous tetramethylammonium fluoride and its 1:1 adduct with trans-3-amino-2-butenenitrile. J Am Chem Soc, 1990. **112**(21): p. 7619-7625.
232. Kim, D.W., et al., Facile nucleophilic fluorination reactions using tert-alcohols as a reaction medium: significantly enhanced reactivity of alkali metal fluorides and improved selectivity. J Org Chem, 2008. **73**(3): p. 957-962.
233. Jacobson, O., D.O. Kiesewetter, and X. Chen, Fluorine-18 Radiochemistry, Labeling Strategies and Synthetic Routes. Bioconjugate Chem, 2015. **26**(1): p. 1-18.
234. Okarvi, S.M., Recent progress in fluorine-18 labelled peptide radiopharmaceuticals. Eur J Nucl Med, 2001. **28**(7): p. 929-938.
235. Wester, H.J., K. Hamacher, and G. Stocklin, A comparative study of N.C.A. fluorine-18 labeling of proteins via acylation and photochemical conjugation. Nucl Med Biol, 1996. **23**(3): p. 365-372.
236. Richter, S. and F. Wuest, 18F-Labeled Peptides: The Future Is Bright. Molecules. 2014;**19**(12):p. 20536-20556.
237. Kuhnast, B. and F. Dollé, The Challenge of Labeling Macromolecules with Fluorine18: Three Decades of Research. Curr Radiopharm, 2010.**3**(3): p. 174-201.
238. Schirrmacher, R., et al., Small Prosthetic Groups in ¹⁸F-Radiochemistry: Useful Auxiliaries for the Design of 18F-PET Tracers. Semin Nucl Med, 2017. **47**(5): p. 474-492.
239. Zhang, M.R. and K. Suzuki, [18F]Fluoroalkyl agents: synthesis, reactivity and application for development of PET ligands in molecular imaging. Curr Top Med Chem, 2007. **7**(18): p. 1817-1828.
240. E. Olberg, D. and O. K. Hjelstuen, Labeling Strategies of Peptides with 18F for Positron Emission Tomography. Curr Top Med Chem, 2010. **10**(16): p. 1669-1679.
241. Block, D., H.H. Coenen, and G. Stöcklin, N.C.A. 18F-fluoroacylation via fluorocarboxylic acid esters. J. Label. Compd. Radiopharm, 1988. **25**(2): p. 185-200.
242. Vaidyanathan, G. and M.R. Zalutsky, Labeling proteins with fluorine-18 using N-succinimidyl 4-[18F]fluorobenzoate. Int J Rad Appl Instrum B, 1992. **19**(3): p. 275-281.
243. Kilbourn, M.R., et al., Fluorine-18 labeling of proteins. J Nucl Med, 1987. **28**(4): p. 462-470.

244. Shiue, C.Y., A.P. Wolf, and J.F. Hainfeld, Synthesis of 18F-labelled N-(p-[18F]fluorophenyl)maleimide and its derivatives for labelling monoclonal antibody with 18F. J. Label. Compd. Radiopharm, 1989. **26**(1-12): p. 287-289.
245. Olberg, D.E. and O.K. Hjelstuen, Labeling strategies of peptides with (1)(8)F for positron emission tomography. Curr Top Med Chem, 2010. **10**(16): p. 1669-1679.
246. Sletten, E.M. and C.R. Bertozzi, Bioorthogonal chemistry: fishing for selectivity in a sea of functionality. Angew Chem Int Ed Engl, 2009. **48**(38): p. 6974-6998.
247. Dirksen, A. and P.E. Dawson, Expanding the scope of chemoselective peptide ligations in chemical biology. Curr Opin Chem Biol, 2008. **12**(6): p. 760-766.
248. Dirksen, A. and P.E. Dawson, Rapid Oxime and Hydrazone Ligations with Aromatic Aldehydes for Biomolecular Labeling. Bioconjugate Chem, 2008. **19**(12): p. 2543-2548.
249. Kölmel, D.K. and E.T. Kool, Oximes and Hydrazones in Bioconjugation: Mechanism and Catalysis. Chem Rev, 2017. **117**(15): p. 10358-10376.
250. Thygesen, M.B., et al., Nucleophilic catalysis of carbohydrate oxime formation by anilines. J Org Chem, 2010. **75**(5): p. 1752-1755.
251. Olberg, D.E., et al., One Step Radiosynthesis of 6-[18F]Fluoronicotinic Acid 2,3,5,6-Tetrafluorophenyl Ester ([18F]F-Py-TFP): A New Prosthetic Group for Efficient Labeling of Biomolecules with Fluorine-18. J Med Chem, 2010. **53**(4): p. 1732-1740.
252. Malik, N., et al., Radiosynthesis of a new PSMA targeting ligand ([18F]FPy-DUPA-Pep). Appl Radiat Isot, 2011. **69**(7): p. 1014-1018.
253. Richarz, R., et al., Neither azeotropic drying, nor base nor other additives: a minimalist approach to (18)F-labeling. Org Biomol Chem, 2014. **12**(40): p. 8094-8099.
254. NEUMAIER, B.Z., Boris; RICHARZ, Raphael; KRAPF, Phillip;, METHOD FOR THE PRODUCTION OF 18F-LABELED ACTIVE ESTERS AND THEIR APPLICATION EXEMPLIFIED BY THE PREPARATION OF A PSMA-SPECIFIC PET-TRACER. 2016, MAX-PLANCK-GESELLSCHAFT ZUR FÖRDERUNG DER WISSENSCHAFTEN E.V.
255. Banerjee, S., M.R. Pillai, and N. Ramamoorthy, Evolution of Tc-99m in diagnostic radiopharmaceuticals. Semin Nucl Med, 2001. **31**(4): p. 260-277.
256. Deutsch, E. and K. Libson, Recent advances in technetium chemistry: bridging inorganic chemistry and nuclear medicine. Comments Inorg Chem, 1984. **3**(2-3): p. 83-103.
257. Zolle, I., Technetium-99m pharmaceuticals. 2007: Springer.
258. Schwochau, K., Technetium Radiopharmaceuticals—Fundamentals, Synthesis, Structure, and Development. Angew Chem Int Ed Engl, 1994. **33**(22): p. 2258-2267.

259. Boyd, R., Technetium-99m generators—the available options. Int J Appl Radiat Isot, 1982. **33**(10): p. 801-809.
260. Papagiannopoulou, D., Technetium-99m Radiochemistry for Pharmaceutical Applications. J. Label. Compd. Radiopharm, 2017. **60**(11):502-520.
261. Banerjee, S.R., et al., Effect of Chelators on the Pharmacokinetics of (99m)Tc-Labeled Imaging Agents for the Prostate-Specific Membrane Antigen (PSMA). J Med Chem, 2013. **56**(15): p. 6108-6121.
262. Decristoforo, C., et al., Comparison of in vitro and in vivo properties of [99mTc]cRGD peptides labeled using different novel Tc-cores. Q J Nucl Med Mol Imaging, 2007. **51**(1): p. 33-41.
263. Lister-James, J., B.R. Moyer, and T. Dean, Small peptides radiolabeled with 99mTc. Q J Nucl Med, 1996. **40**(3): p. 221-233.
264. Jurisson, S.S. and J.D. Lydon, Potential Technetium Small Molecule Radiopharmaceuticals. Chem Rev, 1999. **99**(9): p. 2205-2218.
265. Wong, E., et al., Rhenium(V) and Technetium(V) Oxo Complexes of an N(2)N'S Peptidic Chelator: Evidence of Interconversion between the Syn and Anti Conformations. Inorg Chem, 1997. **36**(25): p. 5799-5808.
266. Scheunemann, M. and B. Johannsen, A simple and efficient synthesis of a derivatized pseudotripeptide containing a methylene thioether isostere and its use for the design of bifunctional rhenium and technetium chelating agents. Tetrahedron Lett, 1997. **38**(8): p. 1371-1372.
267. Morgan, G.F., et al., Synthesis and biological studies of neutral technetium (V) complexes containing NNOS donor sets. Nucl Med Biol, 1992. **19**(1): p. 65-72.
268. Wüst, F., H. Spies, and B. Johannsen, Synthesis of “3+1” mixed-ligand oxorhenium(V) complexes containing modified 3,17β-estradiol. Bioorganic Med Chem Lett, 1996. **6**(22): p. 2729-2734.
269. Chang, F., et al., NHS-MAS3: a bifunctional chelator alternative to NHS-MAG3. Appl Radiat Isot, 1999. **50**(4): p. 723-732.
270. Decristoforo, C. and S. Mather, The influence of chelator on the pharmacokinetics of 99mTc-labelled peptides. Q J Nucl Med, 2002. **46**(3): p. 195-205.
271. Kasina, S., et al., Simplified Preformed Chelate Protein Radiolabeling with Technetium-99m Mercaptoacetamidoadipoylglycylglycine (N3S-Adipate). Bioconjug Chem, 1998. **9**(1): p. 108-117.
272. Hnatowich, D.J., et al., Labeling peptides with technetium-99m using a bifunctional chelator of a N-hydroxysuccinimide ester of mercaptoacetyltriglycine. J Nucl Med, 1998. **39**(1): p. 56-64.

273. Schwartz, D.A., et al., Preparation of hydrazino-modified proteins and their use for the synthesis of technetium-99m-protein conjugates. Bioconjug Chem, 1991. **2**(5): p. 333-336.
274. Edwards, D.S., et al., 99mTc-labeling of hydrazones of a hydrazinonicotinamide conjugated cyclic peptide. Bioconjug Chem, 1999. **10**(5): p. 803-807.
275. Liu, S., et al., Labeling a hydrazino nicotinamide-modified cyclic IIb/IIIa receptor antagonist with 99mTc using aminocarboxylates as coligands. Bioconjug Chem, 1996. **7**(1): p. 63-71.
276. King, R.C., et al., How do HYNIC-conjugated peptides bind technetium? Insights from LC-MS and stability studies. Dalton Trans, 2007(43): p. 4998-5007.
277. Rose, D.J., et al., Synthesis and Characterization of Organohydrazino Complexes of Technetium, Rhenium, and Molybdenum with the {M(η1-HxNNR)(η2-HyNNR)} Core and Their Relationship to Radiolabeled Organohydrazine-Derivatized Chemotactic Peptides with Diagnostic Applications. Inorg Chem, 1998. **37**(11): p. 2701-2716.
278. Edwards, D.S., et al., New and versatile ternary ligand system for technetium radiopharmaceuticals: water soluble phosphines and tricine as coligands in labeling a hydrazinonicotinamide-modified cyclic glycoprotein IIb/IIIa receptor antagonist with 99mTc. Bioconjug Chem, 1997. **8**(2): p. 146-154.
279. Garcia, M.F., et al., Evaluation of tricine and EDDA as Co-ligands for 99mTc-labeled HYNIC-MSH analogs for melanoma imaging. Anticancer Agents Med Chem, 2015. **15**(1): p. 122-130.
280. Ono, M., et al., Control of radioactivity pharmacokinetics of 99mTc-HYNIC-labeled polypeptides derivatized with ternary ligand complexes. Bioconjug Chem, 2002. **13**(3): p. 491-501.
281. La Bella, R., et al., In vitro and in vivo evaluation of a 99mTc(I)-labeled bombesin analogue for imaging of gastrin releasing peptide receptor-positive tumors. Nucl Med Biol, 2002. **29**(5): p. 553-560.
282. Schibli, R., et al., Influence of the Denticity of Ligand Systems on the in Vitro and in Vivo Behavior of 99mTc(I)−Tricarbonyl Complexes: A Hint for the Future Functionalization of Biomolecules. Bioconjug Chem, 2000. **11**(3): p. 345-351.
283. Alberto, R., et al., Synthesis and properties of boranocarbonate: a convenient in situ CO source for the aqueous preparation of [(99m)Tc(OH(2))3(CO)3]+. J Am Chem Soc, 2001. **123**(13): p. 3135-3136.
284. Gorshkov, N.I., et al., 2 + 1 Chelating Systems for Binding Organometallic Fragment Tc(CO) 3 +. Radiochemistry, 2005. **47**(1): p. 45-49.
285. Alberto, R., et al., A Novel Organometallic Aqua Complex of Technetium for the Labeling of Biomolecules: Synthesis of [99mTc(OH2)3(CO)3]+ from [99mTcO4]- in

Aqueous Solution and Its Reaction with a Bifunctional Ligand. J Am Chem Soc, 1998. **120**(31): p. 7987-7988.

286. Mundwiler, S., et al., A new [2+ 1] mixed ligand concept based on [99 (m) Tc (OH 2) 3 (CO) 3]+: a basic study. Dalton Trans, 2004(9): p. 1320-1328.
287. Gorshkov, N.I., et al., "2+1" Dithiocarbamate–isocyanide chelating systems for linking M(CO)3+ (M=99mTc, Re) fragment to biomolecules. J Organomet Chem, 2004. **689**(25): p. 4757-4763.
288. Alvarez, J., Radiopharmaceuticals prepared with stannous chloride. J Radioanal Chem, 1975. **27**(2): p. 475-482.
289. Sampson, C.B., Textbk radiopharmacy. Vol. 3. 1994: CRC Press.
290. Khalil, M., Basic sciences of nuclear medicine. 2010: Springer Science & Business Media.
291. Tofe, A.J. and M.D. Francis, In vitro stabilization of a low-tin bone-imaging agent (99mTc-Sn-HEDP) by ascorbic acid. J Nucl Med, 1976. **17**(9): p. 820-825.
292. Volkert, W.A., D.E. Troutner, and R.A. Holmes, Labeling of amine ligands with 99mTc in aqueous solutions by ligand exchange. Int J Appl Radiat Isot, 1982. **33**(10): p. 891-896.
293. Weineisen, M., et al., Neue und bewährte Radiopharmaka für die Diagnostik und Therapie des Prostatakarzinoms. Nuklearmediziner, 2015. **38**(02): p. 89-98.
294. Kelloff, G.J., P. Choyke, and D.S. Coffey, Challenges in clinical prostate cancer: role of imaging. AJR Am J Roentgenol, 2009. **192**(6): p. 1455-1470.
295. Schöder, H., et al., 2-[18F]Fluoro-2-Deoxyglucose Positron Emission Tomography for the Detection of Disease in Patients with Prostate-Specific Antigen Relapse after Radical Prostatectomy. Clin Cancer Res, 2005. **11**(13): p. 4761-4769.
296. Jadvar, H., Imaging evaluation of prostate cancer with 18F-fluorodeoxyglucose PET/CT: utility and limitations. Eur J Nucl Med Mol Imaging, 2013. **40 Suppl 1**: p. S5-10.
297. Yoshida, S., et al., 11C-choline positron emission tomography in prostate cancer: primary staging and recurrent site staging. Urol Int, 2005. **74**(3): p. 214-220.
298. Heinisch, M., et al., Positron emission tomography/computed tomography with F-18-fluorocholine for restaging of prostate cancer patients: meaningful at PSA < 5 ng/ml? Mol Imaging Biol, 2006. **8**(1): p. 43-48.
299. Mease, R.C., Radionuclide based imaging of prostate cancer. Curr Top Med Chem, 2010. **10**(16): p. 1600-1616.
300. Nanni, C., et al., Comparison of 18F-FACBC and 11C-choline PET/CT in patients with radically treated prostate cancer and biochemical relapse: preliminary results. Eur J Nucl Med Mol Imaging, 2013. **40 Suppl 1**: p. S11-17.

301. Ren, J., et al., The value of anti-1-amino-3-18F-fluorocyclobutane-1-carboxylic acid PET/CT in the diagnosis of recurrent prostate carcinoma: a meta-analysis. Acta Radiol, 2016. **57**(4): p. 487-493.
302. Mansi, R., et al., Bombesin-Targeted PET of Prostate Cancer. J Nucl Med, 2016. **57**(Suppl 3): p. 67s-72s.
303. Afshar-Oromieh, A., et al., The Rise of PSMA Ligands for Diagnosis and Therapy of Prostate Cancer. J Nucl Med, 2016. **57**(Suppl 3): p. 79s-89s.
304. Bander, N.H., et al., Targeting Metastatic Prostate Cancer With Radiolabeled Monoclonal Antibody J591 to the Extracellular Domain of Prostate Specific Membrane Antigen. J Urol, 2003. **170**(5): p. 1717-1721.
305. Eiber, M., et al., Prostate-Specific Membrane Antigen Ligands for Imaging and Therapy. J Nucl Med, 2017. **58**(Suppl 2): p. 67s-76s.
306. Holmes, E.H., PSMA specific antibodies and their diagnostic and therapeutic use. Expert Opin Investig Drugs, 2001. **10**(3): p. 511-519.
307. de Bono , J.S., et al., Abiraterone and Increased Survival in Metastatic Prostate Cancer. New Engl J Med, 2011. **364**(21): p. 1995-2005.
308. Seruga, B. and I.F. Tannock, Chemotherapy-based treatment for castration-resistant prostate cancer. J Clin Oncol, 2011. **29**(27): p. 3686-3694.
309. Parker, C., et al., Alpha Emitter Radium-223 and Survival in Metastatic Prostate Cancer. New Engl J Med, 2013. **369**(3): p. 213-223.
310. Maurer, T., et al., 99mTechnetium-based Prostate-specific Membrane Antigen-radioguided Surgery in Recurrent Prostate Cancer. Eur Urol, 2018. Article in press: https://doi.org/10.1016/j.eururo.2018.03.013.
311. Suardi, N., et al., Long-term outcomes of salvage lymph node dissection for clinically recurrent prostate cancer: results of a single-institution series with a minimum follow-up of 5 years. Eur Urol, 2015. **67**(2): p. 299-309.
312. Rauscher, I., et al., Value of 68Ga-PSMA HBED-CC PET for the Assessment of Lymph Node Metastases in Prostate Cancer Patients with Biochemical Recurrence: Comparison with Histopathology After Salvage Lymphadenectomy. J Nucl Med, 2016. **57**(11): p. 1713-1719.
313. Bandini, M., N. Fossati, and A. Briganti, Salvage surgery for nodal recurrent prostate cancer. Curr Opin Urol, 2017. **27**(6): p. 604-611.
314. Robu, S., et al., Synthesis and preclinical evaluation of novel (18)F-labeled Glu-urea-Glu-based PSMA inhibitors for prostate cancer imaging: a comparison with (18)F-DCFPyl and (18)F-PSMA-1007. EJNMMI Res, 2018. **8**(1): p. 30-41.

VIII. Appendix

Appendix 1: Weineisen M, **Robu S**, Schottelius M, Wester H-J. Novel and Established Radiopharmaceuticals for Diagnosis and Therapy of Prostate Carcinoma. *Nuklearmediziner* 2015; 38(02): 89-98.

Appendix 2: Robu S*, Schottelius M*, Eiber M, Maurer T, Gschwend J, Schwaiger M, Wester H-J. Preclinical Evaluation and First Patient Application of ^{99m}Tc-PSMA-I&S for SPECT Imaging and Radioguided Surgery in Prostate Cancer. *J. Nucl. Med*. 2017; 58(2): 235-242.

Appendix 3: Maurer T*, **Robu S***, Schottelius M, Schwamborn K, Rauscher I, van den Berg N, van Leeuwen F W B, Haller B, Horn T, Heck M M, Gschwend J E, Schwaiger M, Wester H-J, Eiber M. ^{99m}Technetium-based Prostate-specific Membrane Antigen-radioguided Surgery in Recurrent Prostate Cancer. *Eur Urol*. 2019;75(4):659-666.

Appendix 4: Robu S*, Schmidt A, Eiber M, Schottelius M, Günther T, Yousefi B, Schwaiger M, Wester H-J. Synthesis and Preclinical Evaluation of novel ^{18}F-labeled Glu-urea-Glu-based PSMA inhibitors for Prostate Cancer Imaging: a comparison with ^{18}F-DCFPyl and ^{18}F-PSMA-1007. *EJNMMI Res*. 2018; 8(1):30-40.